Review Article:

RC members externally strengthened with FRP composites by grooving methods including EBROG and EBRIG: A state-of-the-art review

Khaled Sanginabadi
Ph.D. candidate, Department of Civil Engineering, University of Kurdistan, Sanandaj, Iran
ksanginabadi@yahoo.com

Azad Yazdani
Prof., Department of Civil Engineering, University of Kurdistan, Sanandaj, Iran
a.yazdani@uok.ac.ir

Davood Mostofinejad
Prof., Department of Civil Engineering, Isfahan University of Technology (IUT), Isfahan, Iran
dmostofi@cc.iut.ac.ir

Christoph Czaderski
Senior Researcher, Swiss Federal Laboratories for Materials Science and Technology (Empa), Dübendorf, Switzerland
christoph.czaderski@empa.ch

Corresponding author: Azad Yazdani
Mailing address: Department of Civil Engineering,
University of Kurdistan,
P.O. Box 416,
Sanandaj, Iran
Phone: +98-87-33668457
E-mail address: a.yazdani@uok.ac.ir

RC members externally strengthened with FRP composites by grooving methods including EBROG and EBRIG: A state-of-the-art review

Abstract

In recent decades, the externally bonded reinforcement (EBR) method has been recognized as a desirable and established choice to strengthen reinforced concrete (RC) structures with fiber-reinforced polymer (FRP) composites. The major weakness of this method is the premature debonding of FRP composites from concrete substrates. The grooving method (GM) has been introduced to prevent or postpone premature debonding. This study aims to review the previous studies on strengthening structural members by the grooving method. More specifically, it sought to examine the studies addressing the behaviors of strengthened beams, slabs, columns, and beam-column joints with FRP composites by grooving methods. The effects of groove dimensions as well as the properties of concrete and FRP materials on the performance of the grooving method were evaluated. The enhancements of flexural, shear, compressive, and seismic behaviors of strengthened RC members by grooving method were assessed and their efficiency was compared with the EBR method. The results showed the considerable efficiency of the grooving method in enhancing the performance of all structural concrete members by postponing or preventing premature debonding. Additionally, this method could considerably decrease the amount of consumed material.

Keywords: Fiber-reinforced polymer (FRP) composites, Externally strengthening, RC beams, RC columns, RC Beam-column joints, Grooving method, Seismic rehabilitation.

1. Introduction

Structures should be retrofitted and strengthened to provide sufficient safety during their life due to errors in design and implementation, updating standard codes, change in occupancy, and natural hazards [1]. The application of fiber-reinforced polymer (FRP) composites for

63 strengthening structures has recently become widespread as compared to other conventional
64 materials. Some of the peculiar features of these composites are lightweight, high tensile
65 strength to weight ratio, durability, and resistance against corrosion, ease of installation, and
66 slight modifications in dimensions of retrofitted members [1-4].

67 FRP composites are used to strengthen concrete elements in two main methods, namely,
68 externally bonded reinforcement (EBR) and near-surface mounted (NSM) (traces a and b in
69 Fig. 1) [1,5]. The EBR method is a conventional strengthening method. Premature debonding
70 is the main challenging problem of this method since it can prevent achieving the full tensile
71 capacity of FRP composites, which can waste expensive FRP materials [1,6-11]. Debonding
72 occurs when the force induced in the FRP composite violates the FRP-to-concrete bond
73 capacity. Accordingly, the debonding of FRP composite from concrete surfaces has a close
74 relationship with a bond capacity [10-15]. Bond capacity was estimated as a function of
75 various factors including the stiffness and tensile strength of adhesive material [14,16-18], the
76 uniaxial stiffness and tensile strength of FRP composite [14,16-20], FRP width to member
77 width ratio [11,16,21], the compressive and tensile strength of concrete [14,16,22-27], FRP
78 materials [19,28], bond length [14,19,29], and dominant loading modes [30-31]. Attaining the
79 full capacity of FRP composite in external reinforcement of concrete structures requires an
80 appropriate surface preparation for eliminating or postponing premature FRP composite
81 debonding [32-43]. To solve this problem, Mostofinejad and Mahmoudabadi suggested a
82 novel method called the grooving method (GM) [44], in which interfacial stress was
83 transferred into firmer layers of beams by creating grooves on the tensile face of the beams.
84 Two installation techniques were adopted in the grooving method (traces c and d in Fig. 1).
85 Externally bonded reinforcement on groove (EBROG) and externally bonded reinforcement
86 in groove (EBRIG) are important techniques to perform the grooving method [44-45].

A large number of studies have been conducted to evaluate the distinguishing capability of FRP-to-concrete bond by grooving method [37,46-66]. In this paper, all previous studies using the grooving method to retrofit structural members were evaluated. A total of 445 tests were performed by these studies, out of which 141 tests were for flexural strengthening of beams and slabs [44-45,67-80], 86 tests for shear strengthening of beams [81-88], 182 tests for strengthening columns [89-105], and 36 tests for strengthening beam-column joints [106-112]. Therefore, this paper considers the flexural strengthening of beams and slabs by EBROG and EBRIG methods, shear strengthening of beams via the EBROG and EBRIG methods, and the strengthened columns by EBROG, EBRIG, and combination of the methods (EBRIOG), respectively. Finally, the seismic rehabilitation of beam-column joints is discussed by using the EBROG method.

2. Flexural strengthening of beams and slabs

The high tensile strength of FRP composites and low tensile strength of concrete are responsible for the flexural strengthening of RC beams, which is considered as one of the main applications of FRP composites [1,6-8,113-116]. Flexural strengthening is performed by adhering FRP composites on the tensile face of beams [100-121]. 16 studies were conducted to evaluate the flexural strengthening of beams and slabs using grooving methods [44-45,67-80]. In these studies, 81 and 6 beams were strengthened by the EBROG and EBRIG methods, respectively. As reference, 30 beams were strengthened by the EBR technique, while 15 beams were not strengthened. All of the beams were tested through a four-point bending apparatus (Fig. 2). Table A.1 presents the properties and results related to the tests for all beams and slabs [44-45,67-80].

2.1. Review of previous studies

Mostofinejad and Mahmoudabadi [44] proposed a novel method called as "grooving method (GM)" to postpone the premature debonding of FRP sheets off the concrete substrate. The

112 results demonstrated that grooves with a 3 mm breadth and 2 mm depth in transversal,
113 diagonal, and longitudinal arrangements could increase the load capacity by 9.0, 15.0, and
114 27.0% in comparison to the beams strengthened through the EBR method (Table A.1).
115 Additionally, the grooves with a 3 mm breadth and 10 mm depth changed the failure mode
116 from debonding FRP composites to rupture and increased the load capacity by about 82.0%
117 [44]. In another study, Mostofinejad and Shameli [45] evaluated the performance of the
118 EBROG method in beams with one, two, and three layers of FRP composite (0.12 mm
119 thickness). In these cases, the bending capacity of the EBROG beams increased 107.0, 146.0,
120 and 94.0% compared to the EBR beams, respectively, by considering the same layers of FRP
121 composite (Table A.1). Mostofinejad and Shameli [67] used EBROG and EBRIG methods to
122 strengthen concrete beams. The bending capacity of EBRIG beams was more than the
123 EBROG beams. The highest increases in ratios of the bending capacity of the EBRIG and
124 EBROG methods were 145.2 and 182.1%, respectively, as compared with the EBR method.
125 Furthermore, Mostofinejad and Hajrasouliha [68] estimated that the bending capacity of the
126 beams increased by increasing the breadth of grooves in all levels of concrete compressive
127 strength and at each constant depth of grooves (7.5, 10.0, and 12.5 mm). The total area under
128 the load displacement curve shows the amount of energy absorbed by the beams. The
129 absorbed energy of the EBROG beams was higher than the EBR beams. The highest growth
130 in absorbed energy was for 30 MPa specimens while the lowest was for 75 MPa
131 specimens. Mostofinejad et al. [69] strengthened some beams by EBRIG and EBROG
132 methods. The bending capacity of the beams strengthened by two layers of CFRP and by the
133 EBROG and EBRIG method was 25.1% more than the two-layer EBR beams. These values
134 were 18.9 and 24.0% for the beams with three layers of CFRP, respectively.

135 Mostofinejad and Moghaddas [70] conducted four-point bending tests to evaluate the
136 failure modes in strengthened RC beams. The EBROG method had a considerably better

performance in comparison to the EBR method for the beams designed to reach FRP rupture failures. Mostofinejad and Khozaei [71] evaluated the effect of the various patterns of the longitudinal grooves (full grooving, end grooving, and intermittent grooving) on the strengthening system. The end grooving pattern caused the highest growth in the bending capacity, and the lowest increase in the bending capacity was attributed to the intermittent grooving pattern. The bending capacity of the EBROG beam with the end grooving pattern and three layers of CFRP experienced a 24.4 and 117.8% increase compared to the EBR beam and unstrengthened beam [71].

Jiang et al. [52] introduced a new method called epoxy interlocking based on grooving methods to improve the bond performance. In this method, when the transverse grooves are created and filled with epoxy, the dowel force of the epoxy grooves will be added to the resistance force components and enhance the bond performance and anchorage behavior. The results displayed that the specimens with grooves filled with epoxy have an 88.8% higher capacity than the specimens with wax-filled grooves. The results may demonstrate the epoxy interlocking effect clearly. Given the analytical results, increasing groove depth augmented the contribution of the concrete surfaces engaged in resistance of filled grooves, and accordingly, the load-slip behavior was improved.

Nader Tehrani et al. [72] evaluated the strengthening of beams by prestressed CFRP up to 0, 20, and 30% of their ultimate strain using the EBROG method. The number and width of flexural cracks cracks diminished by increasing prestressed levels. The results showed that the cracking, yielding, and maximum load of the EBROG beam with a 20% level of prestressing strain increased by 126.7, 48.0, and 62.5% compared to the unstrengthened beams. These values were 6.7, 4.9, and 18.0% compared to the EBR beam, and the maximum strain of CFRP increased by 35.6%.

Azizi and Talaeitaba [73] investigated the EBROG method's capability in punching shear strengthening of flat slabs through a numerical study. The results of 15 numerical specimens emphasized the great efficiency of this method in increasing punching shear capacity. The EBROG specimens experienced 15.0% to 23.0% enhancement in the created strain of the FRP sheet compared to the EBR specimens.

Mashrei et al. [74] evaluated the groove shape and orientation on flexural beam strengthening of RC beams via the EBROG and EBRIG methods. The cross-section of grooves was selected semicircle, triangular and rectangular. The remarkable results can be expressed as follows: the rectangular cross-section showed a higher performance level than the other cross-section shapes in the EBRIG method. As a case, the load-carrying capacity of the EBRIG beams with semicircle, triangular and rectangular groove cross-section was 74.0, 58.0, and 95.0% higher than the load-carrying capacity of the non-strengthened beam, respectively.

Shen et al. [75,122-123] strengthened RC box beams with initial flexural cracks using BFRP strips. A beam (beam B0) remained non-strengthened, and the other beams were strengthened by CFRP strips for shear-strengthening and by the BFRP strips for flexural strengthening. The ends of BFRP strips in the first beam (beam B1), the second beam (beam B2), and the third beam (beam B3) were anchored using U-strips, grooving method, and steel plates as end anchorages, respectively. The results demonstrated that beam B1 underwent BFRP and CFRP strips debonding at its end regions. However, beam B2 and beam B3 experienced debonding BFRP strips on the pure flexure zone. Comparing the load capacity of beam B1, beam B2, and beam B3 with beam B0 illustrated 27.2%, 39.3%, and 42.2% enhancement, respectively. Additionally, beam B2 and beam B3 had a better performance to limit cracks than beam B1. At the ultimate loads, the average depth, distance, and width of

cracks of beam B2 were 2.8, 10.3, and 6.2% less than beam B1. These values were 6.9, 16.2, and 9.3% for beam B3.

Sabzi et al. [76] evaluated the effect of concrete compressive strength and longitudinal reinforcement arrangement on the flexural strengthening of the beams via the EBROG and EBR techniques. On average, the EBROG beams attained a 5.0% increase in the load capacity relative to the EBR beams for normal concrete strength. This value for the beams with high concrete strength was 14.0%.

Al-Rousand and Al-Tahat [60] assessed the FRP-to-concrete bond behavior of heat-damaged concrete. To conduct these tests, they placed the concrete specimens in 250-750 °C for 120 minutes and then strengthened them via the EBROG method. The results illustrated that the transverse grooves have more robust behavior than the longitudinal grooves. For instance, the bond capacity for the EBROG and EBRIG specimens with 115 mm wide FRP sheet and longitudinal grooves under 750 centigrade temperature was 4.1 kN and 5.1 kN, respectively. These values increased to 9.5 kN for the EBROG specimens with transverse grooves.

Torabian et al. [77] assessed flexural strengthening of RC slabs by FRP composites through the EBROG method. The load capacity of the reference specimen was 117.4 kN, and the EBR method could elevate loading capacity by 11.0%. The EBROG technique could increase loading capacity by 38.0% on average, as compared to the reference slab. Further, the strain debonding of the EBROG slabs was 75.0% higher than the EBR slabs. Torabian et al. [78] investigated shear and flexural strengthening of RC slabs with FRP composites and post-installed shear bolts. The load capacity of the non-strengthened slab was 156.3 kN. The combination of post-installed shear bolts and flexural strengthening using the EBROG method led to an increase in loading capacity by 57.0% via preventing premature punching shear failure.

Moshiri et al. [79] investigated the flexural strengthening of beams with the prestressed CFRP up to 26% of their nominal ultimate strength (2800 MPa) using the EBROG method. The results indicated that the bending capacity of prestressed EBROG beams increased by 266.0, 78.0, and 33.0% compared to the unstrengthened beam, EBR beam, and EBROG beam, respectively.

Mohammadi and Mostofinejad [62] categorized grooves in the EBROG method to achieve an optimum design and introduced various layouts regarding groove dimension, space, and direction. The results demonstrated that the groove direction has no substantial effect on the bond capacity. The maximum difference was for the 10×10 mm class with a 30 mm distance (10×10@30 mm) for longitudinal and transverse grooves. In this class, the bond capacity of the specimen with transverse grooves has increased by 28.7% compared to the bond capacity of the similar category with longitudinal grooves [62]. The 5×5@15 mm class was introduced as the most optimum class. The bond capacity of the EBROG of the 5×5@15 mm class has increased by 141.1% and 114.1% for the specimens with longitudinal and transverse grooves compared to the EBR specimens, respectively. The fracture energy of such bonds was measured 5.2 and 4.9 times more than the EBR, respectively [62].

Some researchers evaluated the effect of FRP material types on the EBROG bond behavior [63-65]. Regarding the tests conducted on CFRP-to-concrete and GFRP-to-concrete bonds via the EBROG method, the failure modes of all specimens were sheet debonding in a shallow depth of concrete substrate. Generally, the CFRP-to-concrete bond capacity was measured higher than the GFRP-to-concrete bond capacity. In both bond types, CFRP, and GFRP, the ultimate slip decreased with increasing FRP sheet stiffness, while GFRP specimens experienced a higher ultimate slip compared to CFRP specimens. Some practical models were proposed in these studies to estimate the bond capacity and effective bond length with good accuracy for both types of CFRP and GFRP composites.

Abed et al. [80] evaluated the flexural behavior of the beams strengthened with FRP strips through the EBROG technique. To implement the EBROG strengthening system, they exploited transverse and longitudinal grooves and also their combination. It was observed that the failure mode shifted from FRP debonding to FRP rupture. The ultimate beam deformation also diminished substantially. The load-carrying capacity of the strengthened beams with no grooves, three longitudinal grooves, and eight transverse grooves increased by 48.2, 49.7, and 65.4% compared to a non-strengthened beam. This growth value was 76.7% for a combination of three longitudinal grooves and eight transverse grooves.

2.2. Failure modes

Table A.1 presents the failure modes of all the test specimens. However, in Mostofinejad and Hajrasouliha's investigations [68], the failure mode was not reported independently. In the mentioned study, 116 specimens were strengthened, among these, 38 specimens experienced FRP rupture, 69 specimens underwent the mixed mode of rupture-debonding of FRP sheets, and 9 specimens went through debonding. From the 6 EBRIG beams, Mostofinejad and Shameli [45] reported the FRP rupture failure mode for one beam and concrete cover separation for the two other beams. However, Mostofinejad et al. [69] observed FRP rupture for one EBRIG beam and FRP debonding accompanied with complete concrete cover separation for the two others. Also, according to Table A.1, in all the non-strengthened and EBR beams tests, flexural failure and FRP debonding were reported, respectively. Regarding Table A.1, to scrutinize the failure modes of the EBROG beams, Fig. 3 was presented. Fig. 3a reveals each study's occurrence percentage of FRP debonding (FD), FRP rupture (FR), mixed rupture-debonding of FRP, concrete cover separation (CCS), mixed rupture-debonding of FRP (FR-FD), mixed concrete cover separation-debonding of FRP (CCS-FD), flexural failure (FF), and punching failure of slab (PU) modes. For instance, in Mostofinejad et al.'s [45] tests, 100.0% of the specimens experienced rupture-debonding failure mode. Furthermore,

Mostofinejad and Khozaei [70] observed FRP rupture and concrete cover separation in 33.3%, and 66.7% of their specimens, respectively. Abed et al. [80] recorded this percentage as 12.5% for FRP debonding, 12.5% for FRP rupture, and 75% for the concrete cover separation in their tests. However, the total occurrence percentage of each failure mode may be discussed regarding all the available tests and their failure modes as a collection (Fig. 3b). The failure modes of 33.3, 31.2, and 20.8% of the EBROG beam specimens were FRP debonding, concrete cover separation, and FRP rupture. A combined mode of FRP rupture and FRP debonding occurred for 6.4% of the beams. Only 5.1% of the beams experienced concrete cover separation-FRP debonding mode at failure.

2.3. Load-displacement diagrams

Fig. 4 shows the comparison of the load-displacement diagrams of seven different beams under four-point bending tests. The maximum loads of control beams [45,68] were 6.8 and 12.6 kN, respectively, and the mid-span displacements were 0.40 and 0.65 mm. In addition, the ultimate load and deflection of EBR beams on average reached 15.0 kN and 2.50 mm, respectively. EBROG beams [45,68] had a stiffness similar to the EBR ones until the cracking load. The first crack occurred at about 0.65 mm deflection. The maximum ultimate load and corresponding displacement of the EBROG beam compared to the EBR one were 35.0 kN (133.3% higher load) and 7.00 mm (180.0% higher displacement), respectively (Fig. 4).

The EBRIG beam [45] had the same behavior, and the load remarkably increased due to high stiffness. The apparent difference of this beam with other beams was its higher stiffness. Thus, it experienced only 0.40 mm mid-span displacement at 16.0 kN cracking load. The EBRIG beam [68] exhibited an ultimate load of 41.0 kN at a mid-span displacement of 8.00 mm. The load-displacement diagrams show that the area under the diagram of the EBRIG beam is larger than the EBROG beams. Hence, The EBRIG technique has a higher capacity

to absorb energy in comparison to the EBROG technique. However, compared to the EBR method, the EBROG technique has a considerably higher performance to absorb energy (Fig. 4).

2.4. Parameters affecting the performance of the grooving method

As shown in Table A.1, the properties and characteristics of the tests vary in an extensive range. Therefore, the tests are categorized so that the variation of the intended parameters could be evaluated while the other parameters are almost constant.

2.4.1. FRP composite stiffness ($E_f t_f$) and comparison of the EBROG and EBRIG techniques

Fig. 5 demonstrates the difference between the EBROG and EBRIG performance as well as the effect of stiffness of the FRP composites. In this figure, the horizontal axis denotes the FRP composite stiffness ratio, $\frac{E_f t_f}{E_f t_f^*}$, where $E_f t_f^* = 0.12 \times 230000 = 27600$ N/mm. Fig. 5a shows that there is approximately a linear relationship between the FRP composite stiffness and increasing the load capacity of the strengthened beams. However, the slope of the increasing trend reduces by the growth of stiffness of the FRP composites. The EBRIG beams that were strengthened using FRP composite with $\frac{E_f t_f}{E_f t_f^*} = 1.0$ and 3.0 could achieve the load capacity of 53.8% at least and 672.0% at most more than the corresponding un-strengthened beams, respectively. These values are 54.3 and 502.0%, respectively, for the EBROG beams. Fig. 5a shows that the beams strengthened using FRP composites with $\frac{E_f t_f}{E_f t_f^*} = 1.0$ have the same load capacity for both the EBROG and EBRIG methods. The load capacity of the EBRIG beams increases compared to the EBROG beams when $\frac{E_f t_f}{E_f t_f^*} = 2.0$ and 3.0. For example, the load capacity of the EBRIG beams enhances by 28.0% more than the EBROG beams (compared to un-strengthened beams) when $\frac{E_f t_f}{E_f t_f^*}$ of the FRP composites is 3 (Fig. 5a).

As shown in Fig. 5b, the load capacity of the EBROG and EBRIG beams increases compared to the EBR beams when FRP composite stiffness increases up to a specific value.

The trend becomes reversed after this specific stiffness. This behavior can be attributed to the prevalence of FRP debonding mode at high stiffness. According to Fig. 5b, this specific stiffness value is in the range of $\frac{E_f t_f}{E_f t_f{}^*}$=2.0 to 2.5. Additionally, the EBRIG beams exhibit a higher load capacity than the EBROG beams. For instance, increments in the load capacity of the EBRIG beams compared to EBR beams for $\frac{E_f t_f}{E_f t_f{}^*}$=1.0, $\frac{E_f t_f}{E_f t_f{}^*}$=2.0, and $\frac{E_f t_f}{E_f t_f{}^*}$=3.0 are 117.3, 181.8, and 131.2%, respectively. These values for the EBROG beams are 117, 145, and 81%, respectively. Fig. 5c confirms that utilizing grooving methods can remarkably expand the area under load-displacement curves in comparison to the EBR method in a linear relationship although the slope of this linear relationship diminishes by increasing the stiffness of FRP composites. For instance, the absorbed energy (the area under the load-displacement curves) of the EBRIG beams for $\frac{E_f t_f}{E_f t_f{}^*}$=1.0, $\frac{E_f t_f}{E_f t_f{}^*}$=2.0 and $\frac{E_f t_f}{E_f t_f{}^*}$=3.0 increased by 0.0, 151.2, and 171.2% compared with those of the EBR beams. Such values for the EBROG beams exhibited 6.2, 112.0, and 143.4% growth, respectively.

2.4.2. Concrete compressive strength

Figs. 6-7 show that increasing the concrete compressive strength reduces the load capacity of the EBROG beams compared to the non-strengthened beams and EBR beams. This trend can be also observed for the area under load-displacement diagrams. Among the beams with 28 MPa concrete compressive strength, the load capacity of the EBROG beams increases by at least 53.3% and at most 71.3% compared to the load capacity of the non-strengthened beams. However, the EBROG beams with 75 MPa concrete compressive strength experienced growth by only 6.0% minimum and 10.2% maximum (Fig. 6a). The increase in the load capacity of the EBROG beams concerning the EBR beams with 28 MPa concrete compressive strength is in the range between 18.7% to 34.1%, and the value decreases to less than 5.0% by increasing the concrete compressive strength of the beams to 75 MPa (Fig. 6b).

To explain this behavior, one may refer to the high cracking load in the beams with compressive strength 75 MPa causing serious damage and seriously weak bonding between FRP strip and substrate concrete during cracking, which ultimately leads to premature debonding at the cracking zone.

The ultimate mid-span displacement of the EBROG beams increases as compared to the EBR beams. However, there is no specific trend related to the increase in concrete compressive strength from 28 to 75 MPa. For example, the increase in ultimate mid-span displacement compared to the EBR beams for 28 and 75 MPa concrete compressive strength is in the ranges of 33-50% and 33-44%, respectively (Fig. 7a). In Fig. 7b, the vertical axis is defined as the relative difference between the absorbed energy (the area under the load-displacement curve) of the EBROG specimen to the corresponding value in the EBR specimen. The horizontal axis represents concrete compressive strength. According to Fig. 7b, for the beams with 28 MPa compressive strength of concrete, the relative difference between the area under the load-displacement curve increases 93.4% minimum and 318.0% maximum. For the 45 MPa beams, this ratio ranges between 61.9% and 114.2%. For the beams with 62 MPa, this range is 49.4% to 81.1%. When the concrete compressive strength reaches 75 MPa, the ratio is restricted to 40.7% and 76.8%. Therefore, it may be explicitly observed that this relative difference has a descending trend with increasing concrete compressive strength.

2.4.3. Groove breadth to FRP composite width ratio b_g/b_f

The properties of the tested beams demonstrate that there are different FRP composite widths and groove numbers. Therefore, considering only the groove breadth might not illustrate its effect on the behavior of the beams. Thus, the ratio of groove breadth to FRP composite width (b_g/b_f) is defined based on the sum of the breadth of grooves to the FRP composite width, which covers these grooves.

Increasing the b_g/b_f ratio increases the load capacity of the strengthened beams compared to non-strengthened beams (Fig. 8a). This increase has a slight slope for low b_g/b_f ratio, and growing b_g/b_f ratio heightens the slope. For instance, for the beams strengthened by the grooving methods and a 30 MPa concrete compressive, the load capacity enhances 55.7, 57.7, and 63.3% on average for the b_g/b_f ratios of 0.20, 0.30, and 0.40, respectively. These values for the beams with 45 MPa concrete compressive strength are 26.2, 32.1, and 42.3%, respectively. Additionally, when the compressive strength reaches 75 MPa, the aforementioned values reduce and reach 7.3, 8.4, and 9.3% (Fig. 8a).

Fig. 8b illustrates a similar trend when the beams strengthened by grooving methods are compared to the EBR beams. For example, for the beams strengthened by grooving methods and a 30 MPa concrete compressive strength, the load capacity increases by 21.7, 23.4, and 27.8% (on average) for the b_g/b_f ratios of 0.20, 0.30, and 0.40, respectively. These values for 45 MPa concrete compressive are 8.0, 12.8, and 18.7%, respectively.

As illustrated in Figs. 9a and b, the ultimate mid-span displacement and area under load-displacement curves increase with an increment in the b_g/b_f ratio in comparison to the EBR beams. As a case, when concrete compressive strength is 30 MPa, an increment in the b_g/b_f ratio from 0.20 to 0.40 creates a 51.5% increase in mid-span displacement and a 241.9% increase in the area under load-displacement curves.

2.4.4. Groove depth to FRP composite width ratio (d_g/b_f)

The groove depth to FRP composite width (d_g/b_f) ratio is defined based on the sum of the depth of all grooves to the FRP composite width, which covers these grooves. As shown in Fig. 10, the increase in the load capacity of the strengthened beams by grooving methods compared to the non-strengthened and EBR beams has a linear relationship with increasing the d_g/b_f ratio. However, the load capacity drops when the d_g/b_f ratio exceeds a specific value (about 1.00). As a case, the load capacities of the beams strengthened by grooving

methods compared to the non-strengthened beams and 30 MPa concrete compressive strength increased by 55.5, 66.6, and 59.4% for the d_g/b_f ratios of 0.75, 1.00, and 1.25, respectively (Fig. 10a). When these beams are compared to the EBR beams, the values changed to 21.7, 30.4, and 24.7%, respectively (Fig. 10b). Hence, their optimum value for the d_g/b_f ratio could be about 1.00.

2.4.5. The area ratio of internal reinforcement to external reinforcement (A_s/A_f)

According to Fig. 11, increasing the area ratio of internal to external reinforcement (A_s/A_f) causes the load capacity of the strengthened beams by grooving methods, in comparison to non-strengthened beams, to have a descending trend. The increases in the load capacity of the strengthened beams by grooving methods compared to the non-strengthened beams at the A_s/A_f ratios of 8.37, 12.56, and 18.84 are 56.0, 46.2, and 31.8%, and 1.0, 5.1, and 7.1%, respectively, compared to the EBR beams. Further, the areas under load-displacement curves corresponding to the A_s/A_f ratios of 8.37, 12.56, and 18.84 increase by 3.0, 24.8, and 17.7%, respectively. These values for the ultimate mid-span displacement are 1.1, 18.0, and 10.0% (Fig. 11).

3. Shear strengthening of concrete beams

External shear reinforcement of RC beams was accomplished in three procedures. In the first procedure, FRP composites were installed on two sides of the beams. This method is called the two-side method. The second method was conducted by installing FRP composites on two side faces and bottom face (U-shape). In the third method, all sides of the beams were covered by FRP composites. This technique is called the full-warp method (Fig. 12) [124-131].

The primary challenge in shear strengthening of RC beams is related to the debonding of FRP composites from the concrete substrate [124-131]. The high ability of the EBROG and EBRIG methods in postponing and eliminating the debonding phenomenon motivated

researchers to consider these methods for external shear reinforcement of RC beams. Overall, eight different studies evaluated the shear strengthening of RC beams by FRP composites through EBROG and EBRIG methods [81-88]. Table A.2 presents the characteristics and results of the aforementioned tests [81-88].

3.1. Review of the literature

Mostofinejad and Tabatabayi Kashani [81] performed the first study in external shear reinforcement of RC beams with FRP composites by EBROG method. The use of the EBROG method changed the failure mode from shear to flexural mode. However, the EBR specimen failed due to debonding of FRP sheets. The EBR and EBROG beams had 51.0 and 67.0% growth in the load capacity on average, respectively, compared to the non-strengthened beams. In addition, the EBROG beams had an 11.0% increase in load capacity in comparison to the EBR beams. In the final steps of loading, the load-displacement curves of EBROG beams had a horizontal part. Accordingly, the ultimate displacement of the EBROG beams was 20.0% more than the EBR beams on average [81].

In another study, Mostofinejad and Tabatabaei Kashani [82] tested 32 beams to assess the shear behavior of strengthened beams using EBROG methods. The EBR beams had a 13.5% increase in the load capacity on average in comparison to the non-strengthened beams. This value for the EBROG beams was 26.0%. The decrease of concrete compressive strength from 36.0 to 26.2 MPa led to a reduction in the load capacity from 23.0 to 17.0% for the EBR beams and from 34.0 to 24.0% for the EBROG beams on average. In the EBR beams, because of the weak interface between the FRP sheet and concrete, the FRP sheets were separated from the surface of the concrete beam. The EBROG method changed the failure mode from shear to flexural mode, which led to substantial stretching of the horizontal section of load-displacement curves. Consequently, the ultimate mid-span displacement of

the EBROG beams grew 172.0 and 69.0% compared to the non-strengthened and EBR beams [82].

Furthermore, Mostofinejad et al. [83] tested four beams with the dimension of 560×70×85 mm (length×width×heigt) utilizing a four-point bending test apparatus. The non-strengthened beam suffered a shear failure mode and had a 21.9 kN load capacity. The EBR beam experienced 14.0% load capacity more than the non-shear-strengthened beam, and the failure mode was a shear failure with debonding of CFRP strips off the surface of the concrete beam. Additionally, the EBROG beams had a 22.0% increase in the load capacity on the average and the failure mode changed from shear to flexural.

Mostofinejad et al. [84] strengthened 14 beams, including two non-shear-strengthened beams and six shear-strengthened beams by EBR method as well as six shear-strengthened beams by EBRIG technique (Table A.2). In group A (two-side method), the EBR beams enjoyed 62.2 and 114.9% in the load capacity for vertical and diagonal patterns compared to non-shear strengthened beams. The EBRIG beams in group A (in two vertical and diagonal patterns) had 87.3 and 118.8% growth in the load capacity, respectively, in comparison to the non-shear-strengthened beams [84]. Altering patterns of the CFRP from 90° to 45° for the EBR and EBRIG methods resulted in 33.3 and 17.1% increases in load capacity.

Shomali et al. [85] analytically and experimentally evaluated the EBRIG method for shear strengthening of RC beams. The EBRIG method caused changing failure mode from shear failure to CFRP rupture. For the EBRIG beams, the load capacity increased about 55.4% on average compared to the corresponding non-strengthened beam [85]. Shomali et al. [86] assessed the capability of the EBR and EBRIG methods in shear strengthening of RC beams with different internal reinforcements. The EBR and EBRIG beams showed 33.2 and 74.0% increases in the load capacity at most, respectively, relative to the control beam.

Arabzadeh and Karimizadeh [87] estimated the EBROG and EBR methods efficiency in strengthening the RC deep beams with openings. The load capacity of the EBROG beams increased by 12.0% on average and 24.0% at maximum compared to the EBR beams.

Shomali et al. [88] strengthened 5 RC beams using the EBRIG method to improve the shear capacity. The use of the EBRIG method at 90° (vertical) increased the shear capacity of RC beams with and without stirrups by 37.0 and 71.1% on average, respectively. These values reached 60.2 and 95.3% for the EBRIG method at 45° (diagonal).

3.2. Failure Modes

All unstrengthened beams experienced a shear failure mode, among which 85.0% of the EBR beams suffered shear failure mode accompanied by FRP debonding. The other EBR beams failed due to shear failure mode with FRP rupture. All the EBROG beams enjoyed flexural failure mode, which showed that shear strengthening by the EBROG method could remove shear weaknesses of the beams and shift the shear failure mode to flexural failure mode. Further, 47.8% of the EBRIG beams experienced a shear failure with FRP rupture, 43.5% underwent a shear failure with FRP debonding, and 8.7% failed due to flexural failure mode. Hence, the EBRIG method could improve the failure modes of the beams and alter shear failure modes to flexural failure modes.

3.3. Comparing the results

The experimental results show that with constant FRP width, reducing the spacing of FRP sheets can increase the EBROG/EBRIG beam shear capacity compared to the EBR beam due to postponing the premature debonding. Because of the limited number of studies, the optimal value for FRP materials was not recorded. Fig. 13 demonstrates the comprehensive results of the load capacity of the shear strengthened beams by grooving methods. The highest increase in the load capacity in comparison to the corresponding non-strengthened beam is 155.0%. This increase is associated with an EBRIG beam strengthened by using

single grooves (5×5 mm) which are covered by FRP composites with a 30 mm width, a center-to-center distance of 70 mm, and a full wrap-90° technique. Furthermore, beams strengthened by grooving methods have at least a 19.0% enhancement in the load capacity compared to non-sheer-strengthened beams. This growth is for an EBROG beam with a 40 mm FRP sheet width and an 80 mm center-to-center distance. Under each CFRP sheet, there are two 5×10 mm grooves, and a two-side (vertical pattern) procedure is utilized to shear-strengthen the beams. The highest increase in the load capacity of the strengthened beams by grooving methods compared to the corresponding EBR beams is 46.0%. This growth in the load capacity could be attributed to the EBRIG technique. On the other hand, the lower value recodes 2.0%.

In the two-side installation method of CFRP composites, altering the FRP composite angle from 90° to 45° and changing the EBR technique to ERBIG lead to substantial growth in stiffness, load capacity, and energy absorption. In addition, when the full wrap technique is employed, shifting the angle from 90° to 45° cannot produce a considerable increase in stiffness, load capacity, and energy absorption. In the full wrap technique, even shifting the angle from 90° to 45° causes a slight reduction in the aforementioned parameters. The performance of the U-shaped procedure is between the two-side method and the full wrap technique. For example, the load-displacement curves for some of the beams are presented for comparison (Fig. 14). The non-shear strengthened beams have a brittle failure and fracture with reaching the ultimate load. The EBR beams display the same behavior. However, the beams strengthened by grooving methods have a horizontal zone in their load-displacement curves, which is related to the change of the shear failure mode to the flexural failure mode. In fact, the beams can tolerate and attain large displacements after reaching the ultimate load.

4. Strengthening RC columns

506 The columns are the primary and critical components of a structure which damages to these
507 elements can expose the whole structure to the danger of collapse [132-136]. Hence,
508 strengthening and rehabilitation of RC columns by FRP composites are widely accomplished
509 to improve the loading capacity and ductility of the columns [137-142]. When FRP
510 composite is utilized for RC columns strengthening, it may buckle for compressive stresses
511 induced in the FRP composite and, subsequently, debond from the concrete substrate.
512 Therefore, the FRP composite compressive load capacity is restricted to its probable
513 buckling. [143-145]. The high performance of the grooving methods as an external technique
514 to strengthen beams motivated researchers to conduct a series of investigations on RC
515 columns strengthened by grooving methods [44-45]. Fourteen studies assessed the
516 performance of grooving methods for strengthening the RC column using FRP composites.
517 The results and properties of these specimens are presented in Table A.3. It is worth noting
518 that the results of mutual tests are presented merely one time [89-105].

519 **4.1. Test setups and strengthening patterns**

520 The researchers exercised a machine with a hydraulic jack to apply centric or eccentric loads
521 in quasi-static or cyclic modes. All tests were performed based on controlling displacements
522 with a 1 mm/min rate. The columns were subjected to cyclic loads with 0.1% axial drift in
523 three cycles of loading/unloading. The loading protocols and the test setups are illustrated in
524 Figs. 15a and 15b. It should be noted that the lateral loading protocol was constant for the
525 specimens that were seismically strengthened. The columns were also subjected to a constant
526 axial load equal to 10% of the nominal column capacity under compressive load. The test
527 setup and the lateral loading protocol of the seismic behavior tests are presented in Figs. 15c
528 and 15d.

529 The strengthening of RC columns was accomplished by longitudinal and transversal
530 patterns. A column can be strengthened by one pattern or a combination of some patterns

(Fig. 16 and Fig. 17). In the reviewed studies, the researchers employed longitudinal strengthening by NSM, EBR, EBROG, and EBRIG methods. In all EBROG and EBRIG columns, the dimensions of the grooves were selected as 10×10 mm. However, a novel method called EBRIOG was suggested by mixing EBRIG and EBROG methods to strengthen RC columns. In this method, the groove surfaces were first saturated with resin, and the FRP sheets adhered to the surfaces. Then, the grooves were completely filled with resin, and new sheet layers were installed on the grooves. Finally, the top layer is saturated with resin (Fig. 16e).

The transversal patterns embodied three patterns. In the first pattern, a column was confined with intermittent CFRP wraps (IW). CFRP wraps were connected in a horizontal (transversal) direction. The width and space of CFRP wraps were 30 mm and 55 mm for circular columns, respectively. The width and space of CFRP wraps for other cross-sections was 50 mm (Fig. 16 and Fig. 17). The second pattern can be used for square and rectangular columns. In this pattern, all four corners of the columns were strengthened by corner strips in L shapes in transversal directions. The length of the leg was 45-55 mm. Next, the IW pattern was implemented on these corner strips. This pattern is called CSW (Fig. 16 and Fig. 17). The third pattern was similar to the second pattern, and the corners were strengthened by corner strips with a 45-55 mm leg length. Then, composite battens with 50 mm width and a length equivalent to 90% of the dimension of the column were installed on four sides of the column and corner strips. This pattern is called CSB (Fig. 16 and Fig. 17).

The nomination of the specimens includes the research code, the name of the strengthening pattern, and the number of FRP layers. The letter 'H' is used to name the rectangular and square columns whose tensile face is strengthened and the circular columns whose half of the column is strengthened. In this study, the 'SE' prefix is used to name the EBROG columns whose grooves are filled with a mixture of silica sands and epoxy. In some

studies, the width of the FRP composites was halved, and two layers of FRP composites were installed on each groove. In this paper, the letter 'T' is employed for these groups. The columns whose grooves are filled with epoxy and without installation of FRP composites are named 'MFG'. In addition, an ordinal number is used to demonstrate the number of similar columns. The names, properties, and descriptions of the columns are presented in Table A.3.

4.2. Review of the previous studies

Moshiri et al. [89] and Moshiri and Mostofinejad [90] strengthened square and circular columns by FRP composites. The capacities of the circular and square reference columns were 535.7 and 466.6 kN, respectively. The load capacities of EBR, EBROG, EBRIG, and NSM circular columns were 2.6, 14.1, 18.5, and 2.6% more than the reference columns. These values for square columns were -1, 10.4, 12.7, and 4.8%.

Mostofinejad and Torabian [91] and Torabian and Mostofinejad [92] tested circular columns subjected to eccentric loads and strengthened them through EBR and EBROG methods using the IW pattern. The EBROG columns had the maximum axial load at 0, 30, 60, and 90 mm, which were eccentricities equal to 775.3, 441.0, 260.1, and 175.4 kN. In fact, the maximum axial loads of these columns grew by 8.3, 12.2, 25.8, and 36.0% compared to the reference columns. These values for IW columns were 42.2, 38.4, 35.1, and 29.9%. The columns strengthened by the combination of the EBROG and IW methods had 49.9, 48.6, 57.7, and 59.9% growth. These values were 2.7, 5.1, 10.2, and 14.5% for the EBR columns [91-92].

Mostofinejad and Moshiri [93] evaluated the effect of the strengthening methods and FRP layers on circular columns. The results showed that the EBR and NSM methods did not considerably affect the load capacity of the columns. However, the strengthened columns by the EBROG and EBRIG methods and the EBROG/IW mixed-method had a 13.0, 18.5, and 47.2% increase in comparison to the reference columns, respectively. Increasing the number

of FRP layers enhanced the load capacity of the EBROG columns by 13.0, 14.1, and 20.5% for 1, 2, and 3 layers of FRP, respectively. Employing the EBROG and EBRIG methods engendered ample compressive stress for FRP composites and heightened the load capacity of the columns. For instance, utilizing the EBROG and EBRIG methods increased the compressive stress in FRP composite up to 45.0 and 59.0% of the ultimate stress of the FRP coupon [93].

Saljoughian and Mostofinejad [94] strengthened square columns through IW, CSB, CSB-EBR, and CSB-EBROG methods and subjected them to loads with 0, 30, 60, 90, 120 mm eccentricity. The researchers longitudinally strengthened only the tensile face of the columns. The increased ratio of the ductility of strengthened columns to the reference columns diminished while increasing load eccentricity. For example, CSB-EBROG-0 had a ductility index equal to 11.3 and grew by 569.0% in comparison to the corresponding reference column with a 1.7 ductility index. Additionally, the ductility index of CSB-EBROG-120 was 5.7 and experienced only a 58.0% increase compared to the corresponding reference column with a 2.5 ductility index. However, increasing eccentricity led to a rise in the ductility of the CSB-EBR and the CSB-EBROG columns in comparison to the IW and CSB columns [94].

Saljoughian and Mostofinejad [95] strengthened rectangular columns to compare cross-sectional shapes via EBR-CSB and EBROG-CSB and tested them under loading with 0, 30, 90, and 120 mm eccentricity. The strengthening of the square columns was more effective than the rectangular columns so that the EBROG columns subjected to loads with a 90 mm eccentricity enjoyed a 55.5 and 40.9% increase in the load capacity compared to the reference columns for the square and rectangular columns, respectively. These values were 44.1 and 30.9%, respectively, for centric loadings [94-95].

Saljoughian and Mostofinejad [96-97] assessed the novel technique of EBRIOG to longitudinally strengthen the square columns under cyclic loads. The non-strengthened

column as reference one had a 717.5 kN ultimate load while the EBRIG, EBRIG-IW, EBRIG-CSW, and EBRIG-CSB columns enjoyed 17.1, 48.3, 60.9, and 60.2% increase in comparison to the reference column, respectively. These values were 21.3, 46.0, 66.2, and 71.8% for the EBRIOG, EBRIOG-IW, EBRIOG-CSW, and EBRIOG-CSB, respectively. The ductility index of the non-strengthened columns was 1.6 while the EBRIG, EBRIG-IW, EBRIG-CSW, and EBRIG-CSB columns enjoyed 41.2, 122.0, 217.6, and 173.6% increase, respectively. The EBRIOG, EBRIOG-IW, EBRIOG-CSW, and EBRIOG-CSB columns experienced 46.2, 158.8, 167.2, and 192.1% growth in ductility index [96-97].

Noroozolyaee and Mostofinejad [98] evaluated the effect of slenderness on circular RC columns strengthened by the EBR and EBROG methods. The load capacity of the non-strengthened columns with 15.4, 21.5, and 27.7 slenderness ratios was 103.3, 96.8, and 90.5 kN, respectively. The load capacity of the EBR columns demonstrated 33.1, 25.6, and 32.4% growth compared to the non-strengthened columns, respectively. In addition, the load capacity of the EBROG columns for the aforementioned slenderness ratios, compared to the non-strengthened columns, increased by 49.2, 60.8, and 63.2%. Regarding the EBROG columns, shifting the slenderness ratio from 15.4 to 21.5 and 15.4 to 27.6 caused increases of about 62.0 and 84.0% in the secondary to primary bending moment ratio. These values were 64.0 and 104.0% for the EBR columns and 62.0 and 167.0% for the non-strengthened columns [98].

Saljoughian and Mostofinejad [99] estimated using the grooving methods for seismic strengthening of square RC columns. The maximum load of the un-strengthened column was 39.5 kN. The EBROG and EBRIG columns achieved 42.0 and 51.0% growth in the maximum load, respectively, compared to the un-strengthened column. In contrast, the EBROG-CSB and EBRIG-CSB columns exhibited increases of 64.0 and 77.0% in comparison to the un-strengthened column. Saljoughian and Mostofinejad [100] estimated

631 the behavior of RC columns which strengthened transversally (IW, CSW, and CSB) and
632 longitudinally (EBROG). The non-strengthened column recorded the maximum load of 717.5
633 kN. In comparison to the non-strengthened column, the EBROG-IW, EBROG-CSW, and
634 EBROG-CSB columns showed enhancement in the maximum loads by 39.9, 51.8, and
635 54.9%, respectively.

636 Noroozolyaee and Mostofinejad [101] investigated slender concrete columns reinforced by
637 high-strength steel retrofitted with FRP composite. For slenderness ratios of 15.4, 22.0, and
638 28.0, the maximum loads reached 126.6, 126.2, and 105.2 kN in the reference columns,
639 respectively, while increases of 17.7, 17.5, and 25.1% were recorded for the EBR columns
640 relative to the reference columns. These values were 40.9, 36.7, and 60.8% in the EBROG
641 columns, respectively. Mostofinejad et al. [102] evaluated the behavior of RC slender
642 columns strengthened by FPR composite subjected to loads with eccentricities of 0, 30, 60,
643 and 90 mm. For the un-strengthened columns, the maximum loads reached 647.9 and 85.0 kN
644 subjected to the loads with eccentricities 0 and 90 mm, respectively. The maximum loads
645 increased by 1.3 and 41.7% for the EBR columns, respectively, compared to the un-
646 strengthened columns. Regarding the un-strengthened columns, the maximum load
647 enhancements were 10.6 and 99.3% for the EBROG columns subjected to the loads with
648 eccentricities 0 and 90 mm, respectively.

649 Hosseini and Mostofinejad [103] combined the EBROG technique with the confinement
650 of CFRP warp to develop a method to strengthen short columns against seismic actions via
651 longitudinal FRP sheets. The introduced method resulted in shear and flexural strengthening
652 of RC short columns. The load-carrying capacity, ductility, and energy dissipation of the
653 EBROG columns were 1.8, 2.7, and 13.0 times greater than the non-strengthened columns.
654 Among the EBROG columns, no longitudinal CFRP sheet debonding and buckling were

observed. On the other hand, no improvement was recorded for the EBR columns since they experienced longitudinal CFRP sheet debonding and buckling.

Saljoughian et al. [104] evaluated the seismic performance of high-strength RC columns retrofitted with longitudinal and transverse CFRP sheets. For this purpose, they mixed the EBR, EBROG, and EBRIG methods as a longitudinal strengthening method with Corner Strip Batten (CSB) as a transverse strengthening method. The load-carrying capacity of the EBR-CSB, EBROG-CSB, and EBRIG-CSB increased by 36.4, 64.9, and 75.9% compared with the corresponding non-strengthened column, respectively. The energy dissipation enhancements in the 5.3% drift ratio were 64.5, 89.2, and 111.1%, respectively. Accordingly, the mentioned columns' stiffness growth was 79.2, 124.1, and 142%, and the ductility index also experienced 38.6, 53.7, and 64.3% improvement, respectively.

Razavi et al. [105] invented a new method to simulate column conditions under cyclic loads close to actual conditions of a column in an earthquake. These columns were strengthened through two methods. The first method strengthened the columns transversely using full wrap CFRP sheets. The second technique was the longitudinal strengthening of the two opposite faces of a column by the EBROG method. The load-carrying capacity of the EBROG columns under monotonic and cyclic loads increased by 54.0 and 64.7% compared with non-strengthened columns. These values for full wrap columns were 1.1 and 3.0%. This shows the absolute performance superiority of the EBROG columns over the full wrap columns.

4.3. The most related results

Two different types of FRP sheets of SikaWrap-230 C and SikaWrap-300 C as well as one type of epoxy resin (Sikadur-330 C) were used in all tests. The internal reinforcement conditions were similar for the specimens to a large extent, and there was no considerable difference between the specimens. The grooves were created in 10 mm width and 10 mm

depth in all strengthened specimens by grooving methods. There was no significant variation in the strengthening materials, internal reinforcement, and dimensions of grooves in tests. Hence, the authors assessed the performance of the strengthening methods and the effective parameters including load-strain curves, load-moment, axial load-displacement envelops, the compressive strength of columns, ductility of columns, and compressive stress of fibers. The results are presented in Table A.3.

4.3.1. Load-strain, load-moment, and axial load-displacement envelope curves

Fig. 18 shows the load-strain, load-moment, and axial load-displacement envelope curves for different specimens. The load-strain curves are bi-linear, and the stiffness of the columns is the same for all the columns under the centric load until the end of the ascending branch. The behavior of the columns at the descending branch is different. This branch has a shorter length with a sudden and considerable drop load for the columns with FRP rupture or concrete crushing failure mode (Fig. 18a). The descending branch length is minor and terminates suddenly for the specimens of EBROG-IW and EBR-IW. The specimens strengthened transversally and longitudinally show a considerable drop load in their descending branch due to the domination of the rupture of transversal sheets. The slope of the ascending branch for the columns under 60 mm eccentricity load is less than the columns under centric load. Regarding these columns, when the columns are strengthened longitudinally, the load-strain curves are very similar to the non-strengthened columns. However, adding transversal strengthening can significantly change the ultimate load and slope of the descending branch (Fig. 18a).

As shown in Fig. 18b, strengthening the RC columns increases their capacity to tolerate larger combinations of load and bending moment. The columns strengthened longitudinally by the EBROG method and transversally by the IW method (EBROG-IW) experience an extraordinary capacity in comparison to the non-strengthened columns. The load and bending

moment of these columns at the balance point are 20.0 kN.m and 320.0 kN, respectively. These values for the reference columns are 12.0 kN.m and 200.0 kN, respectively. Furthermore, the EBROG-IW columns demonstrate the highest capacity for pure axial load and pure bending moment.

Axial load-displacement envelope curves are drawn by joining the first point in the unloading for each hysteresis cycle of axial load-displacement curves (Fig. 18c). These curves are bi-linear. The initial stiffness of all the strengthened and non-strengthened columns is equal. The failure begins after passing the maximum load and reaching the descending branch. The failures are step-by-step and give an increase to a gradual decline in the load capacity. The columns strengthened by grooving methods exhibit a more ductile behavior associated with the descending branch. Fig. 18c demonstrates that the energy absorption of the EBROG columns is higher than the non-strengthened columns while the EBRIG-CSB and EBRIOG-CSB columns increase the maximum load and the maximum displacement leading to excellent energy absorption.

4.3.2. The load capacity

The performance of each method in increasing the average values of the load capacity is evaluated (Fig. 19a). When the columns are subjected to centric loads, the EBR columns have a 0.1% increase in the load capacity compared to the non-strengthened columns. This value increases up to 29% when the eccentricity of the load reaches 120 mm. The ERR-IW and EBR-CSB columns enjoy a 27 and 36% increase in the load capacity compared to the non-strengthened columns when centric loads are applied. The increasing eccentricity of the load of the EBR-IW columns to 120 mm gives an increase to 63% growth in the load capacity, and the EBR-CSB columns experience 39% load capacity enhancement at 90 mm eccentricity (Fig. 19a).

729 The EBROG strengthening on average elevates the load capacity of the column under the
730 centric load by 11.0% relative to the non-strengthened columns. However, the EBROG
731 columns have 53.0% higher load capacity than the non-strengthened columns at 120 mm
732 eccentricity of the load. The EBROG-IW columns experience a 46.0% increase in the load
733 capacity, and the EBROG-CSB attain 38.0% growth under centric loads. Elevating the
734 eccentricity up to 120 mm causes 88.0 and 51.0% increments in the load capacity of these
735 columns compared to the non-strengthened columns, respectively (Fig. 19a). The EBRIG
736 columns show a 16.0% increase in the load capacity in comparison to the non-strengthened
737 columns. The EBRIG-IW, EBRIG-CSB, and EBRIG-SW columns have 48.0, 60.0, and
738 61.0% growth in load capacity, respectively, as compared to the non-strengthened columns.
739 Accordingly, the load capacities of the EBRIOG, EBRIOG-IW, EBRIOG-CSB, and
740 EBRIOG-CSW columns enhance by 21.0, 46.0, 72.0, and 66.0%, respectively. The
741 transversal strengthened columns undergo a reduction in load capacity compared to the non-
742 strengthened columns when loading eccentricity increases (Fig. 19a). This trend is in reverse
743 for the longitudinally strengthened columns, and increasing eccentricity causes growth in the
744 load capacity compared to the non-strengthened columns.

745 Based on the results, halving the width of FRP composites on the grooves and doubling
746 FRP composite layers have no significant effect on the load capacity of the columns. In
747 addition, the grooves filled with resin without the installation of FRP composite cannot
748 increase the load capacity of columns alone.

749 ***4.3.3. Ductility***

750 The ductility index of the EBR columns is only 3% higher than the non-strengthened columns
751 under the centric load. The ductility indexes of the IW and CSB columns are 182.0 and
752 328.0% higher than the non-strengthened columns. These values for the EBR-IW and EBR-
753 CSB columns reached 81.0 and 310.0%, respectively (Fig. 19b). The increasing eccentricity

of the load reduces the ratio of the ductility of the strengthened columns to the non-strengthened columns so that the ductility indexes of IW, CSB, and EBR-CSB columns are 5.0, 57.0, and 53.0% higher than the non-strengthened columns at 120 mm eccentricity of the load. The EBROG columns enjoy a 55.0% increase in ductility compared to the non-strengthened columns at centric load. The value is measured for EBROG-IW and EBROG-CSB columns by 149.0 and 318.0%. The growth in the ductility of EBROG-CSB columns is 115.0% at 90 mm eccentricity of the load. However, an increase in the ductility of the EBROG columns enhances from 55.0 to 206.0% when the eccentricity of the load increases from 0 mm to 90 mm. The EBRIG, EBRIG-IW, EBRIG-CSW, and EBRIG-CSB columns experience a 41.0, 122.0, 218.0, and 174.0% increase in ductility index at the centric load condition, respectively. These values for the EBRIOG, EBRIOG-IW, EBRIOG-CSW, and EBRIOG-CSB columns are 46.0, 159.0, 167.0, and 192.0%, respectively (Fig. 19b).

4.3.4. Fiber compressive stress

The experience of the high value of compressive stress by FRP composite is one of the reasons for the increase in load capacity of the strengthened columns. Therefore, the R_{FC} index is introduced as the ratio of the created compressive stress in FRP composite to its ultimate tensile strength. This parameter indicates the amount of ultimate tensile strength of fibers which can be achievable in compression and is evaluated for the columns under centric axial loads. The FRP fibers in strengthened columns by the EBR method suffer a 220 MPa compressive stress, which indicates the R_{FC} is about 9.0%. Additionally, in the EBROG method, the fibers experience 980 MPa compressive stress, which leads to a 31.0% R_{FC} on average. These values for FRP fibers in the EBRIG columns are 1270 MPa and 49.0% (Fig. 20). The FRP fibers of the EBROG-IW and EBRIG-IW columns tolerate 1087 and 1700 MPa compressive stress. Therefore, the R_{FC} for these columns is 42.0 and 69.0%, respectively. Furthermore, the R_{FC} for BERIG-CSW and EBRIG-CSB columns is 53.0 and 55.0%,

779 respectively, which means the compressive stress in the FRP fibers is recorded at 1325 and
780 1377 MPa. The EBRIOG columns can develop 1606 MPa compressive stress in the FRP
781 fibers and have 64.0% R_{FC}. Accordingly, the compressive stress of the FRP composite in the
782 EBRIOG-IW, EBRIOG-CSW, and EBRIOG-CSB columns is 1563, 1726, and 2256 MPa.
783 Hence, the R_{FC} index is computed as 62.0, 69.0, and 90.0%, which indicates that the
784 EBRIOG-CSB method can develop compressive stress in the FRP composite up to 90.0% of
785 its ultimate tensile strength (Fig. 20).

786 **4.4. Discussion**

787 Longitudinal and transverse strengthening of the RC column using FRP composites can
788 improve the failure conditions and behaviors of columns. Longitudinal strengthening by
789 EBROG, EBRIG, and EBRIOG techniques has a better performance than other methods. The
790 grooves filled by the epoxy act as external supports for the FRP composites, and inhibit and
791 postpone buckling on the compressive side and debonding on the tensile side. The EBRIG
792 and EBRIOG methods provide larger contact surfaces between concrete, fibers, and resin
793 matrix to enhance the column performance. Adding transverse strengthening to the grooving
794 methods fails to produce an exceptional improvement in column behaviors. As a case, the
795 load capacity (axial load) of the strengthened columns by CSB, EBRIG, and EBRIG-CSB
796 methods increased by 42.0, 17.0, and 60.0%, respectively. The difference between EBRIG-
797 CSB and CSB methods is 18.0%, which is almost similar to the growth ratio of the EBRIG
798 columns. Such a condition can be extended to ductility and compressive stress of fibers. It
799 seems that transverse strengthening decreases the unbraced length of FRP composites of
800 longitudinal strengthening, which can provide more lateral support.

801 **5. Seismic strengthening of RC beam-column joints**

802 The beam-column joints are one of the primary components of a structure, which are
803 subjected to cyclic and dynamic loads induced by earthquakes. The shear or flexural

804 weaknesses in these joints may lead to the collapse of the whole structure [146-152].
805 Therefore, engineers always pay careful attention to the shear and flexural strengthening of
806 these elements. The use of steel and concrete jackets was the first method for strengthening
807 beam-column joints. Recently, FRP composites have been introduced as one of the most
808 effective methods in seismic retrofits. Among them, CFRP and BFRP may be pointed out.
809 Since CFRP composites enjoy high tensile capacity, these composites are used extensively in
810 strengthening structural members. However, BFRP currently may be more economical than
811 CFRP. It is a relatively new FRP material employed in structural member strengthening,
812 including shear wall and beam-column joint strengthening [153-157]. However, premature
813 debonding is the main challenge in using FRP composites [93-95,157-158]. To overcome this
814 challenge, the EBROG method has been employed in seismic strengthening to postpone or
815 eliminate premature debonding of FRP composites [106-112]. Therefore, 36 beam-column
816 joints were tested in seven studies. The researchers strengthened exterior and corner beam-
817 column joints to resist shear forces and bending moments [106-112]. The properties and
818 results of all tests are presented in Tables A.4-8.

819 **5.1. Test setups and approaches**

820 Fig. 21a shows the setup of all the tests. The support conditions simulated the contra-flexure
821 points of moment-resisting frames subjected to lateral loads. A hydraulic jack applied axial
822 load to apply compressive stress equal to $0.08f_c'$. Two actuators applied a cyclic and quasi-
823 static lateral load by increasing amplitude and controlling the displacement of the top of the
824 column. The lateral loading protocol is based on ACI committee 374.1 [159] (Fig. 21b). The
825 internal reinforcement details and dimensions of specimens are presented in Figs. 21c-e. It is
826 worth mentioning that the size of all grooves in the EBROG method is 10×10 mm with a 30
827 mm free space.

828 The schematic plan of the strengthened specimens and strengthening patterns is illustrated in
829 Fig. 22 and Tables A.4-5. In Ref. [106], the control specimen is called "DSC." "RDS-nHlF"
830 and "RDS-nXl" are designated for the strengthened specimens' naming templates. n is the
831 number of the FRP sheet layers, H and X denote strengthening patterns of the core of the
832 joint. In Refs. [107] and [112], the control specimen is named "CS," and the naming
833 templates of the strengthened specimens are "RS-nHl" and "RS-nLlF," where n is the number
834 of FRP sheet layers. H denotes installing FRP sheets on the top and bottom face of the beam.
835 L means the L-shaped FRP composites installed on the beam and column faces. In [108] and
836 [109] references, CS-3D is the control specimen of the corner joint. The naming format of
837 strengthened specimens is "RDS-nLlF" and "RDS-nXmHlF." In this pattern, n and m signify
838 the number of FRP sheet layers exploited to strengthen the core of joint and FRP sheet layers
839 on the top and bottom faces of the beam, respectively. X and L exhibit the X-shaped and L-
840 shaped strengthening patterns of the core of joints. H indicates strengthening the top and
841 bottom beam faces. In Refs. [106-109] and [112], l is the length of the FRP sheet from the
842 column face toward the mid-span of the beam, and F means the use of an FRP anchor fan.

843 In the Refs. [110-111], the control specimen is named CS, and the "RS-nV-mX-oH," "SnLl-
844 GmX," SoV-nH-FmX," and "SoCSB-nH-FmX," templates are used to designate the
845 strengthened specimens; n, m, and o are the number of FPR sheet layers utilized to strengthen
846 the column, the core of the joint, and the beam. V means strengthening two opposite faces of
847 the column parallel to the bending axis. X means the X-shaped pattern for FRP composite
848 installed on the core of the joint. H stands for installing FRP composites on top and bottom
849 beam faces. L means an L-shaped design of FRP sheets to strengthen the beam and column.
850 G expresses using transverse grooves. F shows the FRP fan anchor, and CSB signifies using
851 corner strip-batten.

852 **5.2. Review of the related studies**

Mostofinejad and Akhlaghi [106] strengthened exterior beam-column joints, which lacked sufficient internal shear reinforcement in their core with CFRP sheet composites by the EBROG method (Figs. 22a-c). The first crack on the DCS (non-strengthened) joint emerged at the vicinity of the column surface with a 0.2% drift ratio. The maximum recorded load was 63.8 kN, and the load started to reduce after a 2.2% drift ratio. Although the maximum load of the RDS-3H75 and RDS-3H325 joints grew 4.2 and 17.4% in comparison to the DCS joint, their behavior did not demonstrate any significant improvement [106].

FRP fans were employed to anchor the end of CFRP sheets for the RDS-3H325F joint. This method resulted in a 35.6% growth in the maximum load as compared to the DCS joint, and the concrete cover separation occurred at a 4.5% drift ratio. The behavior of the RDS-4H500F joint was similar to the RDS-3H325F joint, and the maximum load increased by 52.0% as compared to the DCS joint. However, in the 4.5% drift ratio, the load of the RDS-4H500F joint increased 110.9% compared to the DCS joint. The RDS-1X250 joint could confirm the capability of the EBROG method in eliminating debonding and protecting the strengthening system under large and non-elastic deformations [106].

Mostofinejad and Akhlaghi [107] mixed the EBROG method and FRP fans to invent a novel technique for the flexural strengthening of beam-column joints (Figs. 22d-f). The maximum load was 48.4 kN for the non-strengthened joint (CS). The failure of the beam-column joint occurred with the plastic hinge formation at the column face in the beam. In the RS-1H300 joint, shifting the plastic hinge from the column face to the beam enhanced the maximum load of 32.7% and increased energy absorption and ductility compared to the CS joint. The maximum load of the RS-2H450I joint increased by 41.1%. The plastic hinge position returned to the previous position such as CS joint due to weaknesses in the anchorage of the strengthening system. Hence, a CFRP wrap with a 75 mm width was installed on the FRP fans to prevent such a failure mode for the RS-2H450II joint. The

maximum load and the load at the 4.5% drift ratio increased 38.4 and 44.0% in comparison to the CS joint [107].

For the RS-3H600I joint, the maximum load and the load at 4.5% drift ratio increased by 54.7 and 10.0% compared to the CS joint. To shift the plastic hinge in RS-3H600II, the areas of the CFRP fans elevated from 143 mm^2 (RS-3H600I) to 204 mm^2. Therefore, the plastic hinge was formed on the strengthened part of the beam, and the maximum load increased by 58.1% compared to the non-strengthened joint. The end of CFRP sheets needed more CFRP wraps to shift the plastic hinge position to a non-strengthened part of the beam. To this end, an RS-3L600 joint was designed. The results showed that the maximum load increased by 79.9%, the plastic hinge was completely transferred to the non-strengthened part of the beam, and the energy absorption increased [107].

Mostofinejad and Hajrasouliha [108-109] retrofitted 3D corner joints with CFRP composites using the EBROG technique against shear failure (Figs. 22g-l). The CS-3D joint had a maximum load equal to 55.4 kN in the 0.2% drift ratio. Compared to the CS-3D joint, crack propagation became slow for the SCS-3D joint, and the maximum load and the load in the 4.5% drift ratio grew by 24.5 and 42.8%, respectively. The RDS-3L300 joint experienced the maximum load in the 3.6% drift ratio and was 31.2% higher than the CS-3D joint. Further, the load corresponding to the 4.5% drift ratio caused a 46.0% increment [108]. The RDS-3L300-EBR joint indicated the maximum recorded load (in the 2.8% drift), and the load in the 4.5% drift increased 24.9 and 29.4%, respectively, compared to the CS-3D joint [108]. In the 4.5% drift ratio, the load capacity of the H-RDS-3L300FW joint increased by 56.9%, compared to the CS-3D joint [108].

For the RDS-X joint, the EBROG method could provide energy absorption conditions and undergo large and non-elastic deformations. The maximum load increased by 28.1% as compared to the CS-3D joint. The load increase in the 4.5% drift ratio reached 46.8% [109].

903 However, the maximum load and load in the 4.5% drift ratio of the RDS-X-EBR joint
904 compared to the CS-3D joint grew by 21.0% and 36.8%, respectively. These values for the
905 RDS-1X3H300F joint were 52.7% and 74.9%, respectively. The RDS-1X3H450F joint first
906 experienced flexural cracks on the beam-column intersection and the plastic hinge remained
907 at the edge of the joint, which could be attributed to the longer length of the strengthened part
908 compared to the RDS-1X3H300F joint. Further, the load capacity in the 4.5% drift ratio
909 increased by 49.7% compared to the CS-3D joint [109].

910 Ilia and Mostofinejad [110] seismically retrofitted strong beam-weak column joints by the
911 EBROG method mixed with a CFRP anchorage system (Figs. 22m-p). These joints lacked
912 sufficient internal shear reinforcements. The maximum load of the non-strengthened joint
913 (CS) was 28.4 kN and occurred at the 1.75% drift ratio [110]. For the RS-1V-1X joint, the
914 maximum load was 50.9% higher than the CS joint and occurred in the 2.75% drift ratio. This
915 value reached 28.3% in the 4.5% drift. In the 2.2% drift ratio, the RS-1V-2X joint
916 experienced a 64.1% maximum load higher than the CS joint. This joint had a 33.0% growth
917 in the loading capacity in the 4.5% drift ratio [110]. However, the maximum load of the RS-
918 1V-2X-2H I joint was 57.1% higher than the CS joint and in the 5.2% drift ratio. It is
919 noteworthy that this value was 90.2% for the 4.5% drift ratio. The RS-1V-2X-2H II joint had
920 similar behavior to the RS-1V-2X-2H I joint. The maximum load and load in the 4.5% drift
921 ratio compared to the CS joint increased by 73.3% and 111.0%, respectively [110].

922 Ilia et al. [111] evaluated the seismic strong beam-weak column joints strengthened by
923 FRP composites using the EBROG method and FRP fan anchorage system (Figs. 22q-t). The
924 non-strengthened joint (CS) suffered hinge formation in the column at the final loading
925 stages, which is considered an undesirable failure mode. External strengthening increased the
926 loading capacity by more than 44.6%. The S2CSB-2H-F2X joint experienced the most

increase in the maximum load capacity by 79.4% and the load capacity in the 4.5% drift by 118.4% [111].

Akhlaghi and Mostofinejad [112] estimated the performance of beam-column joint flexural strengthened by a combination of anchorage systems and the CFRP sheets (Figs. 22u-x). The results showed the excellent performance of the 180-degree anchor fan as anchorage system and perfect bond due to the EBROG method, which led to complete plastic hinge relocation along the beam from the column face (RS-1H300.F180 joint). The maximum load of the RS-1H300.F180 joint was 59.4 kN, which showed a 22.7% increase relative to the control joint.

5.3. The comparison of behavior and ductility parameters

The conducted tests reported considerable results related to behavior, load capacity, ductility, and energy absorption.

5.3.1. Load-displacement hysteretic response and the load capacity

Fig. 23 shows the load-displacement hysteretic envelope curves of some different joints. As shown, the non-strengthened joints experienced load capacity reduction from the 2.2% drift ratio. However, the corresponding strengthened joints experienced a significant increase in loading capacity as well as load capacity reduction from the 5.2% drift ratio. Fig. 23 demonstrates that increasing drift ratios leads to a considerable difference in the load capacity and area under load-displacement curves between strengthened and non-strengthened joints. The RDS-3H325F and RDS-1X3H300F joints show the best improvement in terms of behavior and performance.

The highest growths in the maximum load are 79.9, 79.4, 73.3, and 73.4% for the RS-3L600, S2CSB-2H-F2X, RS-1V-2X-2H II, S1V-2H-F2X joints, respectively. The lowest increase in the maximum load is 4.2%, which is related to the RDS-3H75 joint (Fig. 24a). The highest increases in the load capacity at the 4.5% drift ratio reach 118.4, 110.9, 111.0,

and 110.0% for the S2CSB-2H-F2X, RS-4H500F, RS-1V-2X-2H II, and RS-3L600 joints, respectively (Fig. 24b). Additional details are presented in Table A.6.

5.3.2. Ductility

The ductility factor is presented for all the joints in Table A.7. Fig. 25 shows the increased ductility factor in the pull direction for each joint compared to the reference joint. The RS-1V-2X-2H I joint demonstrates that the highest increase value for the ductility factor is equal to 139.0% for the push direction, compared to the reference specimen with a 1.8 ductility index. The RDS-1V-2X-2H II and S1V-2H-F2X joints obtained the second and third highest ductility factor by 110.7 and 113.8% increase in the push direction. The most significant reduction in the ductility index in the push direction is attributed to the RS-3H600II joint by 63.9%. The joints strengthened by the EBROG method and X-shaped pattern experience an average increase of 60.0% in the ductility index in the push direction (Fig. 25).

5.3.3. Energy dissipation

The confined area of a hysteretic curve in each cycle is defined as the dissipated energy of that cycle. Cumulative dissipated energy is the sum of the dissipated energy in all the cycles. Fig. 26a demonstrates the energy dissipation of some joints from the 0.2% drift ratio to the 4.5% drift ratio. Fig. 26a shows a slight difference in the cumulative energy dissipation between strengthened and non-strengthened joints up to the 2.2% drift ratio. However, the difference becomes more tangible by increasing the drift ratio. Regarding the RDS-325F joint compared to the corresponding un-strengthened joint, an increase in energy dissipation in the 2.75, 3.5, and 4.5% drift ratios is 20.0, 50.0, and 100.0%, respectively.

Table A.8 indicates the value of the cumulative energy dissipation of each joint corresponding to the 4.5% drift ratio, and the reference joint of which is compared in Fig. 26b. The cumulative energy dissipations up to the 4.5% drift ratio for the RS-1V-2X-2H-I and RS-1V-2X-2H-II joints as 12437 and 11435 kN.mm, respectively. Since the cumulative

977 energy dissipation of the reference joint is 5056 kN.mm, these joints enjoy 146.0 and 126.2%
978 growth. The cumulative energy dissipation of the RDS-3H325F joint increases by 100.0% in
979 comparison to the corresponding reference joint with 17464 kN.mm cumulative energy
980 dissipation (Fig. 26b). The RS-3H600II joint can dissipate 26288 kN.mm energy, which
981 indicates an 8.5% reduction compared to the reference joint with 28288 kN.mm. On average,
982 the use of the EBROG method can increase the cumulative energy dissipation by 38.0%
983 while the use of the EBROG method and X-shaped pattern can be increased by 61.0% (Fig.
984 26b).

985 ***5.3.4. Stiffness reduction***

986 As shown in Fig. 27a, the initial stiffness of the strengthened joints is somewhat higher
987 than that of the non-strengthened joints. However, continuing loading causes quick stiffness
988 reduction in non-strengthened joints (Fig. 27a). For example, the RS-3L600 joint in 1.00,
989 2.75, and 4.5% drift ratios have 32.0, 79.0, and 97.2% stiffness higher than the reference
990 joint, respectively. These values are 37.0, 76.0, and 94.3% for the RS-1V-2X-2H I joint,
991 respectively (Fig. 27a). In the 4.5% drift ratio, the S2CSB-2H-F2X, RS-1V-2X-2H II, and
992 S1V-2H-F2X joints experience 122.9, 117.1, and 114.3% increment in the stiffness compared
993 to the corresponding reference joints, respectively (Fig. 27b). Regarding the values of the
994 stiffness in the 4.5% drift ratio, the lowest value is 0.35 kN/mm for the CS joint (non-
995 strengthened joint with the strong beam-weak column) while the maximum value is 1.48
996 kN/mm for the RDS-4H500F joint. The EBROG technique can increase the stiffness in the
997 4.5% drift ratio by 55.0% in comparison to the corresponding reference joint (Fig. 27b).
998 Table A.8 and Figs. 27a-b present further details.

999 ***5.3.5. Equivalent hysteretic damping ratio***

1000 Hysteretic damping is a crucial parameter indicating the capacity of a joint to undergo large
1001 and plastic deformation. The equivalent hysteretic damping ratio is defined as the dissipated

1002 energy for each cycle over 2π times of elastic strain energy [106-112]. The equivalent
1003 hysteretic damping ratio for almost all the joints is 0.10 in drift ratios lower than 1.5% (Fig.
1004 28a). However, the equivalent hysteretic damping ratio enhances when the drift ratio is
1005 increased. For instance, the equivalent hysteretic damping ratios of the RDS-3H325F joint in
1006 1.25, 2.75, 3.5, and 4.5% drift ratio increase by 0.0, 20.0, 30.0, and 55.6% in comparison to
1007 the non-strengthened corresponding joint (Fig. 28a).

1008 The maximum equivalent hysteretic damping ratios are 0.27 and 0.24 for the RS-1H300
1009 joint in the 4.5% drift ratio and the non-strengthened corresponding joint, respectively (Fig.
1010 28b). In the 4.5% drift ratio and among all the joints, the RS-1V-2X-2H-I joint experiences
1011 the highest increase (58.8%) with an equivalent hysteretic damping ratio of 0.24 compared to
1012 the reference joint (Fig. 28b). The EBROG method increases the equivalent hysteretic
1013 damping ratio of the strengthened joints compared to the non-strengthened joints by 11.0%
1014 on average.

1015 **5.4. Discussion**

1016 The advantages of the EBROG method in the external strengthening of beam-column joints
1017 could postpone or eliminate FRP composite debonding. Although the EBROG method can
1018 engender a strong bond between the concrete substrate and FRP composites and prevent
1019 debonding, cover separation may occur due to high stress and the presence of the rebar layer.
1020 Consequently, the load capacity increases while ductility has no significant change.
1021 Researchers can prevent cover separation and interfacial debonding to a large extent by
1022 employing the combination of the EBROG method and the FRP fan and FRP wrap anchorage
1023 systems. Hence, the plastic hinge formation is transferred from the columns, joint panels, and
1024 column face into the beam, and converts into a desirable flexural failure mode. Accordingly,
1025 ductility and energy absorption increase significantly. Increasing the FRP length and number
1026 of FRP layers along the beam requires more anchorage systems from FRP fans and FRP

wraps since the test results demonstrate that increasing the FRP length and FRP layers without increasing the anchorage systems can lower ductility and energy absorption of the joints. Thus, the plastic hinge joint is not formed in the desired position.

The combination of the EBROG method, adequate anchorage systems, and the X-shaped pattern results in a low FRP consumption, a higher increase in the load capacity, an improvement in ductility and energy absorption compared to the reference joints. This behavior can be attributed to the favorable performance to control and reduce the diagonal cracks in the joint core. External strengthening of beam-column joints utilizing the EBROG method accompanied by FRP fans or FRP wraps anchorage systems can improve the seismic behavior of joints and alter undesirable and brittle failure modes to desirable and ductile failure modes.

6. Conclusion

This paper reviewed the studies on strengthening structural members via novel grooving methods. The results of shear and flexural strengthening of beams by grooving methods were presented, and its effective parameters, load-displacement behavior, and failure modes were examined. In addition, the studies in strengthening columns by grooving methods subjected to bending moments and axial loads were reviewed. The seismic strengthening of joints using the EBROG method was discussed, and ductility parameters were evaluated.

1. The grooving methods in the flexural strengthening of beams made 20.8% of the beams undergo FRP rupture, 31.2% failed with concrete cover separation mode. Strengthening beam-column joints by EBROG methods to prevent interface debonding and utilizing FRP fans and FRP wraps to hinder concrete cover separation changed the plastic hinge formation in the column, panel zone, and shear failure mode in the joint core into the plastic hinge formation in the beam far from the beam-column intersection.

2. Flexural strengthening of beams by EBROG and EBRIG methods increased the load capacity and energy absorption compared to the EBR method. When the stiffness of FRP sheets was low, there was no remarkable difference between the EBROG and EBRIG methods. However, increasing the CFRP composite stiffness heightened the load capacity and energy absorption of the EBRIG method compared to the EBROG technique. The growth in the concrete compressive strength reduced the ratio of the EBROG to EBR load capacity. Increasing the groove breadth to FRP composite width ratio led to increases in the load capacity. The groove depth to FRP composite width ratio had an optimum value, which was equal to 1.00.
3. Shear strengthening of beams by EBROG and EBRIG methods considerably improved the load-displacement behavior in comparison to the EBR method. Reduction in the distance between FRP sheets improved the load capacity of the beams although the amount of FRP materials, which were expensive to some extent, increased. Regarding the increase in the load capacity, performance, and material consumption, the most suitable pattern for shear strengthening of the beam was strengthening by grooving methods on two sides with a diagonal arrangement (45°).
4. The grooving methods could provide sufficient support for longitudinal FRP sheets and postpone the buckling and debonding of FRP composites. Therefore, the performance, compressive strength, and ductility of the columns were enhanced. Additionally, the novel method of EBRIOG enabled FRP composite to experience compressive stress equal to 64.0% of its ultimate tensile strength.
5. Strengthening beam-column joints with FRP composites by EBROG method and appropriate techniques for the anchorage systems including FRP fans and FRP wraps enhanced load capacity, ductility, and energy absorption. The EBROG method could postpone or eliminate the interface debonding phenomenon to a great extent, and the

anchorage system hampered concrete cover separation. Consequently, the ductility indexes grew significantly. Increasing the length and layers of FRP materials requires the provision of sufficient and secure anchorage systems; otherwise, the ductility increases. The x-shaped pattern compared to the L-shaped and longitudinal pattern enabled the EBROG method to acquire higher performance.

References

[1] American Concrete Institute (ACI). ACI 440.2R-08, Guide for the design and construction of externally bonded FRP systems for strengthening concrete structures. Farmington Hills, MI; 2008.

[2] Nanni A, James G. FRP Composites for Reinforced and Prestressed Concrete Structures: a guide to fundamentals and design for repair and retrofit. Taylor & Francies, 2009.

[3] Ko H, Matthys S, Palmieri A, Sato Y. Development of a simplified bond stress–slip model for bonded FRP–concrete interfaces. Constr Build Mater 2014;68:142-57.

[4] Bilotta A, Ceroni F, Nigro E, Pecce M. Strain assessment for the design of NSM FRP systems for the strengthening of RC members. Constr Build Mater 2014;69:143-58.

[5] Bilotta a, Ceroni F, Di Ludovico M, Nigro E, Pecce M, Manfredi G. Bond Efficiency of EBR and NSM FRP Systems for Strengthening Concrete Members. J Compos Constr 2011;15(5):757–77.

[6] International Federation for Structural Concrete. Fib Bulletin No. 14, Externally bonded FRP reinforcement for RC structures. Lausanne, Switzerland. 2001.

[7] Standards Australia. HB 305-2008, Design handbook for RC structures retrofitted with FRP and metal plates: beams and slabs. Sydney, NSW, Australia. 2008.

[8] National Research Council CNR-DT 200 R1. Guide for the design and construction of externally bonded FRP systems for strengthening existing structures. Rome, Italy. 2013.

[9] Biscaia HC, Chastre C, Silva MAG. Nonlinear numerical analysis of the debonding failure process of FRP-to-concrete interfaces. Compos Part B Eng 2013;50:210–23.

[10] Pan J, Leung CK, Luo M. Effect of multiple secondary cracks on FRP debonding from the substrate of reinforced concrete beams. Constr Build Mater 2010;24(12):2507-16.

[11] Chen JF, Pan WK. Three dimensional stress distribution in FRP-to-concrete bond test specimens. Constr Build Mater 2006;20(1-2):46-58.

[12] Aram MR, Czaderski C, Motavalli M. Debonding failure modes of flexural FRP strengthened RC beams. Compos Part B Eng 2008;39(5):826–41.

[13] Chajes M. J, Januszka T. F, Merta D. R, Thomson T. A, Finch W. W. Shear strengthening of reinforced concrete beams using externally applied composite fabrics. ACI Struct J 1995;92(3):295-303.

[14] Chajes M. J, Finch W. W, Januszka T. F, Merta D. R, Thomson T. A. Bondand force transfer of composite material plates bonded to concrete. ACI Struct J 1996;93(2):209-217.

[15] Taljsten B. Strengthening of concrete prisms using the plate-bonding technique. Int J Fract 1996;82(4):253-266.

[16] Xiao J, Li J, Zha Q. Experimental study on bond behavior between FRP and concrete. Constr Build Mater 2004;18(10):745-52.

[17] Guo YC, Li LJ, Chen GM, Huang PY. Influence of hollow imperfections in adhesive on the interfacial bond behaviors of FRP-plated RC beams. Constr Build Mater 2012;30:597-606.

[18] Ferrier E, Quiertant M, Benzarti K, Hamelin P. Influence of the properties of externally bonded CFRP on the shear behavior of concrete/composite adhesive joints. Compos Part B 2010;41(5):354-362.

[19] Maeda T, Asano Y, Sato Y, Ueda T, Kakuta Y. A. study on bond mechanism of carbon fiber sheet. Proc, 3th Int, Symp, On Non-Metallic (FRP) Reinforcement for concrete structures. Japan Concrete Institute, Sapporo,1997. p. 279-285.

[20] Miller B, Nanni N. Bond between CFRP sheets and concrete. Proceedings, ASCE 5th Materials Congress, Cincinnati, 1999. pp. 240-247.

[21] Sharma S. K, Ali M. S. M, Goldar D, Sikdar P. K. Plate-concrete interfacial bond strength of FRP and metallic plated concrete specimens. Compos Part B Eng 2006;37(1):54–63.

[22] Chen J, Teng J. Anchorage strength models for FRP and steel plates bonded to concrete. J Struct Eng 2001;127(7):784–791.

[23] Bizindavyi L, Neale K. Transfer lengths and bond strengths for composites bonded to concrete. J Compos Constr 1999;4(153):153-160.

[24] Jimenez-Vicaria JD, Pulido MD, Castro-Fresno D. Influence of carbon fibre stiffness and adhesive ductility on CFRP-steel adhesive joints with short bond lengths. Constr Build Mater 2020;260:119758.

[25] Bilotta A, Di Ludovico M, Nigro E. FRP-to-concrete interface debonding: Experimental calibration of a capacity model. Compos Part B Eng 2011;42(6):1539-1553.

[26] Diab H. M, Farghal O. A. Bond strength and effective bond length of FRP sheets/plates bonded to concrete considering the type of adhesive layer. Compos Part B Eng 2014;58: 618–624.

[27] Seracino R, Raizal Saifulnaz M. R, Oehlers D. J. Generic debonding resistance of EB and NSM plate-to-concrete joints. J Compos Constr 2007;1(62):62–70.

[28] Taljsten B. Defining anchor lengths of steel and CFRP plates bonded to concrete. Int J Adhes Adhes 1997;17(4):319-327.

[29] Wu Y, Zhou Z, Yang Q, Chen W. On shear bond strength of FRP-concrete Structures. Eng Struct 2010;32(3):897-905.

[30] Ghorbani M, Mostofinejad D, Hosseini A. Eperimental investigation into bond behavior of FRP-to-concrete under mixed-mode I/II loading. Constr Build Mater 2017;132:303-312.

[31] Ghorbani M, Mostofinejad D, Hosseini A. Bond behavior of CFRP sheets attached to concrete through EBR and EBROG joints subject to mixed-mode I/II loading. J Compos Constr 2017;21(5):04017034.

[32] Smith ST, Teng JG. FRP-strengthened RC beams. I: review of debonding strength models. Eng Struct 2002;24:385–395.

[33] Yuan H, Teng JG, Seracino R, Wu ZS, Yao J. Full-range behavior of FRP-to-concrete bonded joints. Eng Struct 2004;26:553–565.

[34] Zhang P, Lei D, Ren Q, He J, Shen H, Yang Z. Experimental and numerical investigation of debonding process of the FRP plate-concrete interface. Constr Build Mater 2020;235:117457.

[35] Achintha M, Burgoyne C. Fracture energy of the concrete–FRP interface in strengthened beams. Eng Fract Mech 2013;110:38–51.

[36] Su M, Zhong Q, Peng H, Li S. Selected machine learning approaches for predicting the interfacial bond strength between FRPs and concrete. Constr Build Mater 2020;270:121456.

[37] Mohammadi M, Mostofinejad D, Rafieyan A. CFRP-to-concrete bond behavior under aggressive exposure of sewer chamber. J Compos Mater 2021; DOI: 10.1177/00219983211004699.

[38] Mazzotti C, Savoia M, Ferracuti B. A new single-shear set-up for stable debonding of FRP–concrete joints. Constr Build Mater 2009;23(4):1529–137.

[39] Sanginabadi K, Mostofinejad D. Effect of aggregate content on the CFRP-concrete effective bond length: An experimental and analytical study. Compos Struct 2021;269:114044.

[40] Ali-Ahmad M, Subramaniam K, Ghosn M. Experimental investigation and fracture analysis of debonding between concrete and FRP sheets. J Eng Mech 2006;9(914):914–923.

[41] Mostofinejad D, Sanginabadi K, Eftekhar M.R. Effects of coarse aggregate volume on CFRP-concrete bond strength and behavior. Constr Build Mater 2019;198:42-57.

[42] Salimian M.S, Mostofinejad D. Experimental evaluation of CFRP-concrete bond behavior under high loading rates using particle image velocimetry method. J Compos Constr 2019;23(3):04019010.

[43] Yazdani, A., Sanginabadi, K., Shahidzadeh, M.S., Salimi, M.R. and Shamohammadi, A., 2021. Consideration of data correlation to estimate FRP-to-concrete bond capacity models. Construction and Building Materials, 308, p.125106.

[44] Mostofinejad D, Mahmoudabadi E. Grooving as alternative method of surface preparation to postpone debonding of FRP laminates in concrete beams. J Compos Constr 2010; 14(6):804-811.

[45] Mostofinejad D, Shameli S. M. Externally bonded reinforcement in grooves (EBRIG) technique to postpone debonding of FRP sheets in strengthened concrete beams. Constr Build Mater 2013;38:751-758.

[46] Hosseini A, Mostofinejad D. Experimental investigation into bond behavior of CFRP sheets attached to concrete using EBR and EBROG techniques. Compos Part B Eng 2013;51:130–139.

[47] Hosseini A, Mostofinejad D. Effect of groove characteristics on CFRP-to-concrete bond behavior of EBROG joints: Experimental study using particle image velocimetry (PIV). Constr Build Mater 2013;49:364–373.

[48] Hosseini A, Mostofinejad D, Emami M. Influence of bonding technique on bond behavior of CFRP-to-clay brick masonry joints: Experimental study using particle image velocimetry (PIV). Int J Adhes Adhes 2015;59:27-39.

[49] Mohammadi M, Mostofinejad D, Barghian M. Effects of surface preparation method on FRP-concrete bond strength under alkaline conditions. J Compos Constr 2017;21(4): 04017010.

[50] Mohammadi M, Barghian M, Mostofinejad D, Rafieyan A. Alkali and temperature long-term effect on the bond strength of fiber-reinforced polymer-to-concrete interface. J Compos Mater 2018;52(15):2103-2114.

[51] Mostofinejad D, Mofrad M.H, Hosseini A, Mofrad H.H. Investigating the effects of concrete compressive strength, CFRP thickness and groove depth on CFRP-concrete bond strength of EBROG joints. Constr Build Mater 2018;189:323-337.

[52] Jiang C, Wan B, Wu YF, Omboko J. Epoxy interlocking: A novel approach to enhance FRP-to-concrete bond behavior. Constr Build Mater 2018;193:643-53.

[53] Moshiri N, Tajmir-Riahi A, Mostofinejad D, Czaderski C, Motavalli M. Experimental and analytical study on CFRP strips-to-concrete bonded joints using EBROG method. Compos Part B Eng 2019;158:437-447.

[54] Tajmir-Riahi A, Moshiri N, Mostofinejad D. Bond mechanism of EBROG method using a single groove to attach CFRP sheets on concrete. Constr Build Mater 2019;197:693-704.

[55] Moghaddas A, Mostofinejad D. Empirical FRP-concrete bond strength model for externally bonded reinforcement on grooves. J Compos Constr 2019;23(2):04018080.

[56] Mofrad M.H, Mostofinejad D, Hosseini A. A generic non-linear bond-slip model for CFRP composites bonded to concrete substrate using EBR and EBROG techniques. Compos Struct 2019;220:31-44.

[57] Moghaddas A, Mostofinejad D, Ilia E. Empirical FRP-concrete effective bond length model for externally bonded reinforcement on the grooves. Compos Part B Eng 2019;172:323-338.

[58] Tajmir-Riahi A, Moshiri N, Czaderski C, Mostofinejad D. Effect of the EBROG method on strip-to-concrete bond behavior. Constr Build Mater 2019;220:701-711.

[59] Mostofinejad D, Mohammadi M. Effect of Freeze-Thaw Cycles on FRP-Concrete Bond Strength in EBR and EBROG Systems. J Compos Constr 2020;24(3): 04020009.

[60] Al-Rousan R, AL-Tahat M. An Anchoring Groove Technique to Enhance the Bond Behavior between Heat-Damaged Concrete and CFRP Composites. Buildings 2020;10(12):232.

[61] Moshiri N, Czaderski C, Mostofinejad D, Motavalli M. Bond resistance of prestressed CFRP strips attached to concrete by using EBR and EBROG strengthening methods. Constr Build Mater 2021;266:121209.

[62] Mohammadi Ghahsareh F, Mostofinejad D. Groove classification in EBROG FRP-to-concrete joints. Constr Build Mater 2021;275:122169.

[63] Moghaddas A, Mostofinejad D, Saljoughian A, Ilia E. An empirical FRP-concrete bond-slip model for externally-bonded reinforcement on grooves. Constr Build Mater 2021;281:122575.

[64] Arefian B, Mostofinejad D. Experimental Investigation and Modeling of FRP–Concrete Joint Bond Strength Based on Failure Depth. J Compos Constr 2021;25(6):04021050.

[65] Mostofinejad D, Arefian B. Generic assessment of effective bond length of FRP-concrete joint based on the initiation of debonding: Experimental and analytical investigation. Compos Struct 2021;277:114625.

[66] Moshiri N, Czaderski C, Mostofinejad D, Hosseini A, Motavalli M. Effect of Groove Depth on Behavior of Prestressed CFRP Strips Bonded to Concrete by Using EBROG Method. InInternational Conference on Fibre-Reinforced Polymer (FRP) Composites in Civil Engineering 2021 (pp. 2188-2196). Springer, Cham.

[67] Mostofinejad D, Shameli M. Performance of EBROG method under multilayer FRP sheets for flexural strengthening of concrete beams. Procedia Engineering 2011;14:3176-3182.

[68] Mostofinejad D, Hajrasouliha MJ. Effect of concrete strength and groove dimensions on performance of grooving method to postpone debonding of FRP sheets in strengthened concrete beams. IJST, Trans Civ Eng 2013;37(C2):219–232.

[69] Mostofinejad D, Shameli M, Hosseini A. EBROG and EBRIG methods for strengthening of RC beams by FRP sheets. Eur J Environ Civil Eng 2014;18:652–668.

[70] Mostofinejad D, Moghaddas A. Bond efficiency of EBR and EBROG methods in different flexural failure mechanisms of FRP strengthened RC beams. Constr Build Mater 2014;54:605–614.

[71] Mostofinejad D, Khozaei K. Effect of GM patterns on ductility and debonding control of FRP sheets in RC strengthened beams. Constr Build Mater 2015;93:110–120.

[72] Tehrani BN, Mostofinejad D, Hosseini SM. Experimental and analytical study on flexural strengthening of RC beams via prestressed EBROG CFRP plates. Eng Struct 2019;197:109395.

[73] Azizi R, Talaeitaba SB. Punching shear strengthening of flat slabs with CFRP on grooves (EBROG) and external rebars sticking in grooves. I J Ad Struct Eng 2019;11(1):79-95.

[74] Mashrei M, Makki J, Sultan AA. Flexural strengthening of reinforced concrete beams using carbon fiber reinforced polymer (CFRP) sheets with grooves. Latin American Journal of Solids and Structures. 2019;16.

[75] Shen D, Zeng X, Zhang J, Zhou B, Wang AW. Behavior of RC box beam strengthened with basalt FRP using end anchorage with grooving. Journal of Composite Materials. 2019;53(23):3307-24.

[76] Sabzi J, Esfahani MR, Ozbakkaloglu T, Farahi B. Effect of concrete strength and longitudinal reinforcement arrangement on the performance of reinforced concrete beams strengthened using EBR and EBROG methods. Eng Struct 2020;205:110072.

[77] Torabian A, Isufi B, Mostofinejad D, Ramos AP. Flexural strengthening of flat slabs with FRP composites using EBR and EBROG methods. Eng Struct 2020;211:110483.

[78] Torabian A, Isufi B, Mostofinejad D, Pinho Ramos A. Shear and flexural strengthening of deficient flat slabs with post-installed bolts and CFRP composites bonded through EBR and EBROG. Struct Concr 2020;1-18.

[79] Moshiri N, Czaderski C, Mostofinejad D, Hosseini A, Sanginabadi K, Breveglieri M, Motavalli M. Flexural strengthening of RC slabs with non-prestressed and prestressed CFRP strips using EBROG method. Compos Part B Eng 2020;201:108359.

[80] Abed RJ, Mashrei MA, Sultan AA. Flexural behavior of reinforced concrete beams strengthened by carbon fiber reinforced polymer using different strengthening techniques. Advances in Structural Engineering. 2022;25(2):355-73.

[81] Mostofinejad D, Tabatabaei Kashani A. Elimination of Debonging of FRP Strips in Shear Strengthened beams Using Grooving Method. In Advanced Materials Research; Trans Tech Publications Ltd. 2011;250:1077-1081.

[82] Mostofinejad D, Tabatabaei Kashani A. Experimental study on effect of EBR and EBROG methods on debonding of FRP sheets used for shear strengthening of RC beams. Composites Part B 2012;45(1):1704–13.

[83] Mostofinejad D, Mostafavizadeh SA, Kashani A.T. Grooving method to postpone debonding of FRP sheets used for shear strengthening. In Proceedings of World Academy of Science, Engineering and Technology (WASET) 2012;72:795-799.

[84] Mostofinejad D, Hosseini SA, Razavi SB. Influence of different bonding and wrapping techniques on performance of beams strengthened in shear using CFRP reinforcement. Constr Build Mater 2016;116:310-320.

[85] Shomali A, Mostofinejad D, Esfahani MR. Shear strengthening of RC beams using EBRIG CFRP strips: a comparative study. Eur J Environ Civil Eng 2019:1-17.

[86] Shomali A, Mostofinejad D, Esfahani MR. Experimental study on effect of EBRIG shear strengthening method on the behavior of RC beams. Ad Concr Constr 2019;8(2):145-54.

[87] Arabzadeh A, Karimizadeh H. Experimental study of RC deep beams with opening and FRP composites installed by means of EBR and EBROG methods. Constr Build Mater 2019;208:780-91.

[88] Shomali A, Mostofinejad D, Esfahani MR. Experimental and numerical investigation of shear performance of RC beams strengthened with FRP using grooving method. J Build Eng 2020;31:101409.

[89] Moshiri N, Hosseini A, Mostofinejad D. Strengthening of RC columns by longitudinal CFRP sheets: Effect of strengthening technique. Constr Build Mater 2015;79:318-325.

[90] Moshiri N, Mostofinejad D. Compression capacity of RC columns strengthened with longitudinal CFRP composite. As J Civil Eng 2015;16(5):706-620.

[91] Mostofinejad D, Torabian A. Experimental study of circular RC columns strengthened with longitudinal CFRP composites under eccentric loading: comparative evaluation of EBR and EBROG methods. J Compos Constr 2015;20(2):04015055.

[92] Torabian A, Mostofinejad D. Externally Bonded Reinforcement on Grooves Technique in Circular Reinforced Columns Strengthened with Longitudinal Carbon Fiber-Reinforced Polymer under Eccentric Loading. ACI Struct J 2017;114(4):861-873.

[93] Mostofinejad D, Moshiri N. Compressive strength of CFRP composites used for strengthening of RC columns: Comparative evaluation of EBR and grooving methods. J Compos Constr 2015;19(5):04014079.

[94] Saljoughian A, Mostofinejad D. Corner strip-batten technique for FRP-confinement of square RC columns under eccentric loading. J Compos Constr 2016;20(3):04015077.

[95] Saljoughian A, Mostofinejad D. Rectangular Reinforced Concrete Columns Strengthened with Carbon Fiber-Reinforced Polymer Sheets Using Corner Strip-Batten Method. ACI Struct J 2017;114(3):659-671.

[96] Saljoughian A, Mostofinejad D. Grooving methods in square RC columns strengthened with longitudinal CFRP under cyclic axial compression. Eng Struct 2018;174:724-735.

[97] Saljoughian A, Mostofinejad D. RC columns longitudinally strengthened via novel EBRIOG

technique. Struct Concr 2019:1-17.

[98] NoroozOlyaee M, Mostofinejad D. Slenderness Effects in Circular RC Columns Strengthened with CFRP Sheets Using Different External Bonding Techniques. J Compos Constr 2019;23(1):04018068

[99] Saljoughian A, Mostofinejad D. Using grooving and corner strip-batten techniques for seismic strengthening of square reinforced concrete columns with fiber-reinforced polymer composites. Struct Concr 2020;21(5):2066-82.

[100] Saljoughian A, Mostofinejad D. Behavior of RC columns confined with CFRP using CSB method under cyclic axial compression. Constr Build Mater 2020;235:117786.

[101] Noroozolyaee M, Mostofinejad D. Slender Columns Reinforced by High-Strength Steel Reinforcing Bars and Retrofitted by Fiber-Reinforced Polymer Sheets. ACI Struct J 2020;117(5):53-66.

[102] Mostofinejad D, Salimian MS, Taherirani M, Noroozolyaee M. Behavior of Square Slender RC Columns Strengthened with Longitudinal FRP Sheets Subjected to Eccentric Loading. J Compos Constr 2021;25(2):04021006.

[103] Hosseini SM, Mostofinejad D. Seismic Performance of RC Short Columns Retrofitted with a Novel System in Shear and Flexure Using CFRP Composites. Journal of Composites for Construction. 2021;25(5):04021039.

[104] Saljoughian A, Mostofinejad D, Raji A. Retrofit of concrete columns with fibre strips using grooves and corner battens. Proceedings of the Institution of Civil Engineers-Structures and Buildings. 2021:1-5.

[105] Razavi M, Mostofinejad D, Eftekhar M. Behavior of RC columns and those strengthened with FRP composite under an innovative reversing cyclic eccentric axial loading. Engineering Structures. 2021;241:112438.

[106] Mostofinejad D, Akhlaghi A. Experimental investigation of the efficacy of EBROG method in seismic rehabilitation of deficient reinforced concrete beam-column joints using CFRP sheets. J Compos Constr 2016;21(4):04016116.

[107] Mostofinejad D, Akhlaghi A. Flexural strengthening of reinforced concrete beam-column joints using an innovative anchorage system. ACI Struct J 2017;114(06):1603–1614.

[108] Mostofinejad D, Hajrasouliha M.J. Shear retrofitting of corner 3D-reinforced concrete beam-column joints using externally bonded CFRP reinforcement on grooves. J Compos Constr 2018;22(5):04018037.

[109] Mostofinejad D, Hajrasouliha M.J. 3D beam-column corner joints retrofitted with X-shaped FRP sheets attached via the EBROG technique. Eng Struct 2019;183:987–998.

[110] Ilia E, Mostofinejad D. Seismic retrofit of reinforced concrete strong beam–weak column joints using EBROG method combined with CFRP anchorage system. Eng Struct 2019;194:300–319.

[111] Ilia E, Mostofinejad D, Moghaddas A. Cyclic behavior of strong beam–weak column joints strengthened with different configurations of CFRP sheets. Arch Civil Mech Eng 2020;20(2):1-26.

[112] Akhlaghi A, Mostofinejad D. Experimental and analytical assessment of different anchorage

systems used for CFRP flexurally retrofitted exterior RC beam-column connections. Structures 2020;28:881-893.

[113] Biolzi L, Ghittoni C, Fedele R, Rosati G. Experimental and theoretical issues in FRP-concrete bonding. Constr Build Mater 2013;41:182-190.

[114] Shen D, Shi H, Ji Y, Yin F. Strain rate effect on effective bond length of basalt FRP sheet bonded to concrete. Constr Build Mater 2015;82:206-218.

[115] Fazli H, Yassin AM, Shafiq N, Teo W. Effective bond length of CFRP sheets externally bonded to concrete beams under marine environment. Constr Build Mater 2018;167:726-738.

[116] Aram M.R, Czaderski C, Motavalli M. Debonding failure modes of flexural FRP-strengthened RC beams. Compos Part B Eng 2008;39(5):826-841.

[117] Razaqpur AG, Lamberti M, Ascione F. A nonlinear semi-analytical model for predicting debonding of frp laminates from rc beams subjected to uniform or concentrated load. Constr Build Mater 2020;233:117838.

[118] Hosen MA, Jumaat MZ, Alengaram UJ, Sulong NR. CFRP strips for enhancing flexural performance of RC beams by SNSM strengthening technique. Constr Build Mater 2018;165:28-44.

[119] Obaidat YT, Barham WS, Aljarah AH. New anchorage technique for NSM-CFRP flexural strengthened RC beam using steel clamped end plate. Constr Build Mater 2020;263:120246.

[120] Zeng Y, Botte W, Caspeele R. Reliability analysis of FRP strengthened RC beams considering compressive membrane action. Constr Build Mater 2018;169:473-88.

[121] Mahal M, Täljsten B, Blanksvärd T. Experimental performance of RC beams strengthened with FRP materials under monotonic and fatigue loads. Constr Build Mater 2016;122:126-39.

[122] Shen D, Deng S, Zhang J, Wang W, Jiang G. Behavior of reinforced concrete box beam with initial cracks repaired with basalt fiber-reinforced polymer sheet. Journal of Reinforced Plastics and Composites. 2015;34(18):1540-54.

[123] Shen D, Jiao Y, Li M, Liu C, Wang W. Behavior of a 60-year-old Reinforced Concrete Box Beam Strengthened with Basalt Fiber-reinforced Polymers Using Steel Plate Anchorage. Journal of Advanced Concrete Technology. 2021;19(11):1100-19.

[124] Norris T, Saadatmanesh H, Ehsani M.R. Shear and flexural strengthening of R/C beams with carbon fiber sheets. J Struct Eng 1997;123(7):903-911.

[145] De Lorenzis L, Nanni A. Shear strengthening of reinforced concrete beams with near-surface mounted fiber-reinforced polymer rods. Struct J 2001;98(1):60-68.

[126] Ascione L, Berardi V.P, Feo L, Mancusi G. A numerical evaluation of the interlaminar stress state in externally FRP plated RC beams. Compos Part B Eng 2005;36(1):83-90.

[127] Aprile A, Feo L. Concrete cover rip-off of R/C beams strengthened with FRP composites. Compos Part B Eng 2007;38(5-6):759-771.

[128] De Lorenzis L, Teng JG. Near-surface mounted FRP reinforcement: An emerging technique for strengthening structures. Compos Part B Eng 2007;38(2):119-143.

[129] Kim G, Sim J, Oh H. Shear strength of strengthened RC beams with FRPs in shear. Constr Build Mater 2008;22(6):1261-1270.

[130] Rizzo A, De Lorenzis L. Behavior and capacity of RC beams strengthened in shear with NSM FRP reinforcement. Constr Build Mater 2009;23(4):1555-1567.

[131] Shen D, Yang Q, Jiao Y, Cui Z, Zhang J. Experimental investigations on reinforced concrete shear walls strengthened with basalt fiber-reinforced polymers under cyclic load. Constr Build Mater 2017;136:217-29.

[132] Parvin A, Wang W. Behavior of FRP jacketed concrete columns under eccentric loading. J Compos Constr 2001;5(3):146-152.

[133] Theriault M, Neale KW, Claude S. Fiber-reinforced polymer confined circular concrete columns: investigation of size and slenderness effects. J Compos Constr 2004;8(4):323-331.

[134] Campione G. Influence of FRP wrapping techniques on the compressive behavior of concrete prisms. Cem Concr Compos 2006;28(5):497-505.

[135] Siddiqui NA, Alsayed SH, Al-Salloum YA, Iqbal RA, Abbas H. Experimental investigation of slender circular RC columns strengthened with FRP composites. Constr Build Mater 2014;69:323-34.

[136] Eshaghi-Milasi S, Mostofinejad D, Saljoughian A, Bahmani H. Behavior of RC columns strengthened with UHPFRC jackets through grooving method under eccentric loading: A comparative evaluation of steel and synthetic macro fibers in UHPFRC. Structural Concrete.

[137] Youssef MN, Feng MQ, Mosallam AS. Stress-strain model for concrete confined by FRP composites. Compos Part B Eng 2007;38:614-628.

[138] Wu G, Wu ZS, Lu ZT. Design-oriented stress-strain model for concrete prisms confined with FRP composites. Constr Build Mater 2007;21:1107-1121.

[139] Park TW, Na UJ, Chung L, Feng MQ. Compressive behavior of concrete cylinder confined by narrow strips of CFRP with spacing. Compos Part B Eng 2008;39:1093-1103.

[140] Hadi MNS. Behavior of FRP wrapped normal strength concrete columns under eccentric loading. Compos Struct 2006;72(4):503-511.

[141] Quiertant M, Clement JL. Behavior of RC columns strengthened with different CFRP systems under eccentric loading. Constr Build Mater 2011;25(2):452-60.

[142] Dadvar SA, Mostofinejad D, Bahmani H. Strengthening of reinforced concrete columns with combined ultra-high-performance fiber-reinforced concrete and glass fiber-reinforced polymer jacketing. ACI Structural Journal. 2021 Sep 1;118(5):285-97.

[143] Realfonzo R, Napoli A, Pinilla JG. Cyclic behavior of RC beam-column joints strengthened with FRP systems. Constr Build Mater 2014;54:282-97.

[144] Mostofinejad D, Ilia E. Confining of square RC columns with FRP sheets using corner strip-batten technique. Constr Build Mater 2014;70:269-278.

[145] Saljoughian A, Mostofinejad D. Axial-flexural interaction in square RC columns confined by intermittent CFRP wraps. Compos Part B Eng 2016;89:85-95.

[146] Mosallam AS. Strength and ductility of reinforced concrete moment frame connections

strengthened with quasi-isotropic laminates. Compos Part B: Eng 2000;31:481–497.

[147] Ghobarah A, Said A. Seismic rehabilitation of beam-column joints using FRP laminates. J Earthquake Eng 2001;5(1):113–129.

[148] El-Amoury T, Ghobarah A. Seismic rehabilitation of beam-column joint using GFRP sheets. Eng Struct 2002;24(11):1397–407.

[149] Ghobarah A, Said A. Shear strengthening of beam-column joints. Eng Struct 2002;24(7):881–8.

[150] Said AM, Nehdi ML. Use of FRP for RC frames in seismic zones: part I. Evaluation of FRP beam-column joint rehabilitation techniques. Appl Compos Mater 2004;11:205–26.

[151] Chalioris CE, Favvata MJ, Karayannis CG. Reinforced concrete beam-column joints with crossed inclined bars under cyclic deformations. J Earthquake Eng Struct Dyn 2008;37(6):881–97.

[152] Realfonzo R, Napoli A, Pinilla JG. Cyclic behavior of RC beam-column joints strengthened with FRP systems. Constr Build Mater 2014;54:282-97.

[153] Shen D, Ojha B, Shi X, Zhang H, Shen J. Bond stress–slip relationship between basalt fiber-reinforced polymer bars and concrete using a pull-out test. Journal of Reinforced Plastics and Composites. 2016 May;35(9):747-63.

[154] Shen D, Ji Y, Yin F, Zhang J. Dynamic bond stress-slip relationship between basalt FRP sheet and concrete under initial static loading. Journal of Composites for Construction. 2015 Dec 1;19(6):04015012.

[155] Shen D, Yang Q, Huang C, Cui Z, Zhang J. Tests on seismic performance of corroded reinforced concrete shear walls repaired with basalt fiber-reinforced polymers. Construction and Building Materials. 2019 Jun 10;209:508-21.

[156] Shen D, Li M, Liu C, Kang J, Li C, Yang J. Seismic performance of corroded reinforced concrete beam-column joints repaired with BFRP sheets. Construction and Building Materials. 2021 Nov 8;307:124731.

[157] Shen D, Li M, Kang J, Liu C, Li C. Experimental studies on the seismic behavior of reinforced concrete beam-column joints strengthened with basalt fiber-reinforced polymer sheets. Constr Build Mater 2021;287:122901.

[158] Borujerdi AS, Mostofinejad D, Hwang HJ. Cyclic loading test for shear-deficient reinforced concrete exterior beam-column joints with high-strength bars. Eng Struct 2021;237:112140.

[159] ACI Committee 374.1. Acceptance criteria for moment frames based on structural testing and commentary. ACI 374.1-05, Farmington Hills, MI; 2005.

List of Figures

Fig. 20. Effect of various methods strengthening of RC column on compressive stress of FRP composite to ultimate tensile strength (R_{FC})

Fig. 21. Test setup and seismic loading protocol of RC beam-column joints

Fig. 22. Various patterns of external strengthening RC beam-column joints by grooving methods

Fig. 23. Load-displacement envelope curves for RC beam-column joints

Fig. 24. Increase in load capacity of strengthened joints compared to the control joints: (a) peak load, (b) Load in the 4.5% drift ratio

Fig. 25. Enhancement in ductility factor (in pulling) of strengthened joints compared to the control joints

Fig. 26. Energy dissipation of strengthened joints: (a) cumulative dissipated energy versus drift ratio, (b) increase of energy dissipation compared to the control joint in the 4.5% drift ratio

Fig. 27. Stiffness degradation of strengthened joints: (a) stiffness degradation versus drift ratio, (b) increment in stiffness compared to the control joint in the 4.5% drift ratio

Fig. 28. Equivalent damping ratio of strengthened joints: (a) equivalent hysteretic damping versus drift ratio, (b) increase in equivalent hysteretic damping ratio compared to the control joint in the 4.5% drift ratio

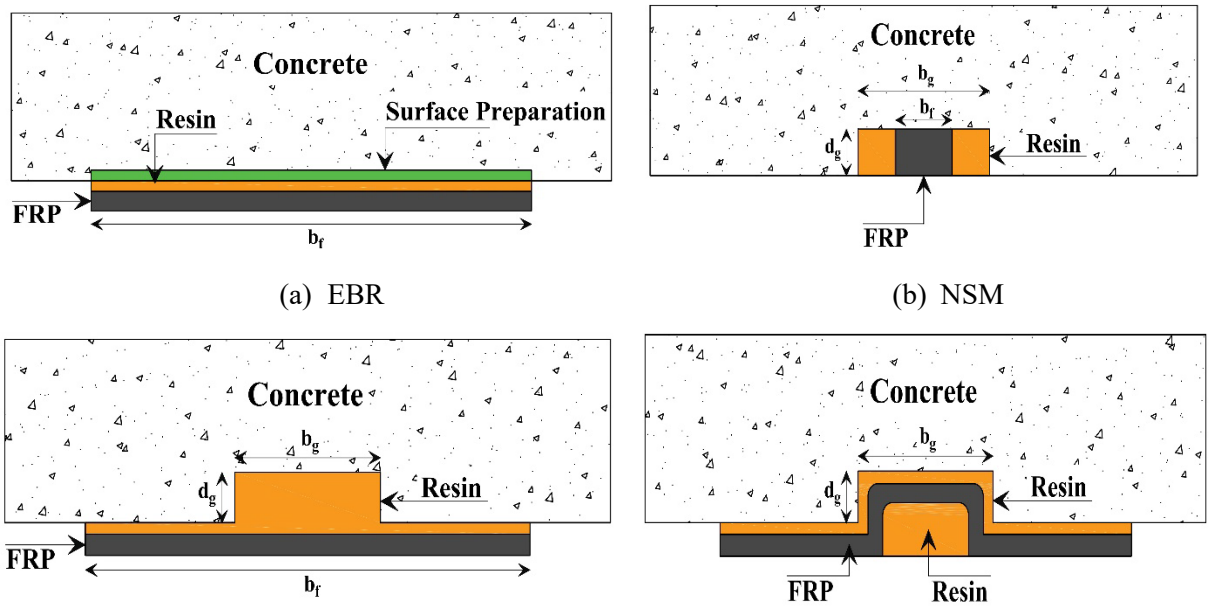

(a) EBR (b) NSM

(c) EBROG (d) EBRIG

Fig. 1. Methods for strengthening structural members

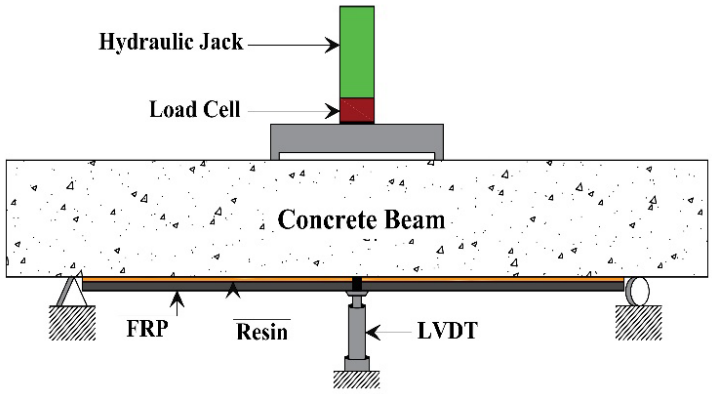

Fig. 2. Setup of the four-point bending test

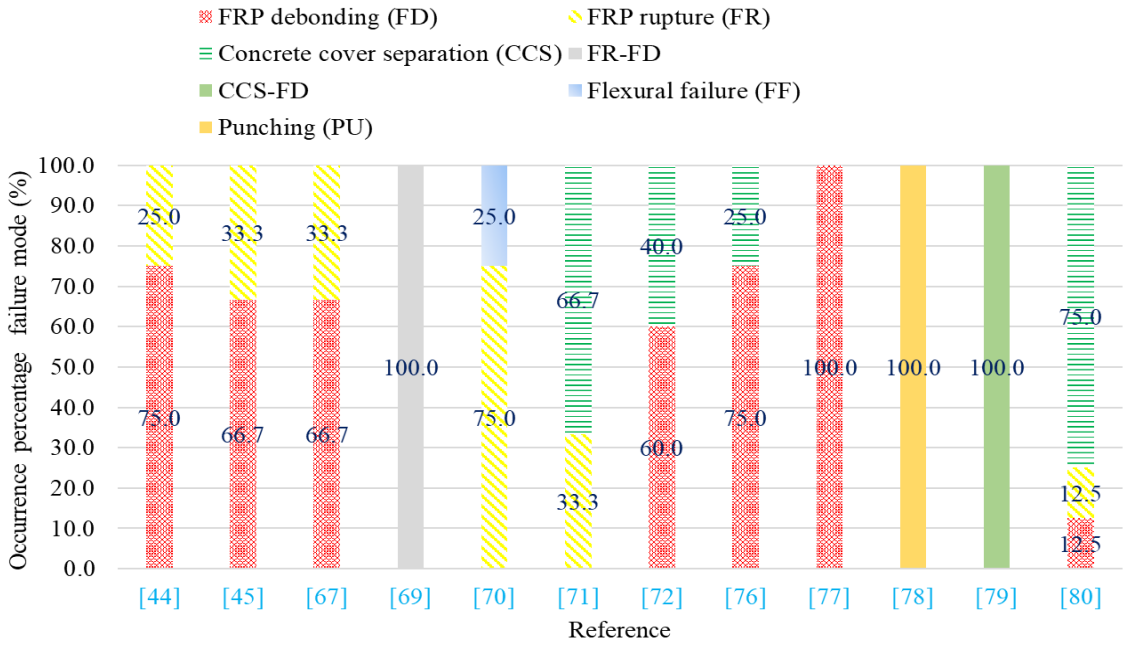

(a)

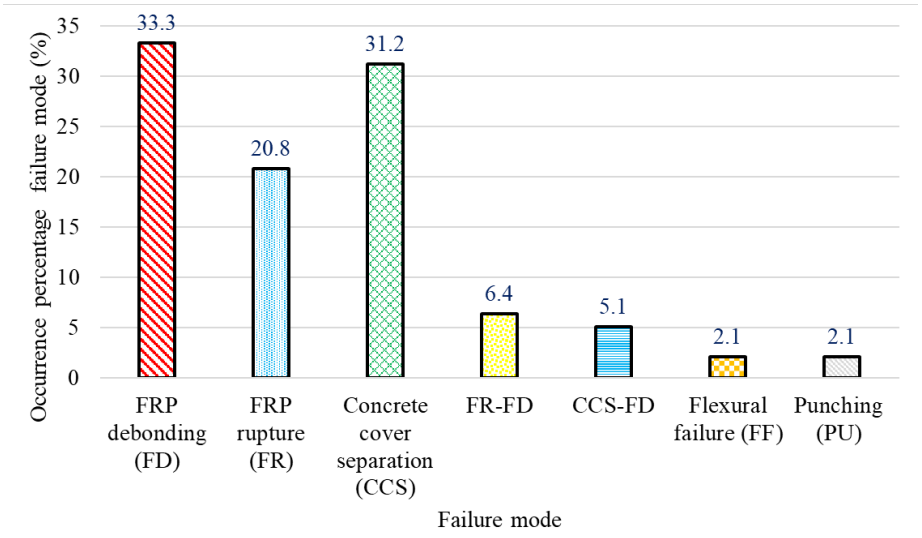

(b)

Fig. 3. Occurrence percentage of failure modes: (a) in each study, (b) in the total studies

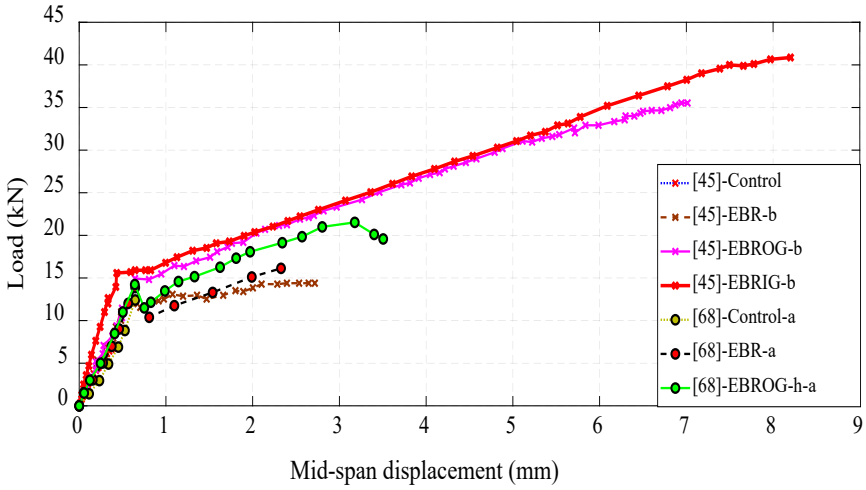

Fig. 4. Load-displacement curves for some flexural-strengthened beams

(a)

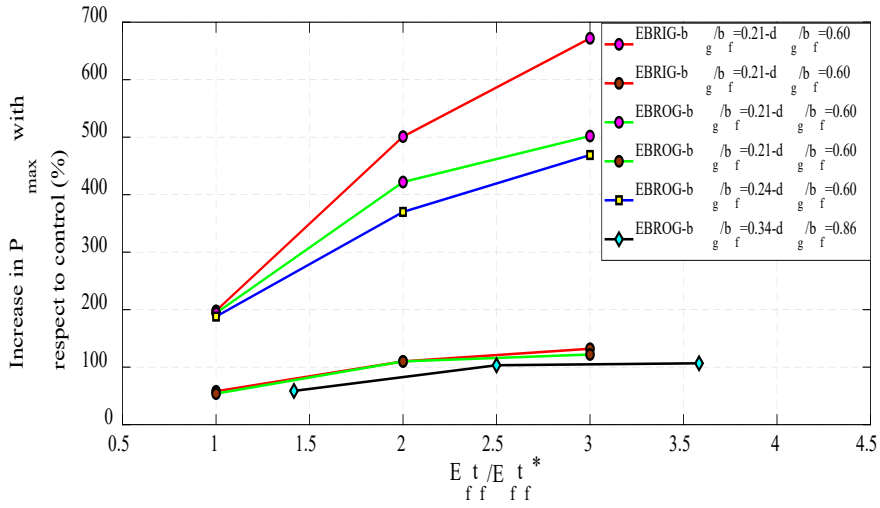

(b)

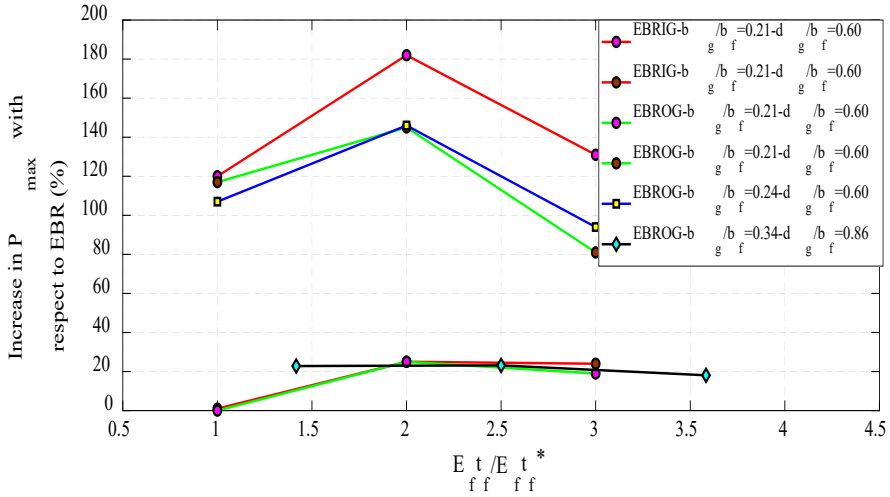

(c)

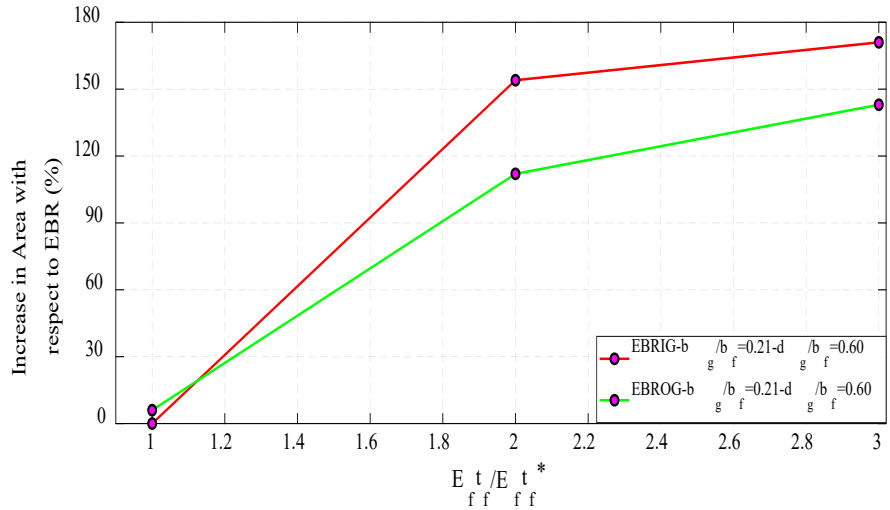

Fig. 5. Effect of FRP composite stiffness of flexural-strengthened beams on: (a) Load capacity increase compared to reference specimens, (b) load capacity increase compared to EBR specimens, (c) growth in the area under load-displacement curves of EBROG beams compared to EBR beams

(a)

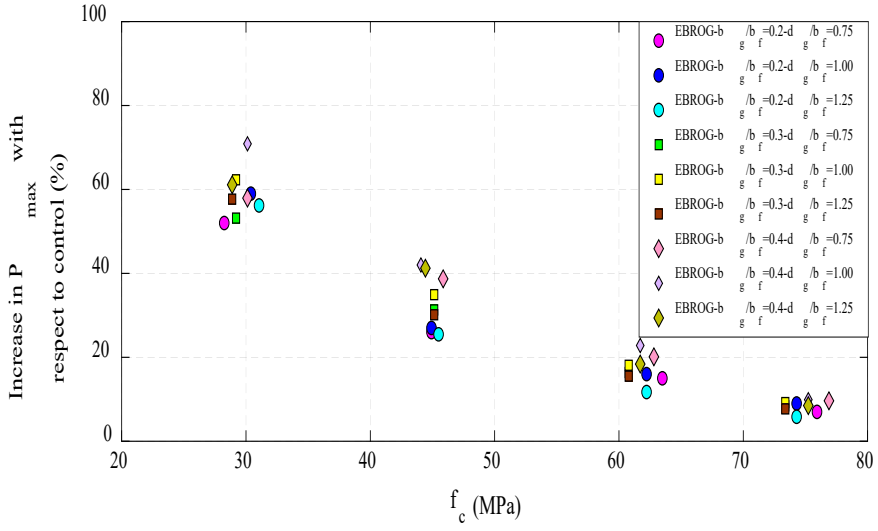

(b)

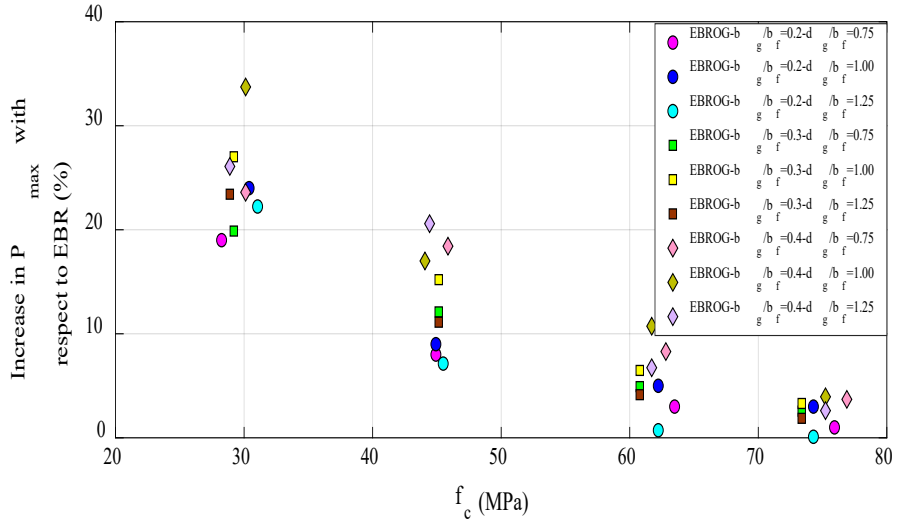

Fig. 6. Effect of concrete compressive strength on: (a) load capacity increase of EBROG beams compared to reference beams, (b) load capacity increase of EBROG beams compared to EBR beams

(a)

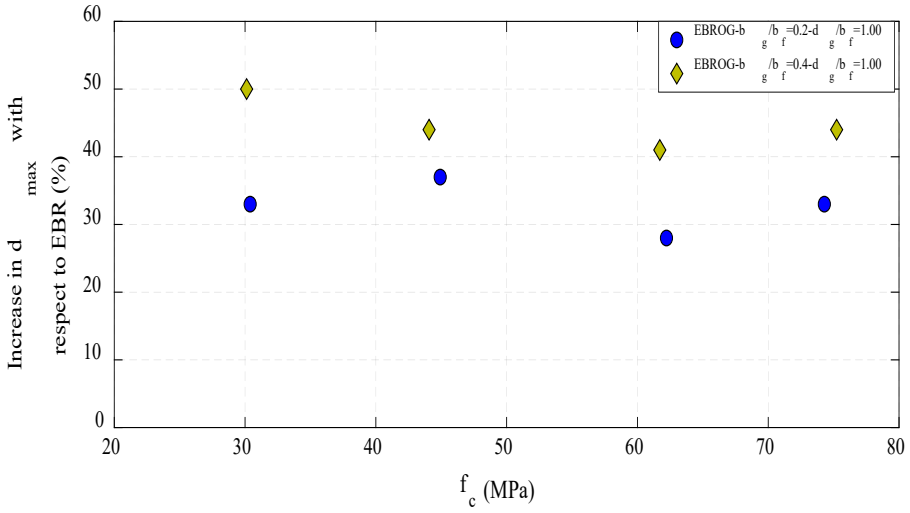

(b)

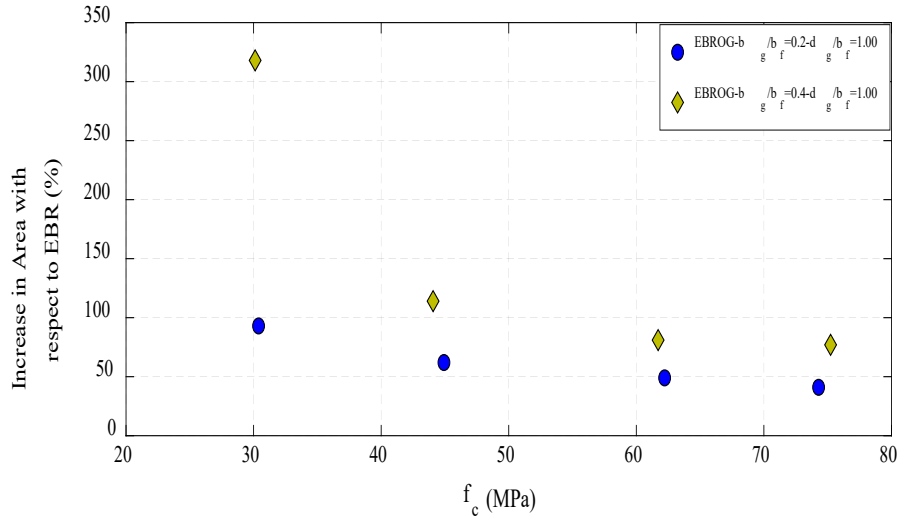

Fig. 7. Effect of concrete compressive strength on: (a) maximum mid-span displacement of EBROG beams compared to EBR beams, (b) value of growth in the area under load-displacement of EBROG beams compared to EBR beams

(a)

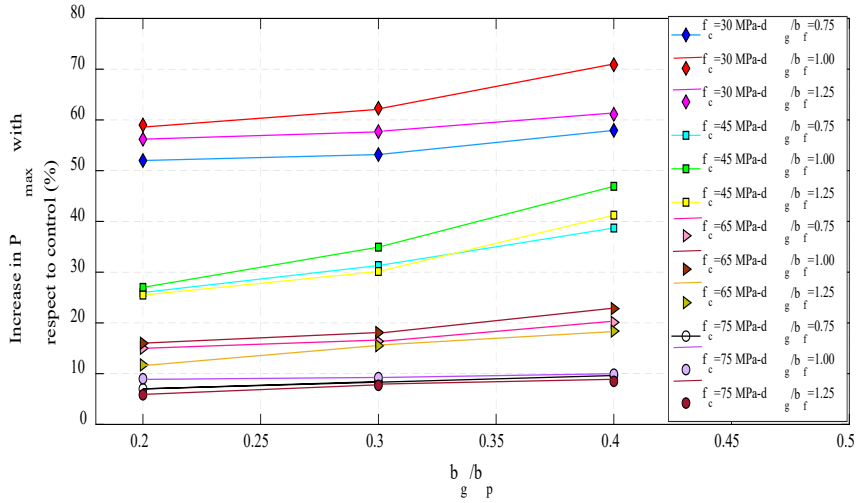

(b)

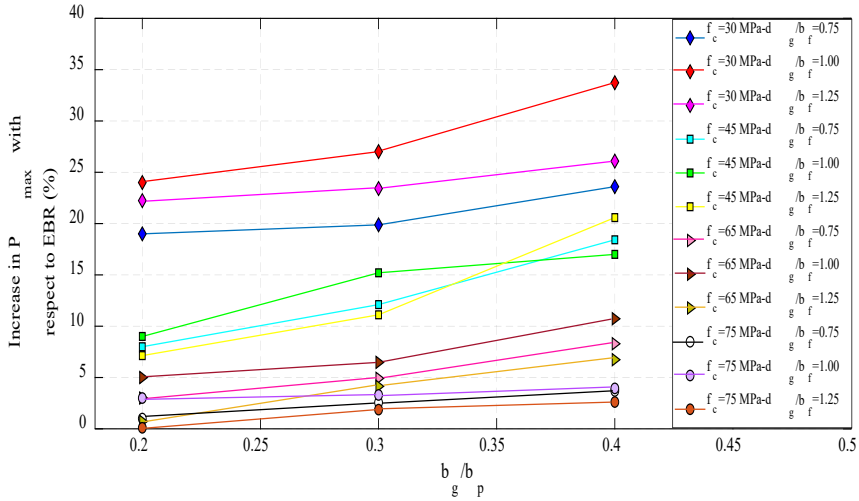

Fig. 8. Effect of groove breadth to FRP sheet width ratio: (a) load capacity enhancement compared of EBROG beams to reference specimens, (b) load capacity enhancement of EBROG beams compared to EBR specimens

(a)

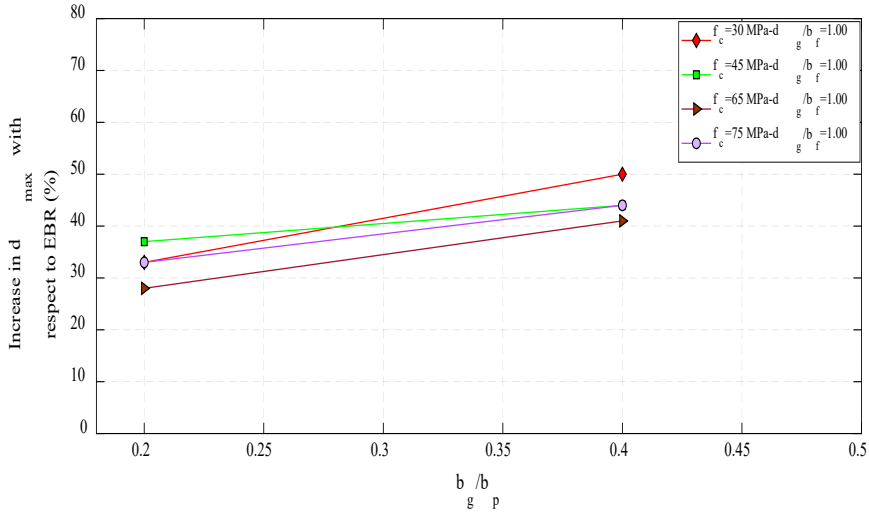

(b)

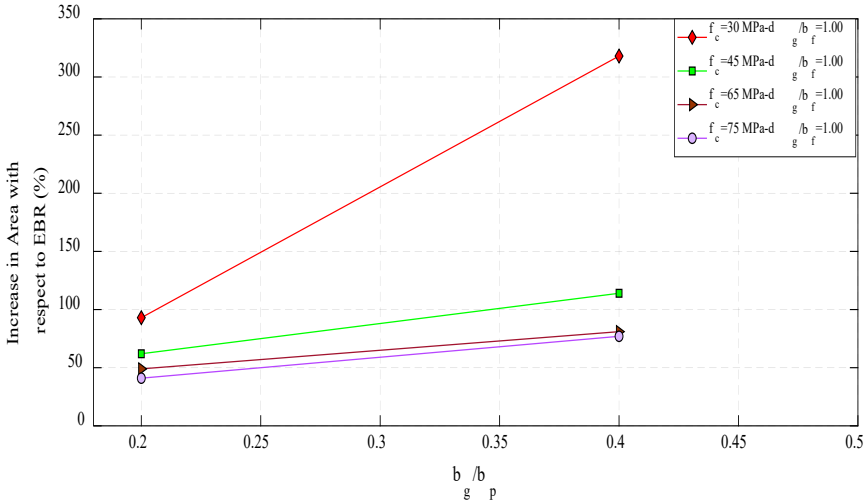

Fig. 9. Effect of groove breadth to FRP sheet width ratio: (a) maximum mid-span displacement of EBROG beams compared to EBR beams, (b) value of growth in the area under load-displacement curves of EBROG beams compared to EBR beams

(a)

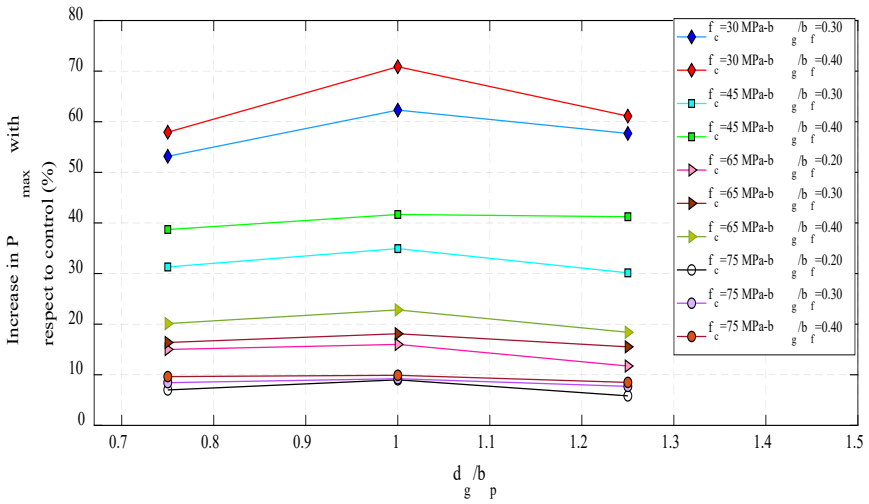

(b)

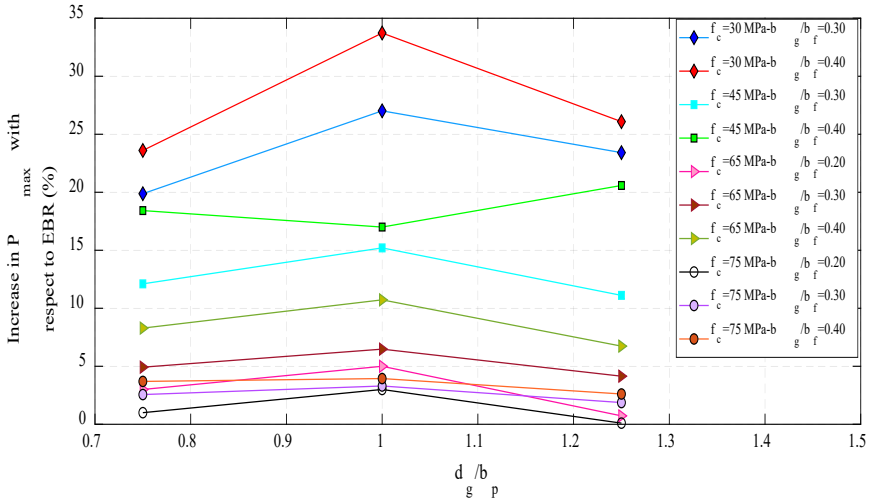

Fig. 10. Effect of groove depth to FRP sheet width ratio: (a) load capacity increase compared to reference specimens, (b) load capacity increase compared to EBR specimens

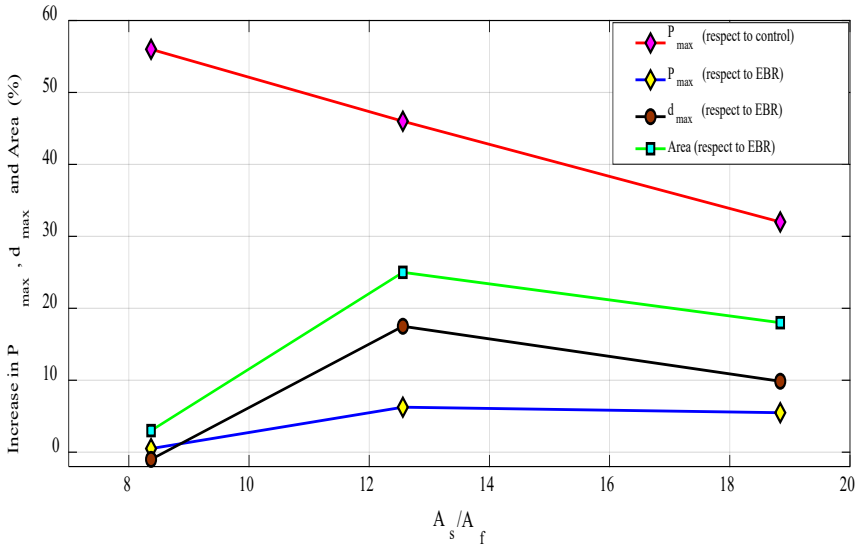

Fig. 11. Load capacity, maximum mid-span displacement, and area under load-displacement curves versus the ratio of external strengthening area to internal reinforcement area

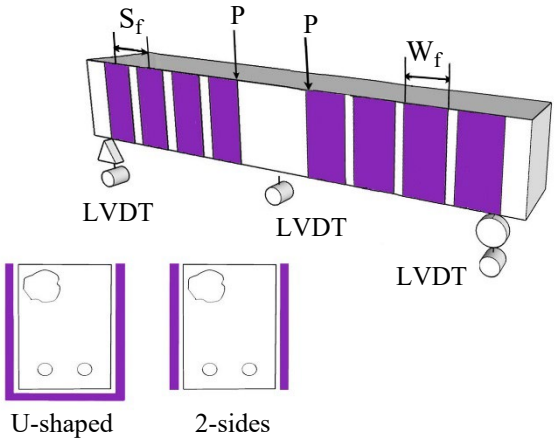

(a) Vertical pattern, U-shaped and 2-sides methods

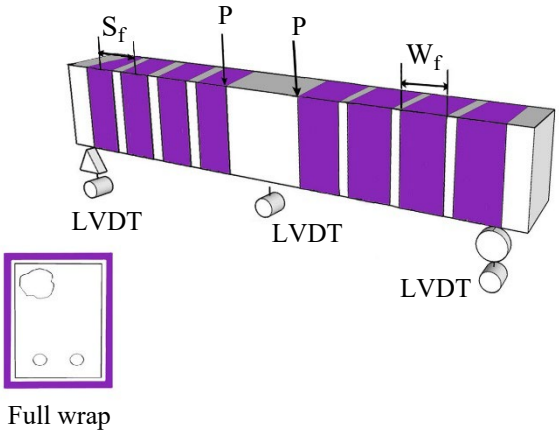

(b) Vertical pattern, Full wrap method

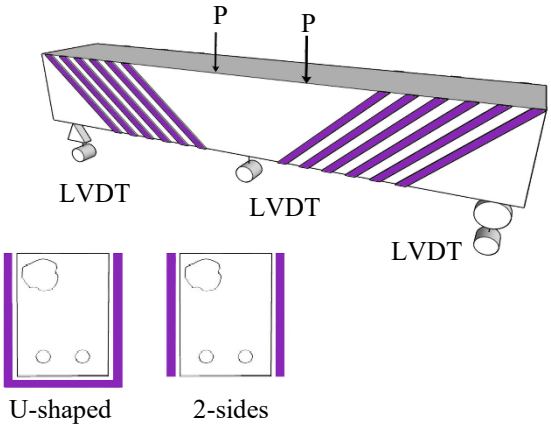

(c) Diagonal pattern, U-shaped and 2-sides methods

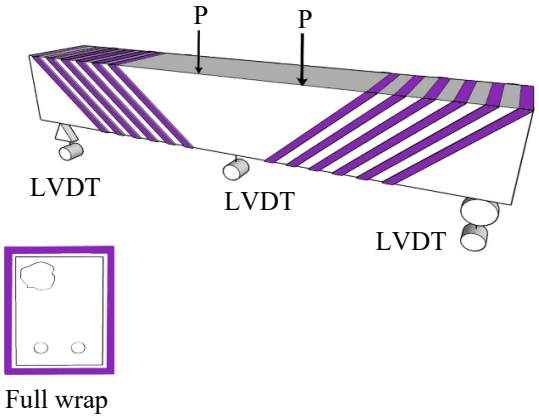

(d) Diagonal pattern, Full wrap method

Fig. 12. Test setup and different shear strengthening patterns

(a)

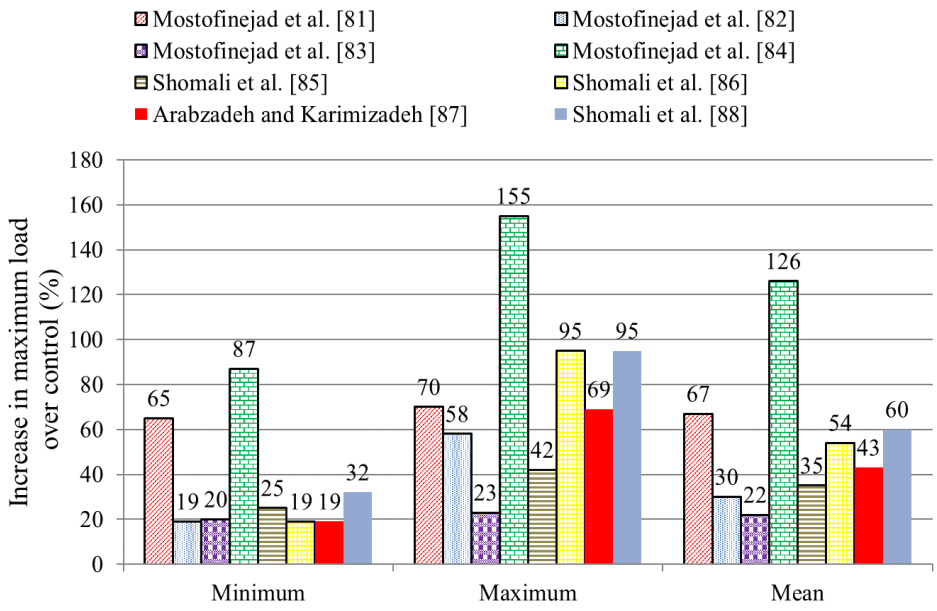

(b)

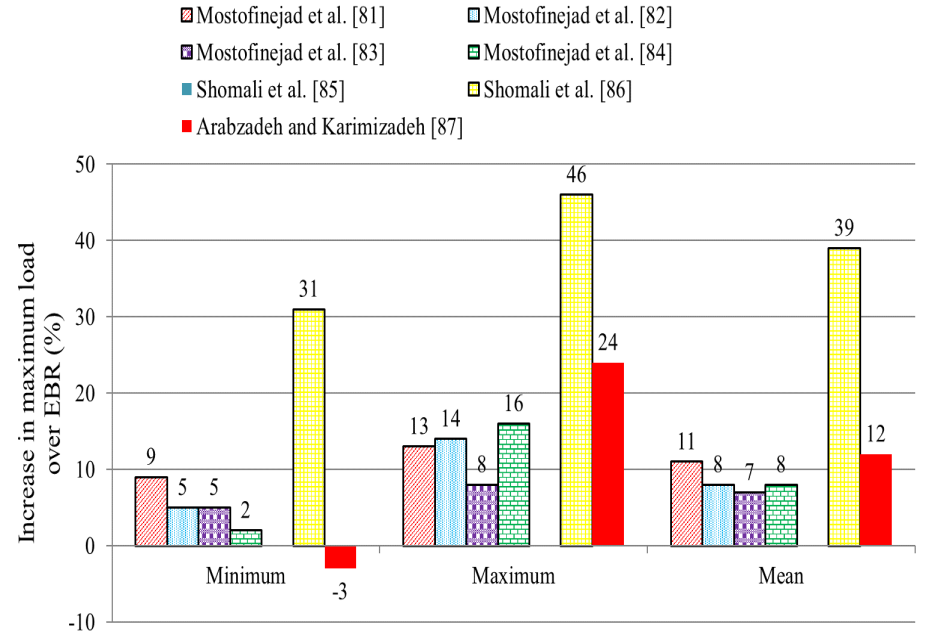

Fig. 13. Increase in load capacity of shear strengthened beams: (a) compared to non-strengthened beams, (b) compared to EBR beams

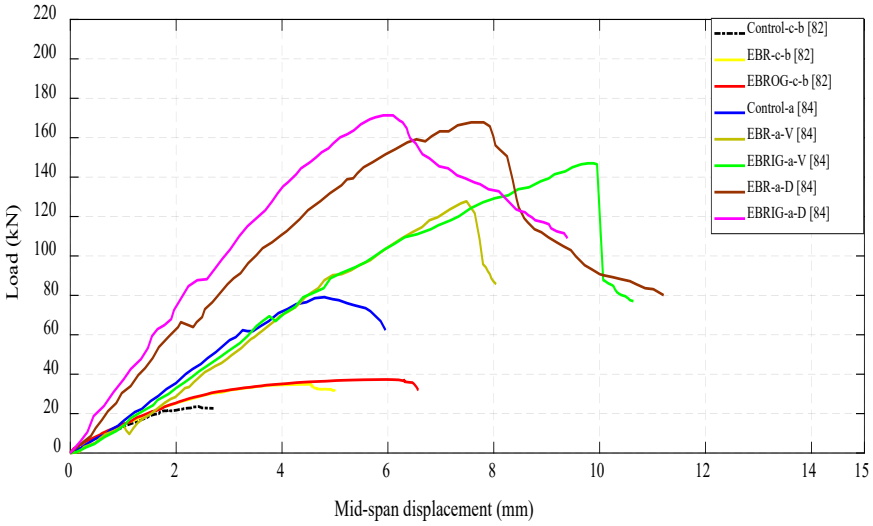

Fig. 14. Load-displacement curves at mid-span of some shear strengthened beams

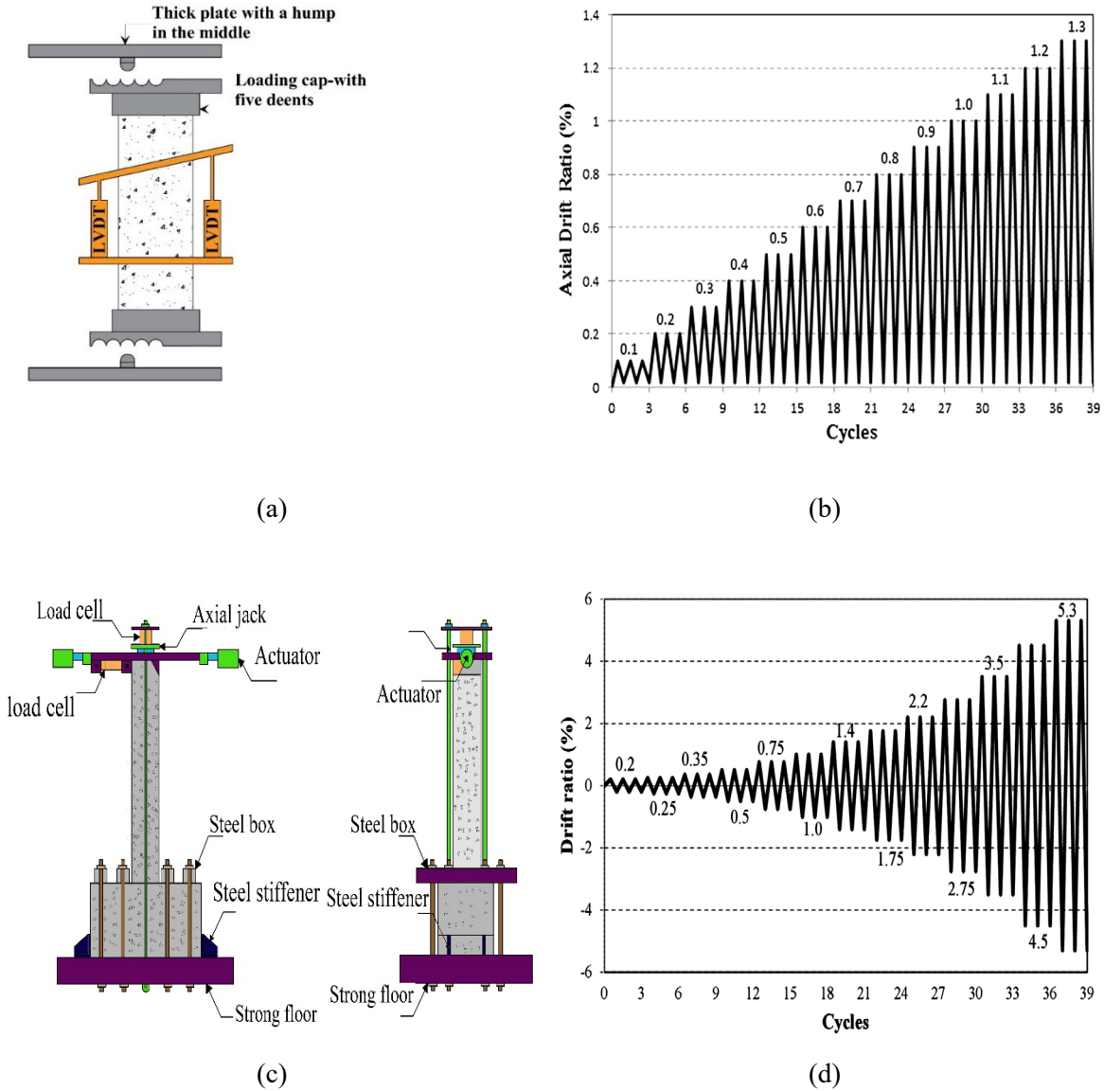

Fig. 15. Testing strengthened columns, (a) schematic view of the axial test setup, (b) axial cyclic loading protocol, (c) schematic view of the seismic test setup , (d) lateral cyclic loading history

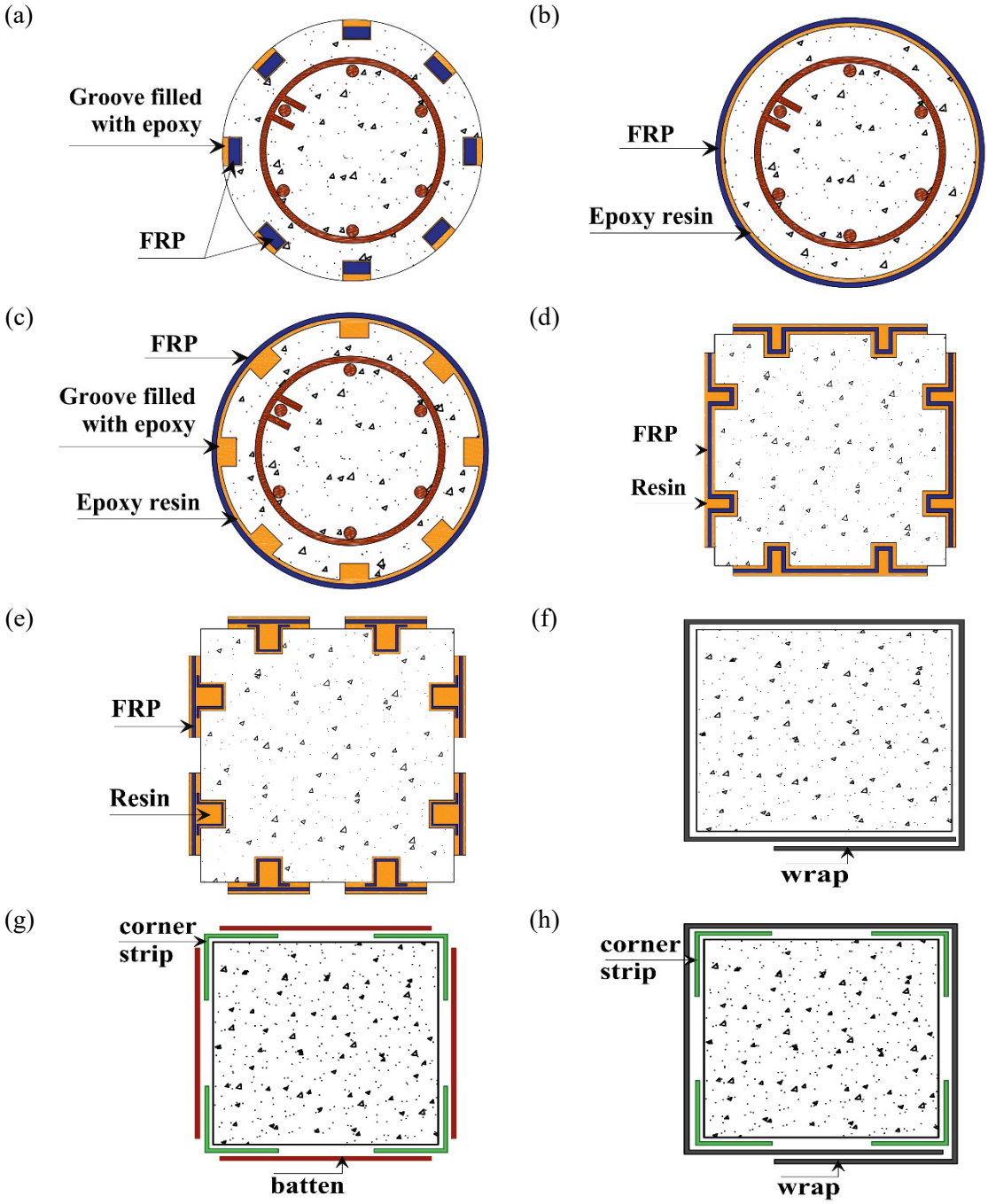

Fig. 16. Section views of external strengthening of RC columns: longitudinal patterns (a) NSM, (b) EBR, (c) EBROG, (d) EBRIG, (e) EBRIOG; transverse patterns (f) IW, (g) CSB, (h) CSW

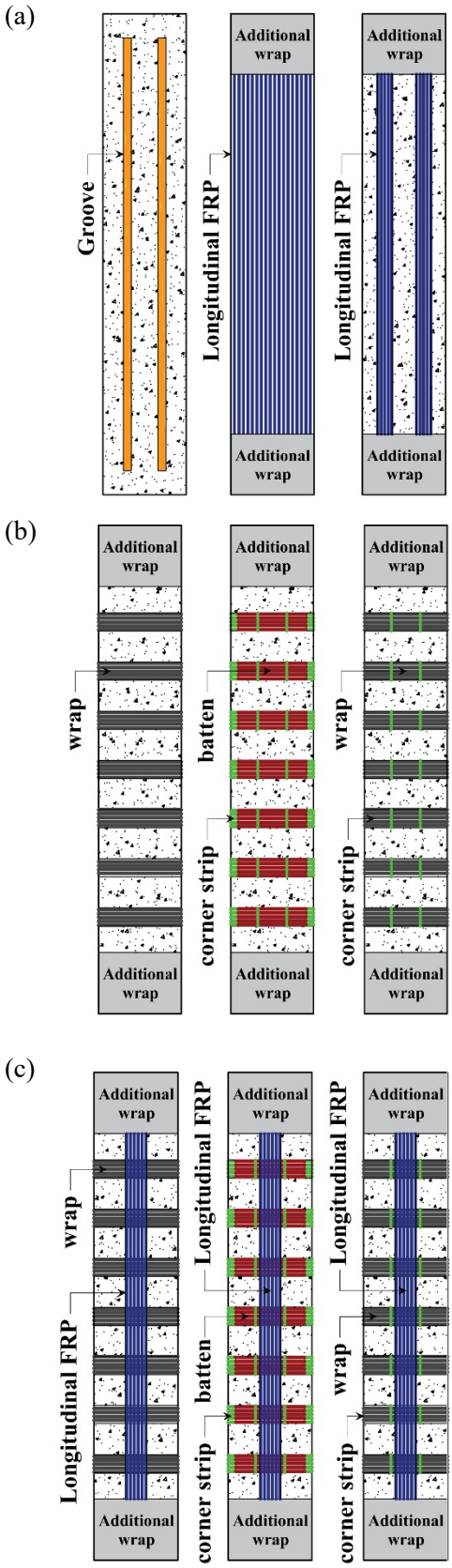

Fig. 17. Side views of external strengthening of RC columns: (a) longitudinal, (b) transverse, (c) longitudinal and transverse

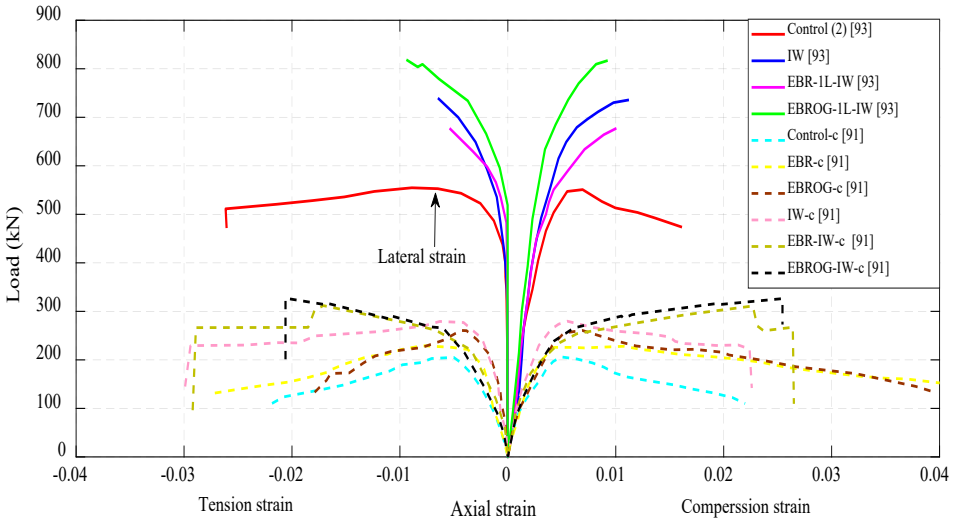

(a)

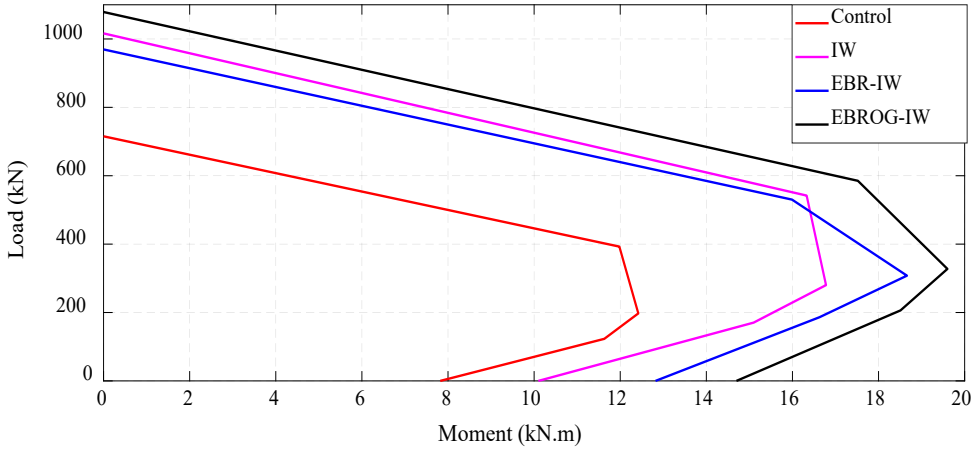

(b)

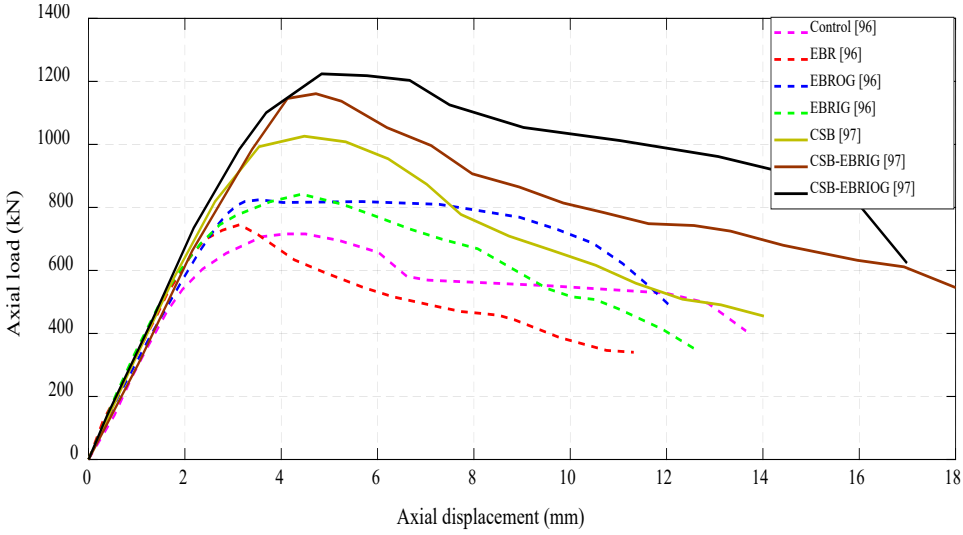

(c)

Fig. 18. Behavioral diagrams of some external strengthened RC columns: (a) load-strain curves, (b) P-M diagrams, (c) axial load-displacement envelope curves

(a)

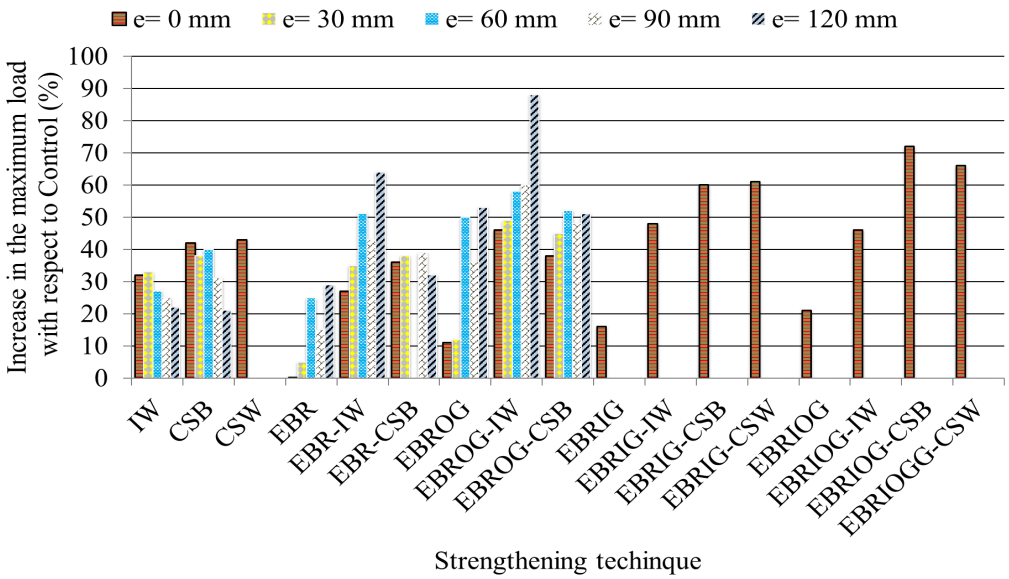

(b)

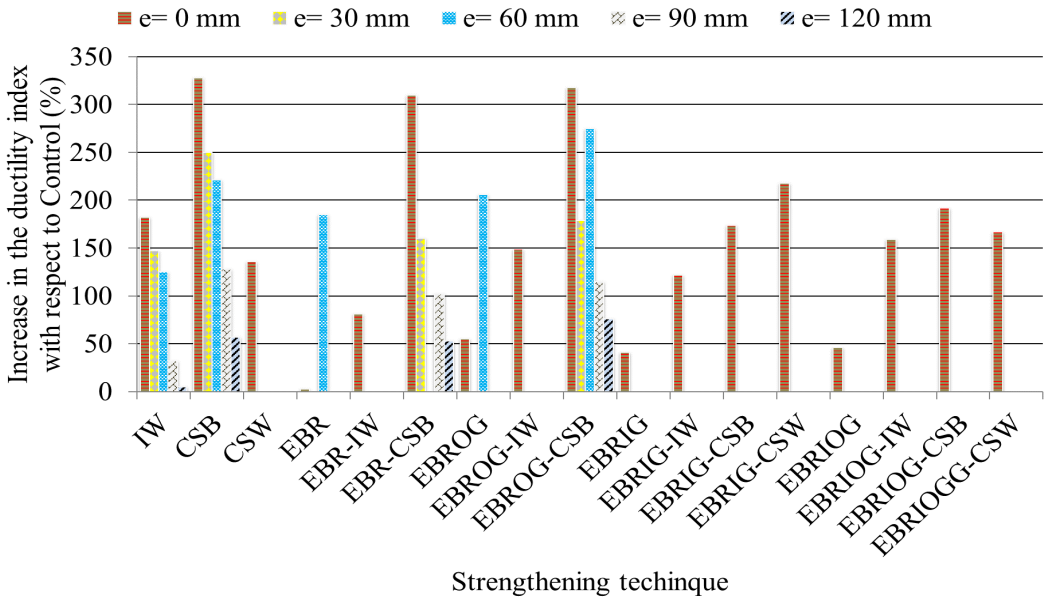

Fig. 19. Effect of various methods of longitudinal and transverse strengthening of columns: (a) maximum load capacity, (b) ductility index

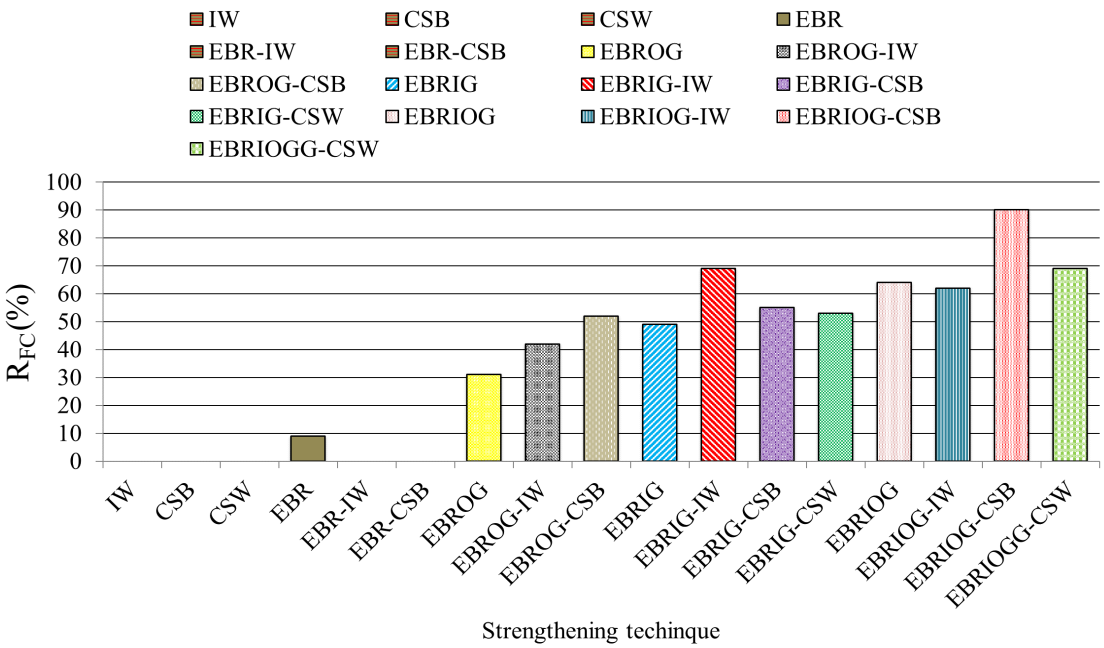

Fig. 20. Effect of various methods strengthening of RC column on compressive stress of FRP composite to ultimate tensile strength (R_{FC})

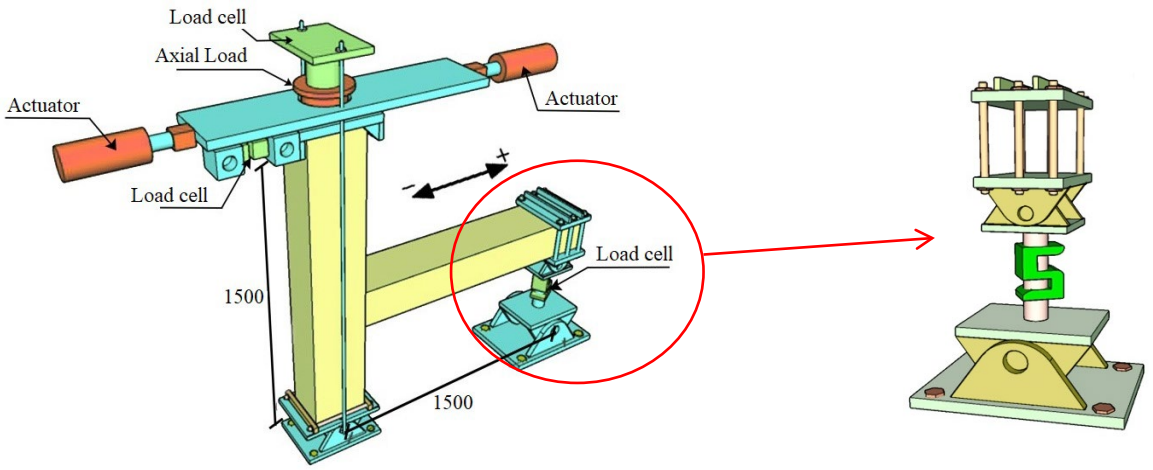

(a) Test setup [106-112]

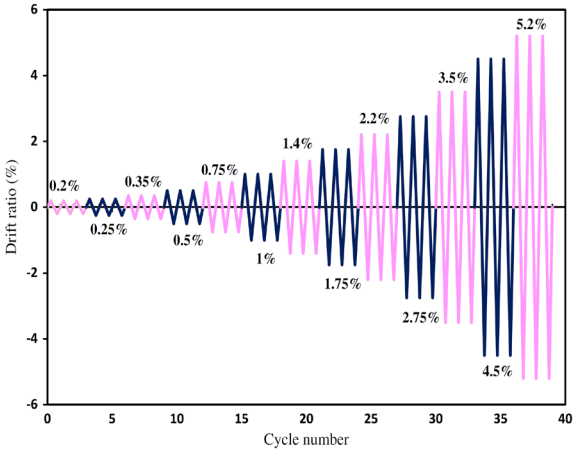

(b) Cyclic loading history [106-112,159]

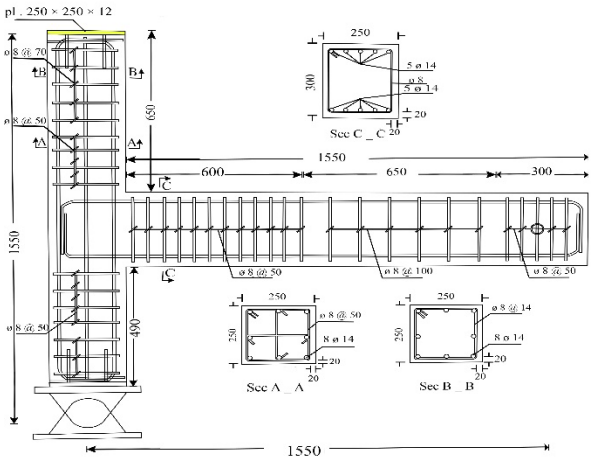

(c) Reinforcement details and dimensions [106-107,112]

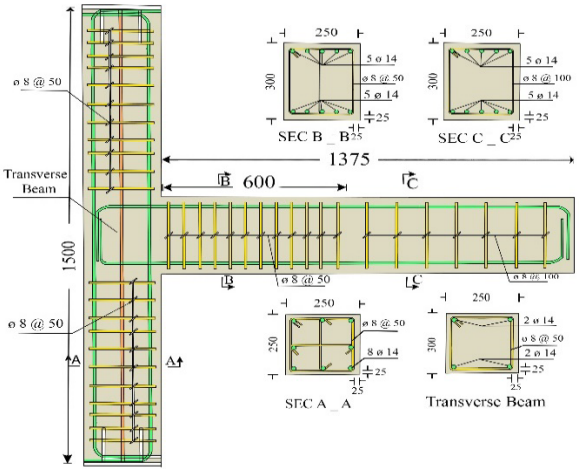

(d) Reinforcement details and dimensions [108-109]

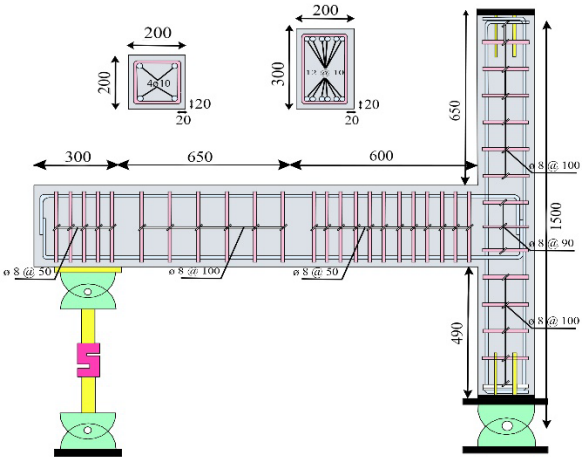

(e) Reinforcement details and dimensions [110-111]

Fig. 21. Test setup and seismic loading protocol of RC beam-column joints

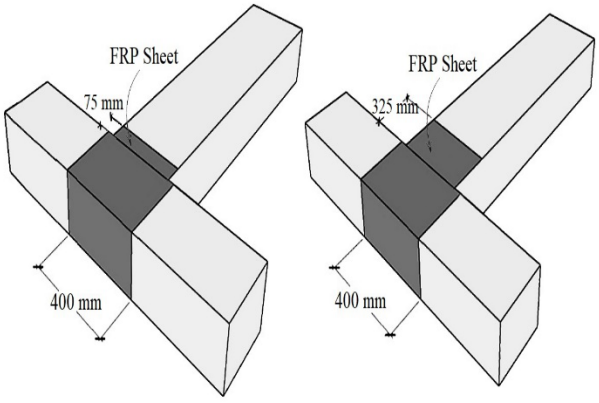

(a) RDS-3H75 and RDS-3H325 [106]

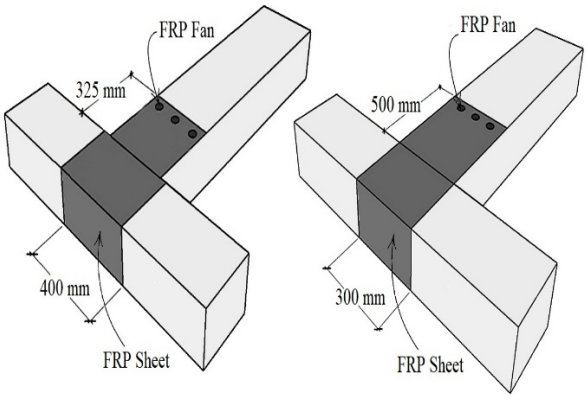

(b) RDS-3H325F and RDS-4H500F [106]

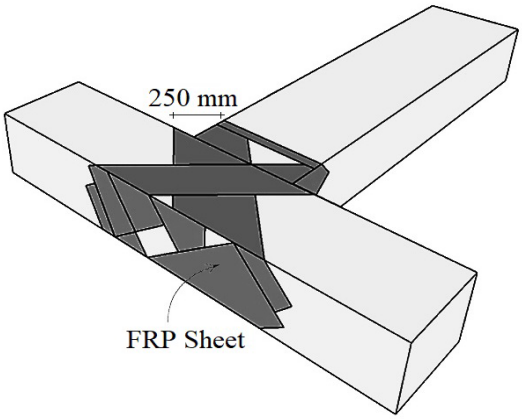

(c) RDS-1H250 [106]

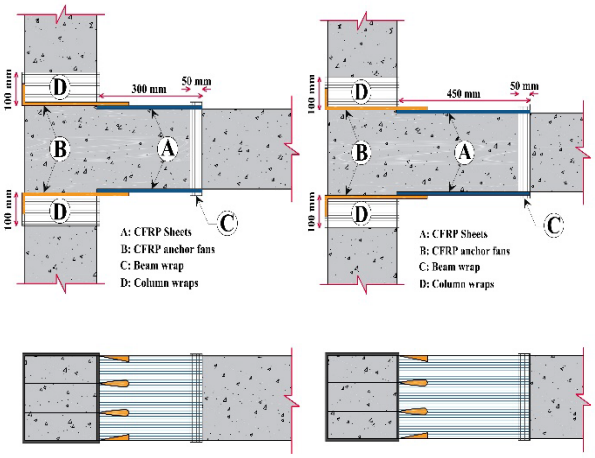

(d) RS-1H300 and RS-2H450I [107]

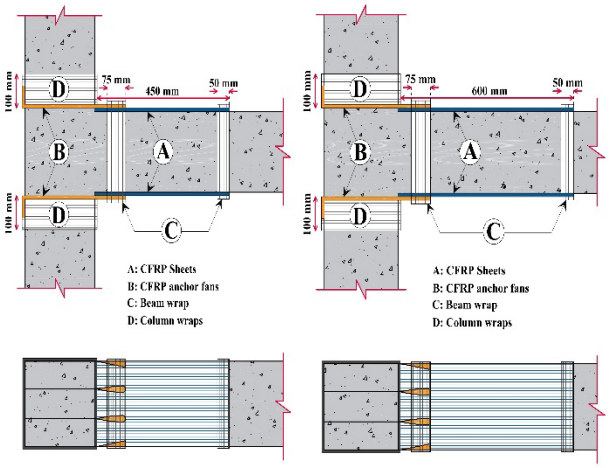

(e) RS-2H450II and RS-3H600I,II [107]

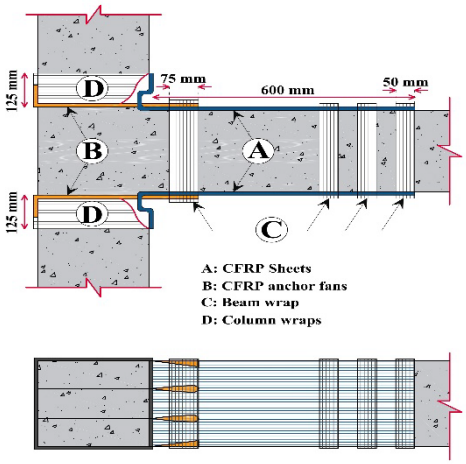

(f) RS-2L600 [107]

Fig. 22. Various patterns of external strengthening RC beam-column joints by grooving methods

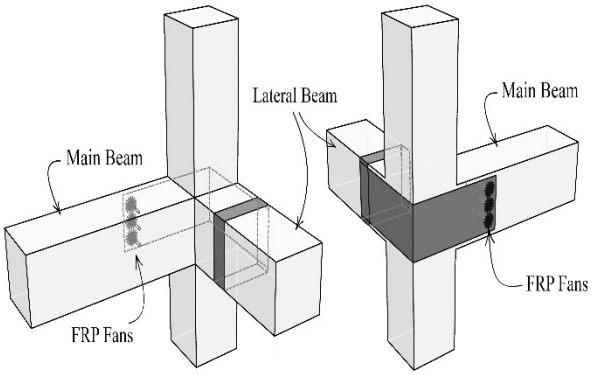

(g) RDS-3L300 [108]

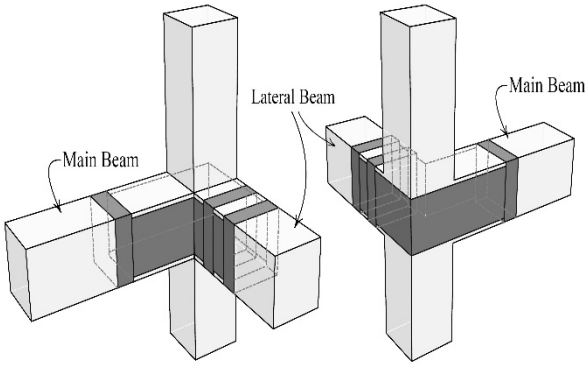

(h) RDS-3L300-EBR [108]

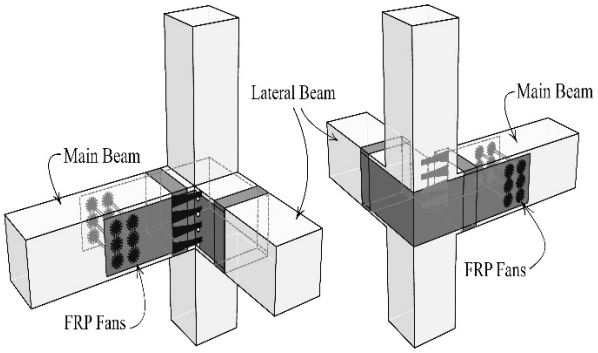

(i) RDS-3L300FW [108]

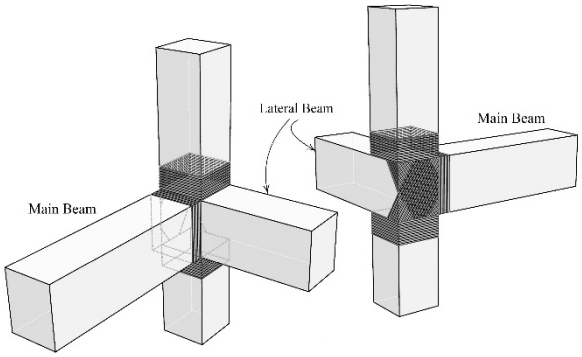

(j) RDS-X and RDS-X-EBR [109]

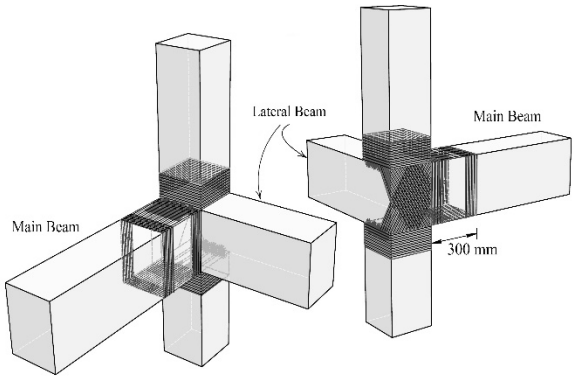

(k) RDS-1X3H300F [109]

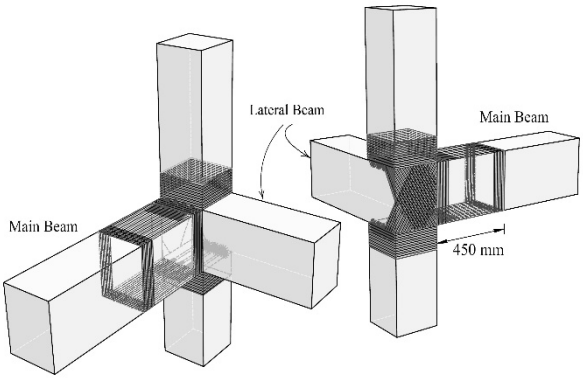

(l) RDS-1X3H450F [109]

Fig. 22. (Continued)

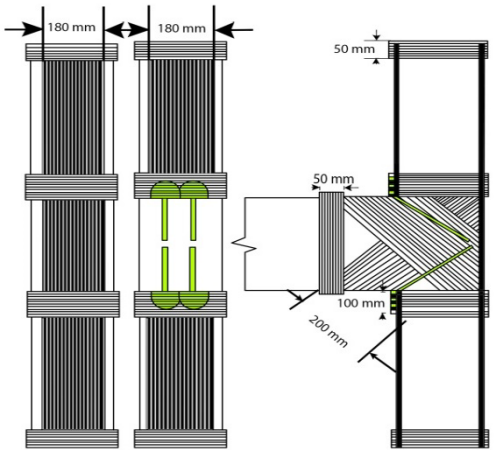

(m) 1V-1X [110]

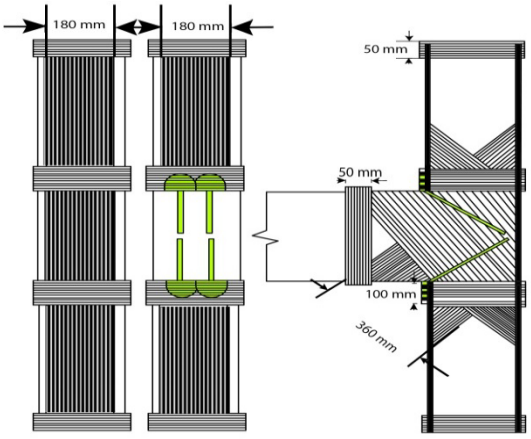

(n) 1V-2X [110]

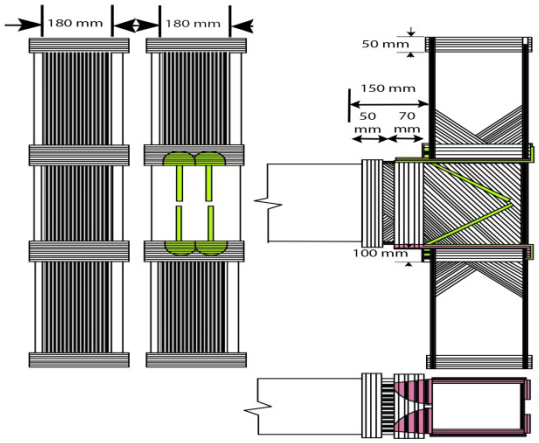

(o) 1V-2X-2H.I [110]

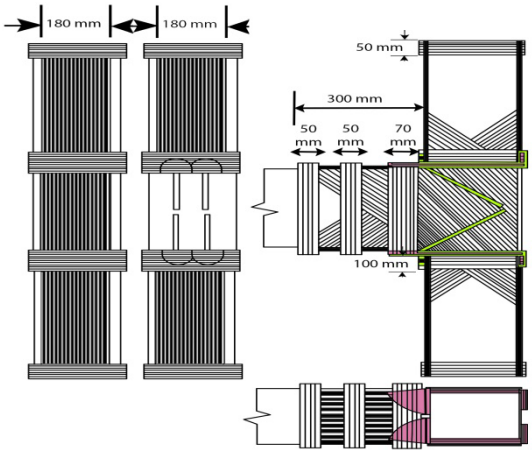

(p) 1V-2X-2H.II [110]

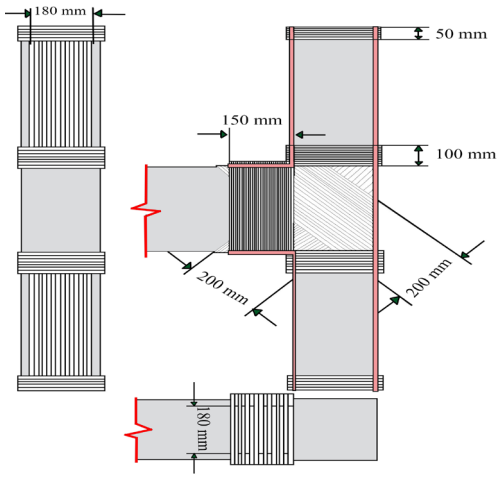

(q) S1L150-1X [111]

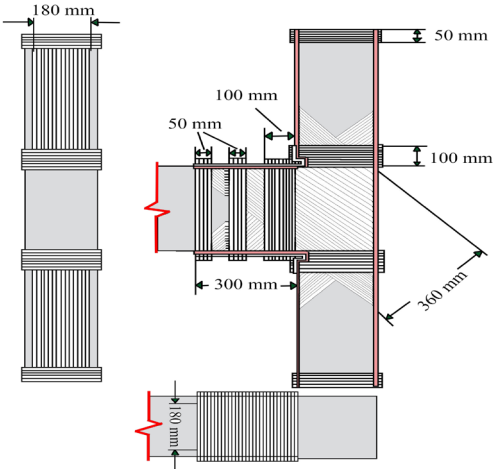

(r) S2L300-G2X [111]

Fig. 22. (Continued)

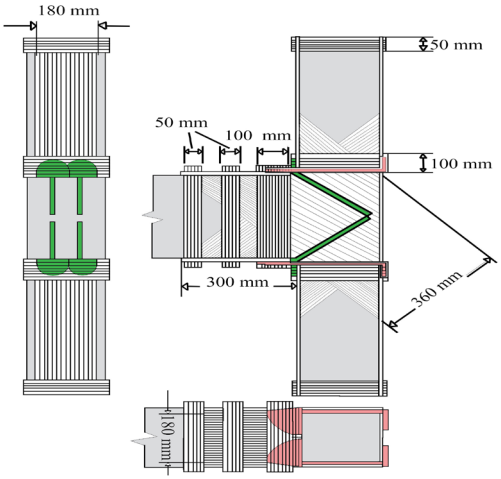

(s) S1V-2H-F2X [111]

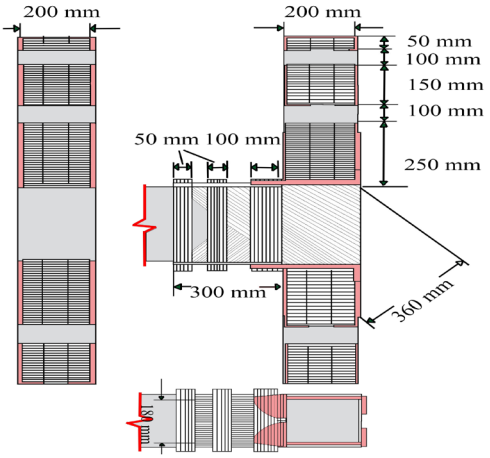

(t) S2CSB-2H-F2X [111]

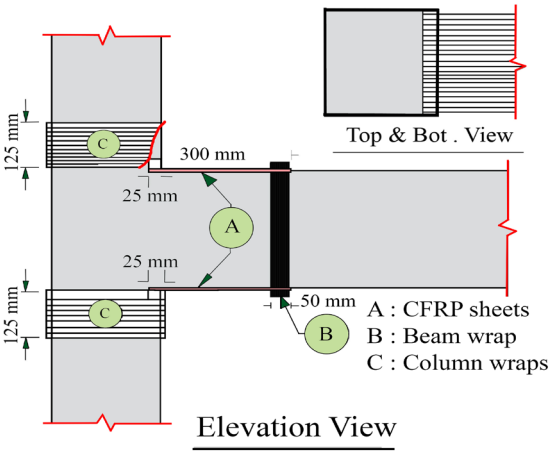

(u) RS-1H300 [112]

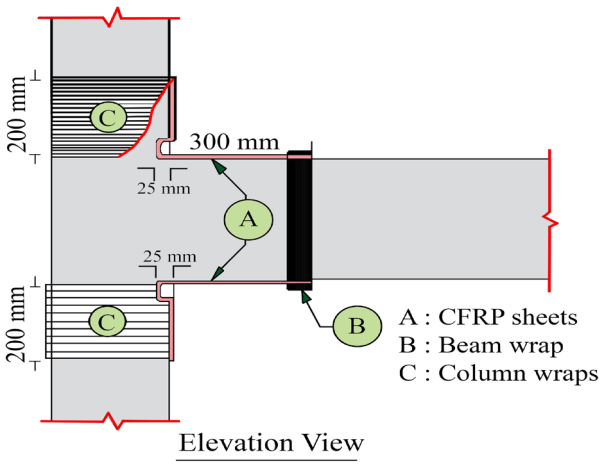

(v) RS-2L300 [112]

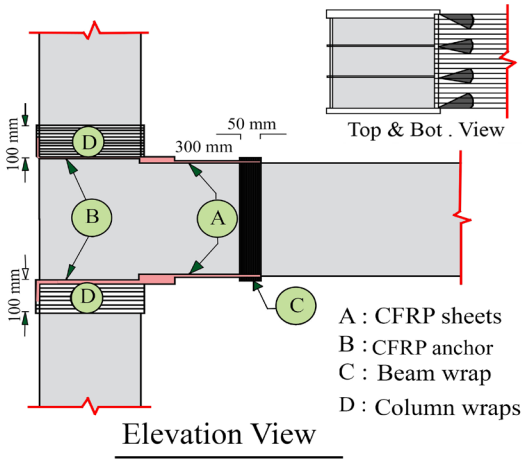

(w) RS-1H300.F180 [112]

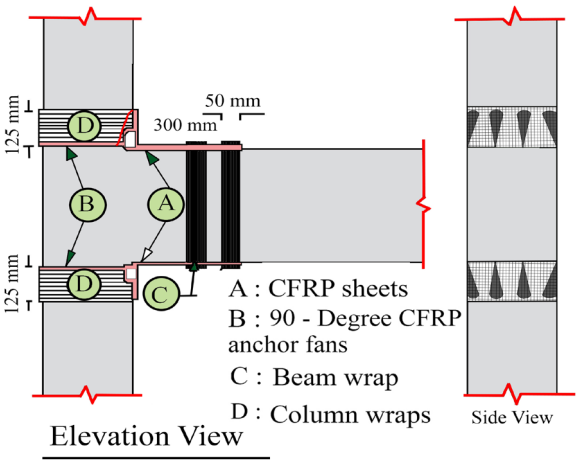

(x) RS-1L300.F90 [112]

Fig. 22. (Continued)

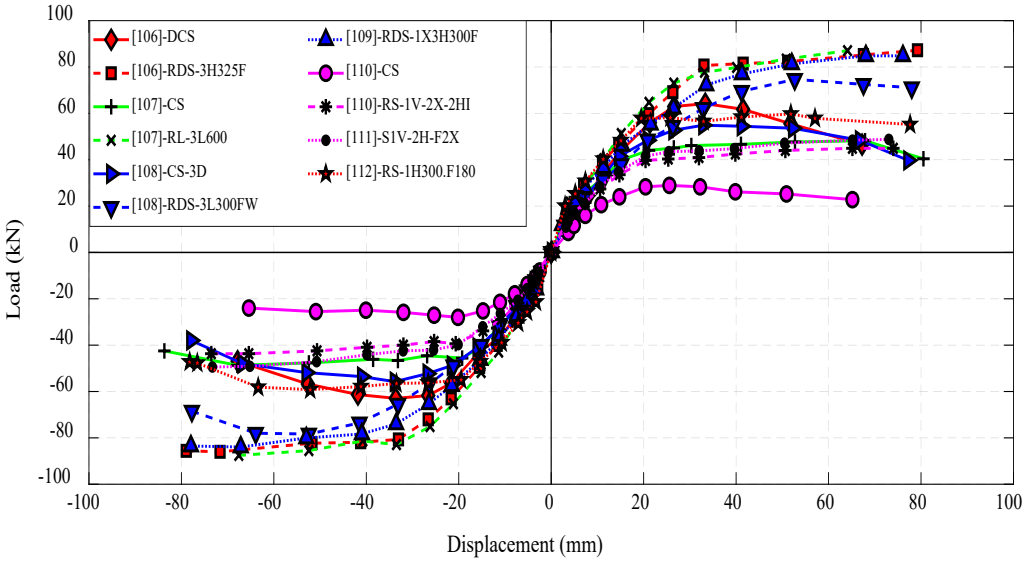

Fig. 23. Load-displacement envelope curves for RC beam-column joints

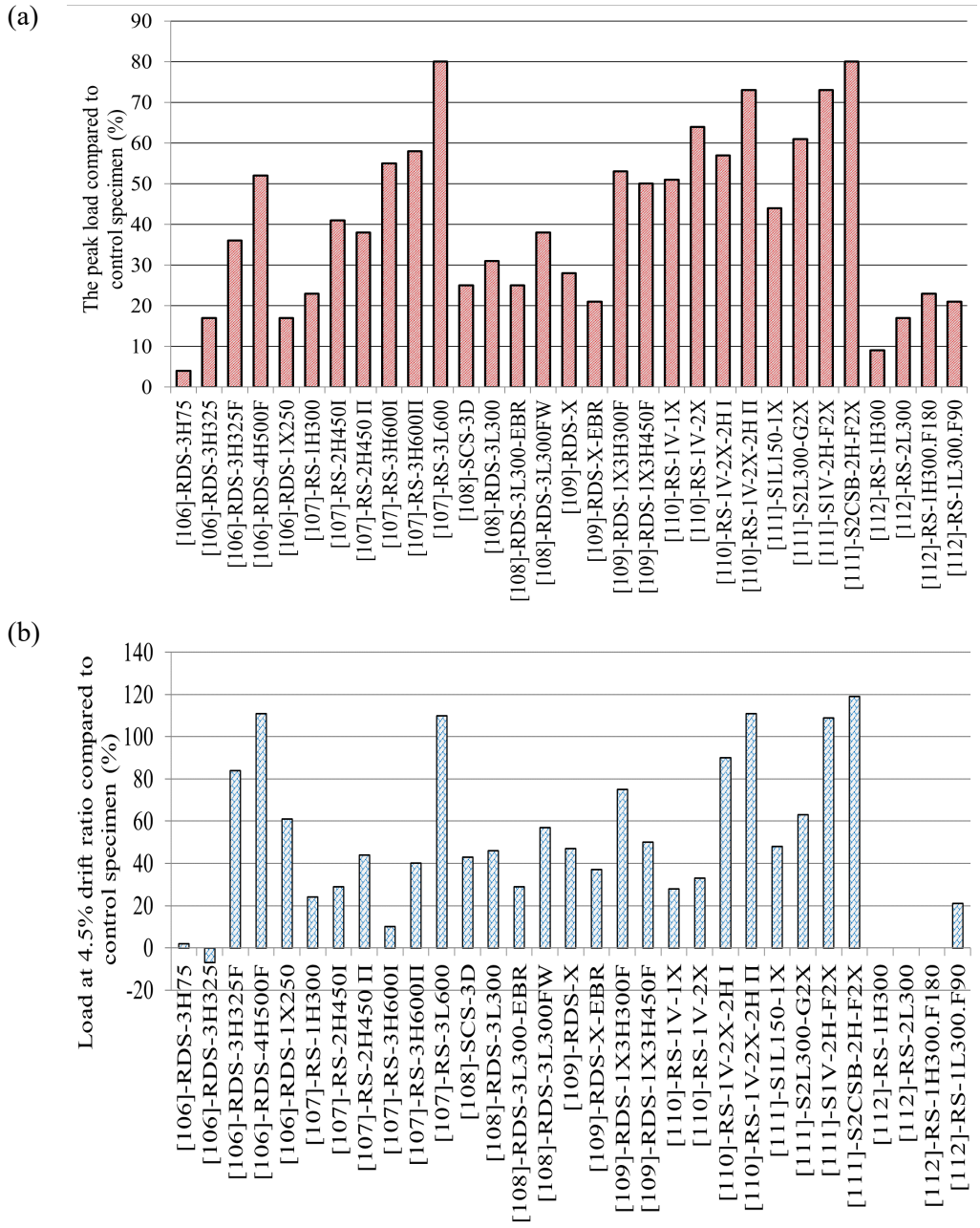

Fig. 24. Increase in load capacity of strengthened joints compared to the control joints: (a) peak load, (b) Load in the 4.5% drift ratio

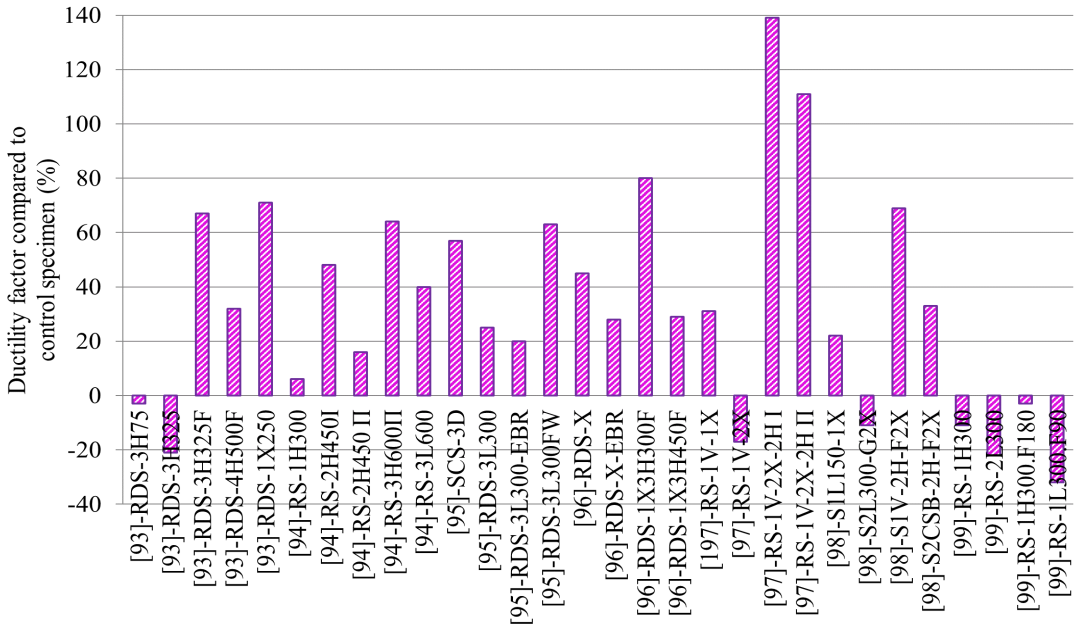

Fig. 25. Enhancement in ductility factor (in pulling) of strengthened joints compared to the control joints

(a)

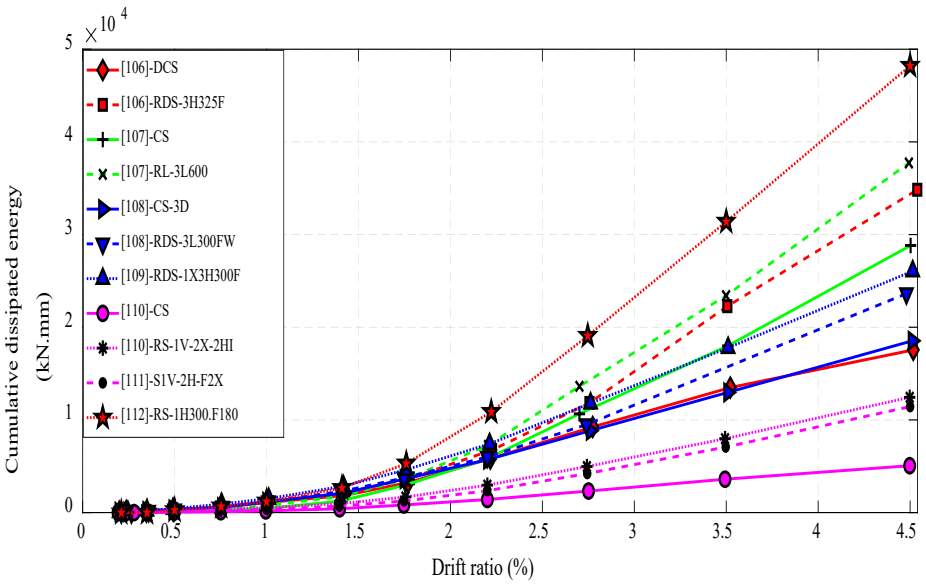

(b)

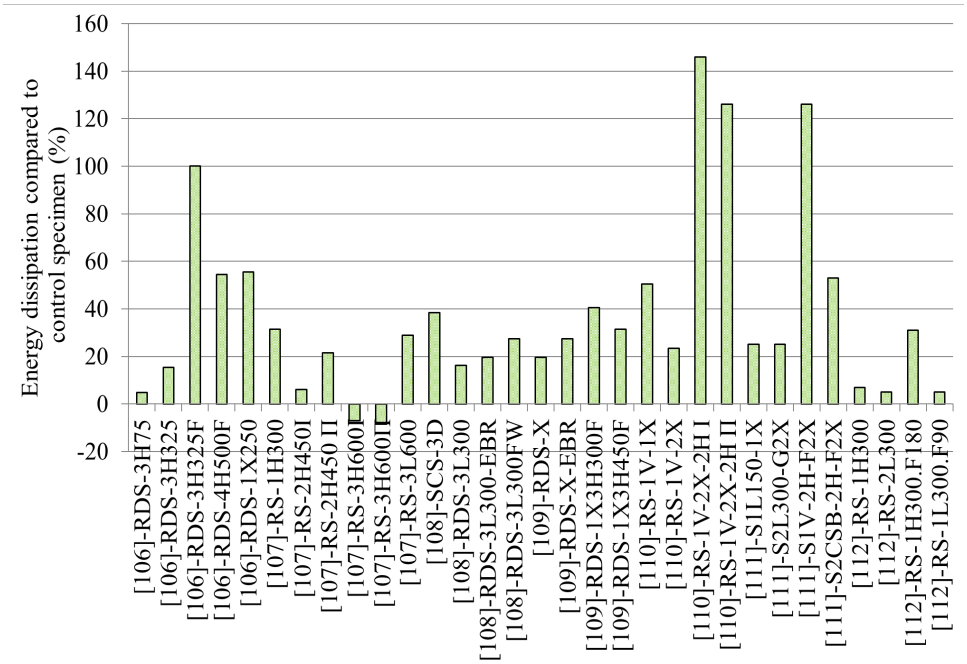

Fig. 26. Energy dissipation of strengthened joints: (a) cumulative dissipated energy versus drift ratio, (b) increase of energy dissipation compared to the control joint in the 4.5% drift ratio

(a)

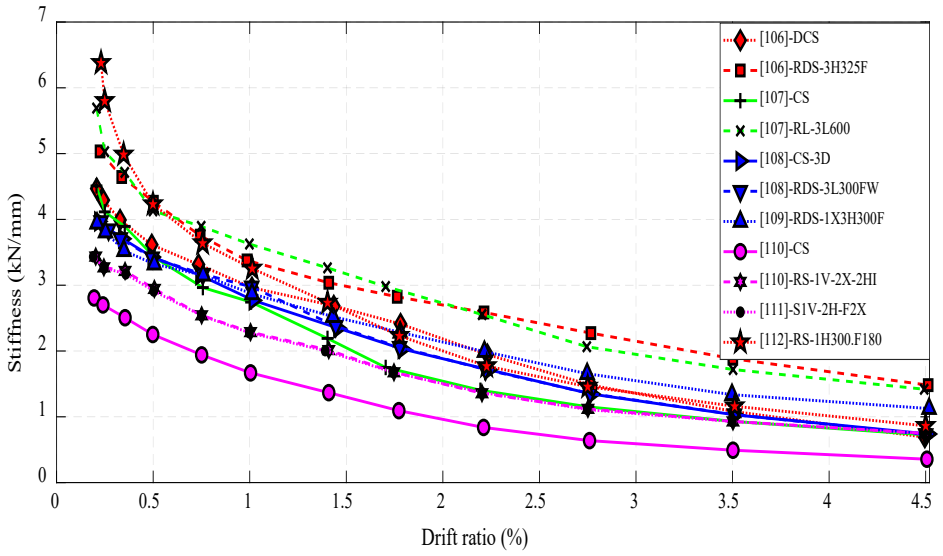

(b)

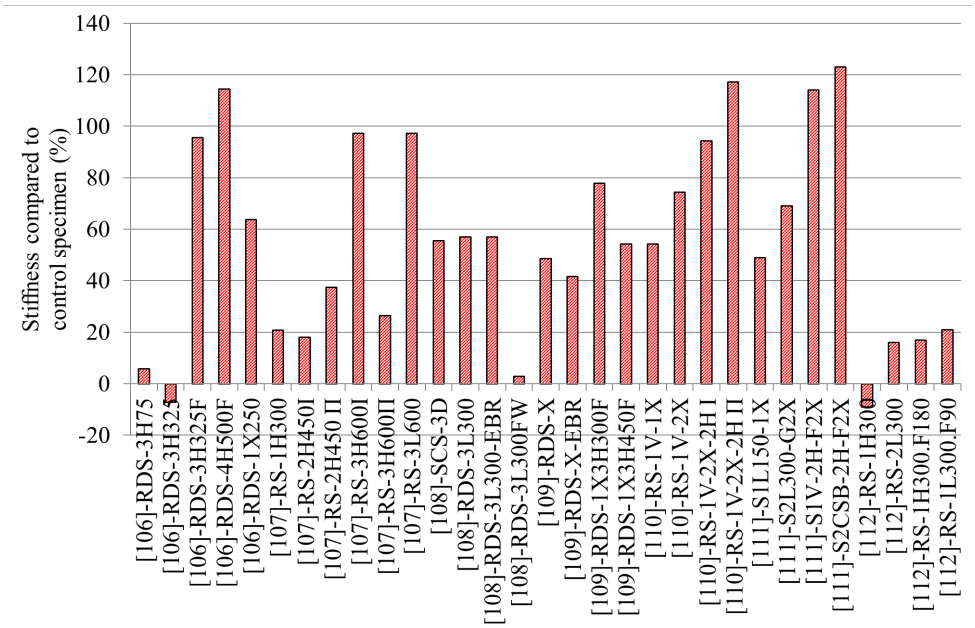

Fig. 27. Stiffness degradation of strengthened joints: (a) stiffness degradation versus drift ratio, (b) increment in stiffness compared to the control joint in the 4.5% drift ratio

(a)

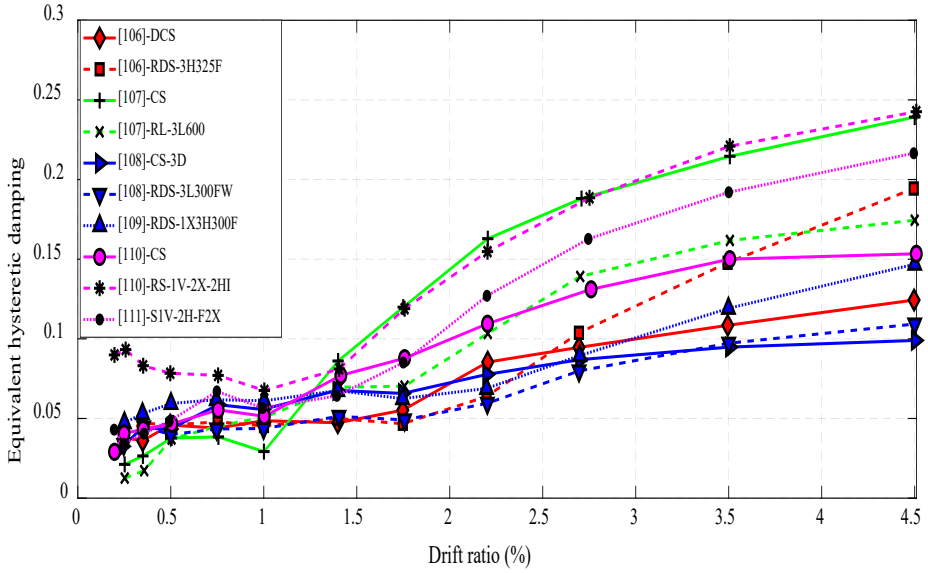

(b)

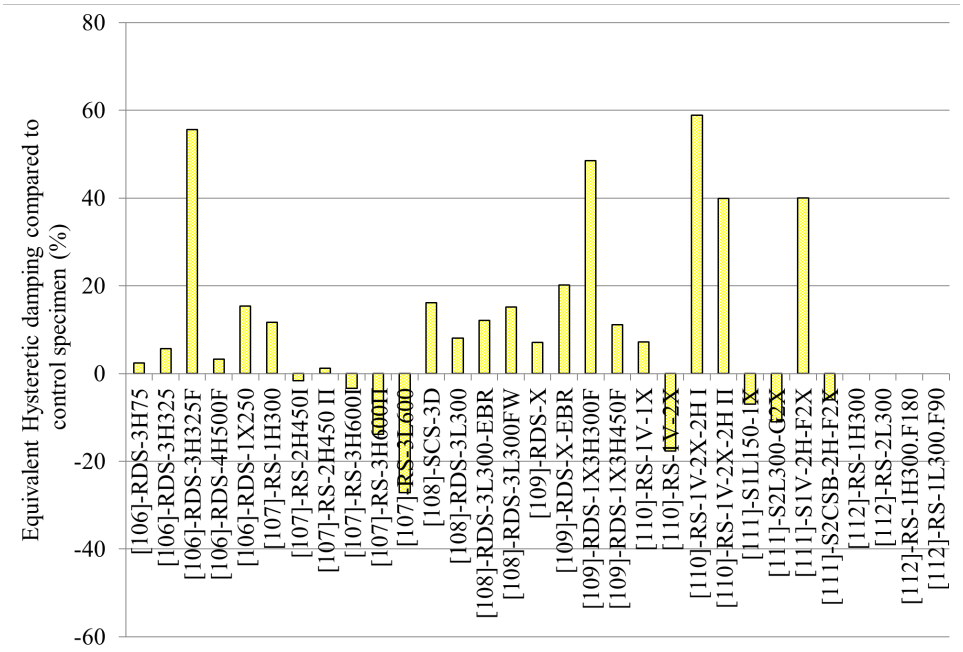

Fig. 28. Equivalent damping ratio of strengthened joints: (a) equivalent hysteretic damping versus drift ratio, (b) increase in equivalent hysteretic damping ratio compared to the control joint in the 4.5% drift ratio